NEUTRINO OSCILLATION EXPERIMENTS USING ACCELERATORS AND REACTORS

Stanley Wojcicki
Physics Department, Stanford University
Stanford, CA 94305
e-mail: sgweg@slac.stanford.edu

ABSTRACT

These lectures emphasize neutrino oscillation experiments using accelerators and reactors. We describe past, present, and proposed experiments. A brief introduction to neutrino oscillations is given at the beginning. The technology of beams and detectors for neutrino experiments is described briefly.

Table of Contents

1 Introduction

The existence of the neutrino was postulated in 1930 by W. Pauli[1] to explain the apparent energy nonconservation in nuclear weak decays. It was another 23 years before this bold theoretical proposal was verified experimentally in a reactor experiment performed by C. Cowan and F. Reines.[2] The most fundamental properties of the neutrino were verified during the subsequent decade. The neutrino was shown to be left- handed in an ingenious experiment by Goldhaber, Grodzins, and Sunyar[3] in 1957. The distinct nature of ν_e and ν_μ was demonstrated in 1962 in a pioneering accelerator neutrino experiment at BNL by Danby *et al.*[4]

The following years saw a remarkable progress in neutrino experiments, especially those utilizing accelerators as their sources. Increases in available accelerator energies and intensities, advances in neutrino beam technology, and more sophisticated and more massive neutrino detectors were all instrumental in our ability to do ever more precise neutrino experiments. The focus of those experiments, however, was until very recently mainly on using neutrinos as a probe in two different areas. Together with experiments utilizing electrons and muons, the worldwide neutrino program played a key role in measuring the nucleon structure functions. And together with a variety of other efforts (especially e^+e^- annihilations and deep inelastic electron scattering) the neutrino experiments played a key role in establishing the validity of the Standard Model (SM), through the discovery of neutral currents,[5] measurements of the NC/CC ratio,[6] and measurements of the neutrino lepton scattering cross sections.[7]

I believe that we are now entering a new phase in experimental neutrino physics. The main thrust in the future will probably be twofold: better understanding of the nature of the neutrino, i.e., a study of neutrino properties; and use of the neutrino in astrophysics and cosmology as an alternative window on the universe, complementing the information obtained from studies of the electromagnetic spectrum. In these lectures I shall deal with the subject of neutrino oscillations, i.e., a part of the first program.

We believe that neutrinos are among the fundamental constituents in nature. In addition, the space around us is permeated with neutrinos which are relics of the Big Bang, to the tune of about 110 ν's/cc for every neutrino flavor. But our knowledge of the neutrino's properties lags far behind our knowledge of other elementary constituents, for example, the charged leptons. A few examples may illustrate this point. (We quote the lepton values from the latest compendium by the Particle Data Group.[8])

We do not know whether neutrinos have a mass; our current information gives us only upper limits ranging from a few eV for ν_e to some 20 MeV for ν_τ. We can contrast that with a fractional mass error of about 3×10^{-7} for the electron and muon and about 2×10^{-4} for the tau.

We do not know if neutrinos are stable or decay, either into neutrinos of other flavors or into some new, as yet undiscovered, particles. In contrast, we know that electron is stable, and know the μ lifetime with a fractional error of 2×10^{-5} and the τ lifetime at the level of 0.5%.

Finally, we do not know if the neutrinos have electromagnetic structure, like for example, a magnetic moment. The electron moment is known with a precision of about one part in 10^{11}; the magnetic moment of the muon to one part in 10^8.

The study of neutrino oscillations offers us what is potentially a most sensitive investigation or measurement of neutrino masses (neutrino mass squared differences to be precise). Observation of a non-zero neutrino mass, which would follow directly from observation of neutrino oscillations, would be a clear example of breakdown of the SM and thus an indication of physics beyond it. Many of the popular extensions of the SM do indeed predict non-zero neutrino masses and existence of neutrino oscillations.[9] Furthermore, neutrino oscillations are not only an attractive theoretical concept, but also a phenomenon hinted at by several experimental observations.

These observations are:

(a) An apparent need for dark (i.e., non-shining) matter.[10] One example of this need is the observed deficit of sufficient matter to account for the gravitational forces needed to explain the rotation velocity of stars in spiral galaxies. Neutrinos, since they are present in abundance everywhere, could account for at least a part of this deficit if they had a finite mass.

(b) The solar neutrino deficit, i.e., observation of fewer sun-originated neutrinos on earth than expected from the known solar luminosity.[11]

(c) The atmospheric neutrino anomaly,[12] i.e., a measured ν_μ/ν_e ratio for neutrinos from cosmic ray interactions in our atmosphere which is significantly smaller than predicted.

(d) The apparent observation of $\bar{\nu}_e$ in an almost pure $\bar{\nu}_\mu$ beam in a Los Alamos experiment[13] (the LSND effect).

As discussed in parallel lectures by K. Martens,[14] the second and third effects could be explained by neutrino oscillations: ν_e oscillations into another flavor in the case of the solar neutrino deficit and ν_μ oscillating into ν_e or (more likely) into ν_τ in the case of the atmospheric neutrino anomaly. The LSND effect will be discussed later in these lectures (see Sec. 6.2.1).

These lectures start out with a very brief description of neutrino oscillation phenomenology and of the customary method of classification of neutrino oscillation experiments. The next two chapters deal with the general experimental aspects of the neutrino experiments: neutrino beams and neutrino detectors. The following two chapters discuss what is known today about neutrino oscillations from the accelerator and reactor experiments and also describe the current experimental program in the field. The final chapter concludes those lectures by discussing the current plans around the world for future accelerator and reactor experiments which could investigate more fully the four categories of hints alluded to above. The past, present, and future efforts in the non-accelerator, non-reactor area are discussed in the parallel Martens lectures.

2 Formalism of Neutrino Oscillations

2.1 Phenomenology

The underlying principle behind neutrino oscillations[15] is the fact that if neutrinos have mass, then a generalized neutrino state can be expressed either as a superposition of different mass eigenstates or of different flavor eigenstates. This is mainly a restatement of a well-known quantum mechanics theorem that, in general, several different basis vector representations are possible, these different representations being connected by a unitary transformation. Other well-known examples of this principle in particle physics are the $K^0\overline{K}^0$ system (strong interaction and weak interaction eigenstates) and the quark system (weak interaction and flavor eigenstates connected by the CKM matrix).

From the study of e^+e^- annihilations at the Z^0 peak,[16] we know that there are only three neutrino flavor eigenstates if we limit the potential neutrino mass to less than $m_Z/2$. Accordingly, the most likely situation is that we have three mass eigenstates and that the connecting unitary matrix is a 3×3 matrix. This is not rigorously required since we could have states with $m_\nu > m_Z/2$, or flavor states that do not couple[17] to the Z^o. Even though such possibilities appear *a priori* unaesthetic, there has been recently significant theoretical effort to see whether such mechanisms could be possible explanations of some of the anomalous effects seen in neutrino experiments.

Thus, for the three-flavor case, the weak eigenstates $|\nu_\alpha\rangle = \nu_e, \nu_\mu, \nu_\tau$ and the mass eigenstates $|\nu_i\rangle = \nu_1, \nu_2, \nu_3$ are related by

$$\begin{bmatrix} \nu_e \\ \nu_\mu \\ \nu_\tau \end{bmatrix} = \begin{bmatrix} \\ U \\ \ \end{bmatrix} \begin{bmatrix} \nu_1 \\ \nu_2 \\ \nu_3 \end{bmatrix},$$

i.e., $\nu_\alpha = U\nu_i$, where U is a unitary matrix that can be parameterized as (in analogy with the CKM matrix):

$$U = \begin{bmatrix} C_{12}C_{13} & S_{12}C_{13} & S_{13} \\ -S_{12}C_{23} - C_{12}S_{23}S_{13} & C_{12}C_{23} - S_{12}S_{23}S_{13} & S_{23}C_{13} \\ S_{12}S_{23} - C_{12}C_{23}S_{13} & -C_{12}S_{23} - S_{12}C_{23}S_{13} & C_{23}C_{13} \end{bmatrix}.$$

where $C_{ij} = \cos\theta_{ij}$ and $S_{ij} = \sin\theta_{ij}$, and for simplicity, we have taken the phase $\delta = 0$, i.e., assumed CP conservation.

The probability, then, that a state which is pure ν_α at $t = 0$ is transformed into another flavor β at a time t later (or distance L further) is

$$P_{\alpha\beta} = \delta_{\alpha\beta} - 4\sum_{j>i} U_{\alpha i}U_{\beta i}U_{\alpha j}U_{\beta j}\sin^2\left(\frac{\Delta m^2_{ij}L}{2E}\right)$$

with E being the energy of the neutrino and

$$\Delta m^2_{ij} = m^2(\nu_i) - m^2(\nu_j)\,.$$

Thus (assuming CP invariance) we have five independent parameters: three angles, θ_{12}, θ_{23}, and θ_{13} and two Δm^2_{ij} (the third Δm^2_{ij} must be linearly related to the first two). All of the neutrino oscillation data must then be capable of being described in terms of these five parameters.

Clearly, the above expression is complicated and the relationship of experimental results to the five basic parameters is somewhat obscure. Partly due to a desire for simplicity and partly because of the possibility (likelihood to some) that the leptonic mixing matrix U has a similar structure to the CKM matrix (i.e., is almost diagonal), it has become customary to represent the results of a single experiment in terms of oscillation between two flavors and involving only two mass eigenstates, hence only one Δm^2_{ij}. These two basis representations are then related by

$$\begin{bmatrix} \nu_\alpha \\ \nu_\beta \end{bmatrix} = \begin{bmatrix} \cos\theta & \sin\theta \\ -\sin\theta & \cos\theta \end{bmatrix} \begin{bmatrix} \nu_1 \\ \nu_2 \end{bmatrix}.$$

Clearly, such a representation will be a good approximation if the pattern of the U matrix is similar to the CKM matrix.

We can now consider a state which is a pure $|\nu_\alpha>$ at t = 0. Decomposing it into mass eigenstates, we have

$$|\nu_\alpha\rangle = \cos\theta\, |\nu_1\rangle + \sin\theta\, |\nu_2\rangle.$$

At subsequent times t, we have

$$|\nu(t)\rangle = \cos\theta e^{-iE_1 t}\, |\nu_1\rangle + \sin\theta^{-iE_2 t}\, |\nu_2\rangle.$$

Treating neutrinos as stable particles and assuming that $E^2 >> m^2$, we obtain

$$|\nu(t)\rangle = e^{-ipt}\left[\cos\theta e^{-\frac{1}{2}i\frac{m_1^2}{p}t}\, |\nu_1\rangle + \sin\theta e^{-\frac{1}{2}i\frac{m_2^2}{p}t}\, |\nu_2\rangle\right].$$

We now transform back to the flavor basis, using

$$|\nu_1\rangle = \cos\theta\, |\nu_\alpha\rangle - \sin\theta\, |\nu_\beta\rangle,$$

$$|\nu_2\rangle = \sin\theta\, |\nu_\alpha\rangle + \cos\theta\, |\nu_\beta\rangle,$$

and ignore the initial phase factor since eventually we shall be interested in the square of the coefficient of $|\nu_\beta\rangle$. We obtain

$$|\nu(t)\rangle = \left[\cos^2\theta e^{-\frac{1}{2}i\frac{m_1^2}{p}t} + \sin^2\theta e^{-\frac{1}{2}i\frac{m_2^2}{p}t}\right] |\nu_\alpha\rangle - \left[e^{-\frac{1}{2}i\frac{m_2^2}{p}t} - e^{-\frac{1}{2}i\frac{m_1^2}{p}t}\right] \sin\theta\cos\theta\, |\nu_\beta\rangle.$$

We now take the magnitude squared of the coefficient of $|\nu_\beta\rangle$ and use trigonometric identities to simplify the equation. This magnitude squared is then the probability $P(\alpha \rightarrow \beta)$, the probability of transition of a neutrino of flavor α into a neutrino of flavor β. If L is expressed in Km (m) and E in GeV (MeV) then the expression reduces to

$$P\,(\nu_\alpha \rightarrow \nu_\beta) \;=\; \sin^2 2\theta\; \sin^2(1.27\Delta m^2 \frac{L}{E})\ ,$$

where $\Delta m^2 = m_1^2 - m_2^2$ and is expressed in eV^2. This expression is obviously much simpler than the one for the three flavor case, and the results of an experiment analyzed in this formalism can be easily displayed in a two-dimensional plot since only two parameters, θ and Δm^2, are involved.

2.2 Classification of Oscillation Experiments

As can be seen from the last equation, results of any neutrino oscillation experiment can be displayed graphically on a two dimensional plot, the two axes traditionally being $\sin^2 2\theta$ (abscissa) and Δm^2 (ordinate). It is customary to use log-log representation, but sometimes $\sin^2 2\theta$ is expressed on a linear scale. An experiment claiming a positive result delineates a contour in this space (1σ, 90% C.L., etc.) within which the true answer must lie if the experiment is correct. A negative result can be represented by a curve delineating the region (again at 1σ, 90% C.L., etc.) excluded by that particular experiment.

It is clear that if one wants to probe a region of small $\sin^2 2\theta$, one needs good statistics since the effect will be small. Since the neutrino flux, and hence the event rate, falls off with source-detector distance L like

$$\phi_\nu \propto (1/L)^2,$$

we need to be relatively close to the source to have a large event rate. In addition, we need to keep the second factor large, i.e., the argument—$1.27 \cdot \Delta m^2 \cdot \frac{L}{E}$—has to be of the order of unity. Hence, we need

$$\Delta m^2 \approx E/L\,,$$

and thus for large E/L, such an experiment will be limited to probing large values of Δm^2. This basically defines a <u>short</u> <u>baseline</u> experiment, one where the source-detector distance is relatively small and where the region probed extends to small values of $\sin^2 2\theta$ but is limited to large values of Δm^2.

On the opposite end of the spectrum are the long baseline experiments which try to focus on investigation of low values of Δm^2. Again, to keep the argument of the second factor close to unity, L/E has to be large, i.e., the detector has to be far away. But that results in a flux penalty and hence the region covered in $\sin^2 2\theta$ is smaller. Clearly, it is the value of the ratio L/E that provides the factor determining the category of the experiment.

Thus, long baseline experiments are able to probe low values of Δm^2 but their reach in $\sin^2 2\theta$ is more limited. Solar neutrino studies are clearly long baseline experiments; the initial reactor and accelerator oscillation searches would be classified as short baseline experiments. We illustrate the regions covered by each kind of experiment graphically in Fig. 1.

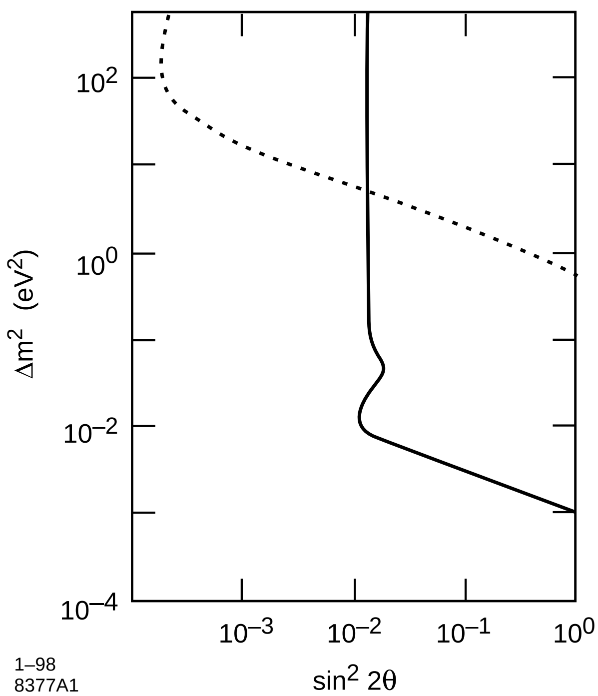

FIG. 1. A rough illustration of the regions in oscillation parameter space that might be covered by a long baseline experiment (solid line) and a short baseline experiment (dashed line).

An alternative classification of experiments is between appearance and disappearance experiments. Considering a search for the possible oscillation $\nu_\alpha \rightarrow \nu_\beta$, the latter kind of experiment would measure the ν_α interaction rate at one or more locations and compare it with the expected signal, based on the knowledge of the neutrino flux at (or near) the source. Use of two detectors, one near and one far from the source, can reduce systematic errors in this kind of an experiment. Such experiments cannot see very small signals because their observation would involve subtraction of two large numbers from each other; they also cannot tell the mode of oscillation, i.e., whether we see $\nu_\alpha \to \nu_\beta$ or $\nu_\alpha \to \nu_\gamma$, since only the ν_α interaction rate is measured. Study of solar neutrinos is clearly via disappearance experiments.

Appearance experiments try to detect the potentially created new flavor, i.e., ν_β in our case. Their sensitivity for small signals is much better and is generally limited by the knowledge of the amount of ν_β in the initial beam and the ability of the detector to distinguish clearly ν_β from ν_α. Searches for ν_τ, identified by τ production and decay in emulsion with essentially no background in a predominantly ν_μ beam are examples of appearance experiments.

2.3 Sensitivities

In this section we discuss how the reach of a given experiment depends on the experimental parameters, i.e., L, E, and N, the number of events. We distinguish between two qualitatively different situations: a background-free experiment (e.g., search for ν_τ in emulsion), and an experiment relying on a statistical subtraction, e.g., a disappearance experiment or a measurement of the NC/CC ratio. The reach can be parametrized by the lowest value of Δm^2 accessible and by the lowest value of $\sin^2 2\theta$ that can be explored.

The number of signal events, N_β, is given by

$$N_\beta = N_\alpha \sin^2 2\theta \ \sin^2(1.27 \cdot \Delta m^2 \cdot \frac{L}{E}),$$

where N_α is the expected number of events of the original flavor in the absence of oscillations at a given location L and varies as

$$N_\alpha \propto N_\alpha^o (\frac{1}{L})^2 \ ,$$

with N_α^o being the number of ν_α interactions at the source (L = 0). We may write

$$N_\alpha^o = I f(E) \quad ,$$

where I is the total proton intensity on target, and f(E) is a function describing energy dependence of the neutrino flux which is determined by the initial hadronic production spectrum, details of the focusing system, length of the decay volume, and energy dependence of the neutrino cross section (which is proportional to E in the GeV region).

To investigate sensitivity at low Δm^2 ($\Delta m^2 << 1$ eV^2), i.e., the lowest value of Δm^2 that can be detected, we can write

$$N_\beta = N_\alpha \sin^2 2\theta \cdot \left(1.27 \cdot \Delta m^2 \cdot \frac{L}{E}\right)^2 \propto N^o_\alpha \cdot \left(\frac{1.27 \cdot \Delta m^2}{E}\right)^2 ,$$

where N_β is the number of β flavor events detected necessary to establish presence of a signal. For the truly background-free case, $N_\beta = 1$ (or 2 or 3 for very small background case). Thus the sensitivity for background-free case is $\Delta m^2 \propto \sqrt{1/N^o_\alpha}$, i.e, <u>independent</u> of L.

For the statistical case, the figure of merit for determination of sensitivity is the quantity δ defined by

$$\delta = N_\beta / \sqrt{N_\alpha},$$

i.e., the number of standard deviations away from zero, namely from no effect. For low Δm^2 we have

$$\delta \propto N^o_\alpha \cdot \left(\frac{1.27 \cdot \Delta m^2}{E}\right)^2 / \sqrt{N_\alpha} = N^o_\alpha \left(\frac{1.27 \cdot \Delta m^2}{E}\right)^2 / \sqrt{N^o_\alpha \frac{1}{L}} = \sqrt{N^o_\alpha}\left(\frac{\Delta m^2}{E}\right)^2 L.$$

Thus, the sensitivity in Δm^2 in this case goes as $(N^o_\alpha)^{-1/4}\left(\frac{E}{\sqrt{L}}\right)$. (Note that in this definition of sensitivity a lower number means further reach, and that N^o_α has very likely a strong dependence on E as discussed above). The above arguments illustrate the importance of choosing as small a value of E/L as feasible for good low Δm^2 sensitivity; because of fourth root dependence on N^o_α, it is laborious and expensive to gain more sensitivity by increasing the running time (or the neutrino flux or the tonnage of the detector).

We turn now to the question of sensitivity in $\sin^2 2\theta$. Maximum sensitivity is generally taken as one that will occur at values of Δm^2 high enough so that we shall have

$$\overline{\sin^2(1.27 \cdot \Delta m^2 \cdot L / E)} = \frac{1}{2} ,$$

where the average is over the energy spectrum. Hence we have

$$N_\beta = \frac{1}{2} N_\alpha \sin^2 2\theta \propto N^o_\alpha \left(\frac{1}{L}\right)^2 \sin^2 2\theta.$$

For the background-free case the sensitivity in $\sin^2 2\theta$ will vary inversely with N^o_α (i.e., $\propto 1/N^o_\alpha$) and as L^2. For statistical analyses

$$\delta \propto N^o_\alpha \left(\frac{1}{L}\right)^2 \sin^2 2\theta / \sqrt{N^o_\alpha}\,\frac{1}{L} \;=\; \sqrt{N^o_\alpha}\,\frac{1}{L}\sin^2 2\theta .$$

The sensitivity will be proportional to $1/\sqrt{N^o_\alpha}$ and L. Thus, clearly a mistake in the proper choice of E/L is less costly in the reach for $\sin^2 2\theta$ than for Δm^2.

Knowing now the dependence of the intercepts of our sensitivity contour, it remains to ask about the shape of the contour in the intermediate region. Taking the log of our probability equation for low Δm^2 we have

$$\log N_\beta \;=\; \log N_\alpha + \log\left(\sin^2 2\theta\right) + 2\log\left(1.27 \cdot \frac{L}{E}\right) + 2\log\left(\Delta m^2\right) .$$

Thus the slope of the sensitivity curve on a log-log plot will be 1/2. The general shape of a typical sensitivity plot is shown in Fig. 2. The turnaround point corresponds roughly to

$$1.27 \cdot \Delta m^2 \cdot \frac{L}{E} \;=\; \frac{\pi}{2},$$

and the sharpness of the wiggles near that region increases for a relatively narrow beam energy spectrum and is washed out for a broad spectrum.

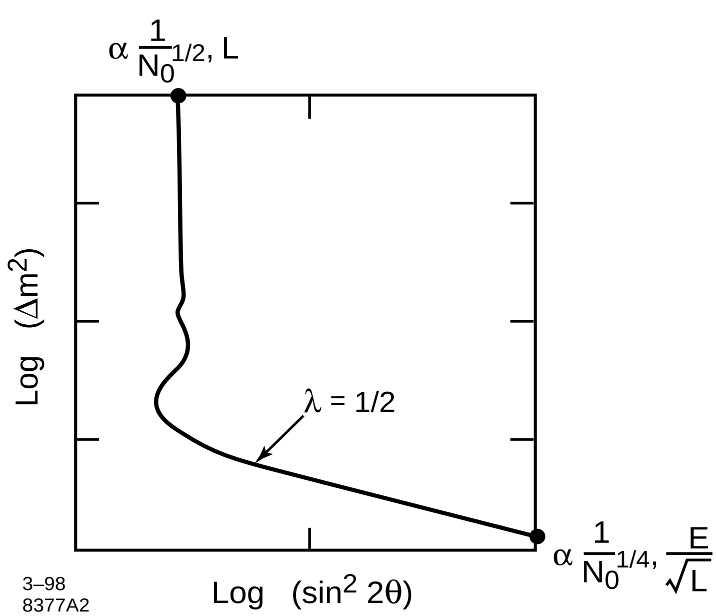

FIG. 2. A typical shape of a sensitivity plot for an oscillation experiment. We note the dependence of the limiting points on initial flux and the values of L and E. One must remember, of course, the additional, implicit dependence of N_0 on E as discussed in the text.

3 Neutrino Beams

3.1 General Considerations

In discussing neutrino beams and neutrino experiments one has to keep in mind two basic facts:

(a) Neutrino cross sections are very low.

(b) Neutrino beams, being tertiary in nature and not capable of being focused, tend to be large in transverse dimensions.

These two facts strongly influence the design of the neutrino experiments. We elaborate further on these points below.

The neutrino charged current cross section on a single nucleon at high energies is very roughly[18]

$$\sigma_{\nu}^{CC} \approx 0.7 \times 10^{-38} E_{\nu}\,(\mathrm{GeV})\ \mathrm{cm}^2$$

and the neutral current cross section

$$\sigma_{\nu}^{NC} \approx 0.3 \times 10^{-38} E_{\nu}\,(\mathrm{GeV})\ \mathrm{cm}^2 \quad .$$

The antineutrino cross sections are smaller by roughly a factor of 2.5.

The purely leptonic processes, e.g., $\nu_e e^- \to \nu_e e^-$, have even smaller cross sections. The $\nu_e e^-$ cross section[19] is

$$\sigma^{\nu e} \approx 0.933 \times 10^{-43}\,(E_{\nu}/10\mathrm{Mev})\ \mathrm{cm}^2$$

and the corresponding cross sections of $\bar{\nu}_e$, ν_μ, and $\bar{\nu}_\mu$, are about a factor of 2.4–7.1 smaller. These values have to be contrasted with a typical hadronic cross section of about 10^{-26}–10^{-25} cm^2.

As far as the beam transverse size is concerned, a typical neutrino beam in the GeV energy range will be of the order of 1 m^2 or larger. In contrast, hadron beams can be focused to spot sizes of the order of 1 mm^2 or even smaller.

Putting all of these numbers together, we see that per atom the neutrino interaction probability of a neutrino in a neutrino beam is about 18 orders of magnitude smaller than for a hadron in a hadron beam. This great disparity means that large beam intensities and massive detectors form a necessary requirement for neutrino experiments.

3.2 Beams From Accelerators

Accelerator-produced neutrino beams have played a key role in the neutrino experimental program to date. The obvious neutrino sources can be divided into three general categories, depending on the typical decay length scale of the parent particles. Examples of these three categories are enumerated in Table 1 below where the typical decay length quoted corresponds to parent energies in the multi-GeV range.

TABLE 1.
Potential sources of neutrinos from an accelerator.

Long lived sources: $\lambda \approx 1$ km	BR ≈ 50-100%
$\pi^+ \to \mu^+ \nu_\mu$	
$K^+ \to \mu^+ \nu_\mu, \quad \pi^\circ \mu^+ \nu_\mu, \quad \pi^\circ e^+ \nu_e$	
$K_L^0 \to \pi^- \mu^+ \nu_\mu, \quad \pi^- e^+ \nu_e, \quad \pi^+ \mu^- \bar{\nu}_\mu, \quad \pi^+ e^- \bar{\nu}_e$	
$\mu^+ \to e^+ \bar{\nu}_\mu \nu_e$	
Medium lived sources: $\lambda \approx 1$ m	BR ≈ 0.1%
$\Lambda \to p e^- \bar{\nu}_e$	
$K_S^0 \to \pi^- \mu^+ \nu_\mu, \quad \pi^- e^+ \nu_e, \quad \pi^+ \mu^- \bar{\nu}_\mu, \quad \pi^+ e^- \bar{\nu}_e$	
$\Sigma^- \to n e^- \bar{\nu}_e$	
Short lived sources: $\lambda \approx 1$ mm - 1cm	BR ≈ 2-20%
$D^+ \to K^0 \mu^+ \nu_\mu, \quad K^0 e^+ \nu_e$	
$D_s^+ \to \tau^+ \nu_\tau$	
$\tau^+ \to \mu^+ \nu_\mu \bar{\nu}_\tau, \quad e^+ \nu_e \bar{\nu}_\tau$	
$B^o \to D^- \mu^+ \nu_\mu, \quad D^- e^+ \nu_e$	

It is the first category of sources that gives us the classical neutrino beams. The parent particles are relatively long lived for a variety of reasons: no lower-mass hadronic state for π, $\Delta I = 1/2$ rule for K^+, CP conservation to a high accuracy for K_L^0, and a purely leptonic process for μ^+. The last category of processes is interesting as a potential source of beam-dump neutrinos, where one wants to suppress contributions from the long lived sources.

3.2.1 Neutrinos from Hadron Beams

Even though the neutrino beams produced from hadron beams are quite diverse in their nature and the relevant beam design, the basic principle in all the cases is the same. The "generic" hadron-produced neutrino beam is shown in Fig. 3. Accelerator primary beam (generally protons) strikes a target where different hadrons are produced. Some initial focusing and momentum and/or sign selection may be done immediately downstream and hadrons are allowed subsequently to drift for some distance L. A fraction of them will decay in that space and create neutrinos collimated in a cone around the hadronic propagation direction. The drift space is terminated by a beam stop to eliminate residual hadrons; it is then followed by a shield (earth and/or iron) to absorb and stop resulting hadronic debris but also, more importantly, to range out the muons created together with the neutrinos in the hadron decays. After some distance l, generally chosen by the criterion that it has to be sufficiently long to range out even the most energetic μ's, a detector is placed where neutrino interactions are observed.

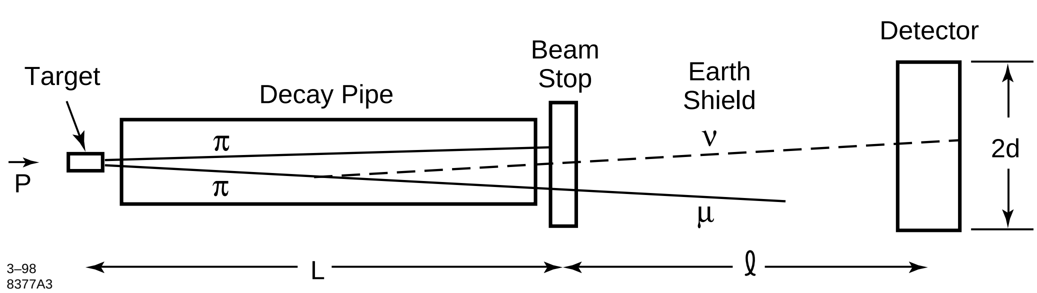

FIG. 3. Schematic of a typical accelerator neutrino beam.

To discuss the optimization of neutrino beams, we need to review first some basic kinematics. We recall that

$$E_\nu^{lab} = \gamma\,(\beta P_\nu^{*} \cos\theta_\nu^{*} + E_\nu^{*}),$$

where the starred quantities refer to π or K rest frame. Because $m_\pi \sim m_\mu$, but $m_K >> m_\mu$ we have

$$E_\nu^{lab,\ \ max} \approx 0.41\ \ P_\pi^{lab}\ \ \text{(for } \pi \text{ decay)},$$

$$E_\nu^{lab,\ \ max} \approx P_K^{lab}\ \ \text{(for } K \to \mu\nu \text{ decay)}.$$

The median laboratory angle, corresponding to $\theta_\nu^{*} = \pi/2$ will be given by $\theta^{med} = 1/\gamma$.

We can now ask what should be the values of L, l, and 2d (transverse size of the detector) required so that the detector can intercept a significant fraction of potentially produced ν's. Such a condition might be defined as one corresponding to L of the order of hadronic lifetime ($\approx \gamma c \tau_{had}$) and the detector size sufficient to intercept more than half of the neutrino flux. The requirement that even the most energetic μ's are absorbed means that for the earth shield

$$l\ (km) \approx 2P_{had}\ (GeV),$$

since μ's lose roughly 0.5 GeV/m of earth shield. We have then $L \approx \gamma c \tau$ and $d \propto (L + l)\,\theta^{med} = \frac{1}{\gamma}(L + l)$. We see that for such a design d is independent of the primary hadron energy, since both L and l scale as this energy.

For 50 GeV π's, we would have

$$\gamma \approx 350,$$

$$L \approx 2.7 \text{ km},$$

$$l \approx 100 \text{ m, and}$$

$$d \approx 8 \text{ m}.$$

Clearly, such a detector is uncomfortably large and drift space uncomfortably long. Obviously, the above parameters need to be scaled down and we need to consider how to optimize the overall design.

To zeroth order, the number of observed ν interactions near 0° scales as d^2z, z being the depth of the detector. The cost, also to zeroth order (i.e., ignoring initial fixed costs and economies of scale), scales similarly as d^2z. To go beyond zeroth order analysis, we must consider factors which break this degeneracy, i.e.,

(a) ν spectrum is not flat but falls off as we go away from 0° (towards larger d).

(b) E_ν variation with θ near 0° is

$$E_\nu = \frac{E_\nu^{max}}{1 + (\gamma\theta)^2} \quad .$$

Thus E_ν, and hence σ_ν, falls off as θ increases.

Both of these factors argue for largest possible z (i.e., small d). However, we have to consider the need to define a fiducial volume; this requirement establishes some minimum transverse dimension of the detector, d. Thus the dimensions of the detector need to be optimized in light of these three conditions and the precise cost dependence.

To optimize L for maximum flux, we need to find an optimum compromise between the decreasing hadron flux as one goes away from the target production due to exponential decay of the hadrons and an increasing acceptance as the decays occur closer to the detector, and hence further away from the production target. We generally try to make l as small as possible, consistent with adequate shielding. The conditions chosen in the past for a typical experiment were

$$l < L < 2l$$

and d of the order of 1–2 m. We emphasize that such values are appropriate for optimization which tries to maximize the number of detected neutrino events.

We can turn now to the discussion of specific hadron-beam originated neutrino beams. The simplest such beam is a “bare target” beam which was used in the first neutrino accelerator experiment.[4] No focusing of the hadrons is attempted in this situation and hence, the neutrino yield at the detector is rather low. Since that first experiment, many different schemes have been developed to obtain enhanced neutrino yields or beams with specific neutrino properties.

Clearly, the neutrinos themselves cannot be focused. Thus, we always have to live with the neutrino divergence due to the intrinsic P_T in the decay: 30 MeV/c for $\pi \to \mu\nu$ decay, 236 MeV/c for $K^+ \to \mu^+\nu$ decay. However, in a bare target beam, there is also the additional divergence of the hadronic beam, characterized by a typical P_T in the production process of about 300 MeV/c. This component could be eliminated or drastically reduced by the appropriate focusing. In an ideal case, never achieved in practice, the hadrons would form a perfectly parallel pencil beam in the drift space.

One of the earliest schemes[20] used to obtain hadron focusing (still in use today) relies on pulsing a current through an appropriate conducting surface, shaped so as to generate a focusing magnetic field. Several such elements, referred to as “horns,” can be combined to obtain focusing over a broad momentum range. One such geometry, proposed for the MINOS experiment to be discussed later, is illustrated in Fig. 4. The current flows on the inside surface and returns on the outside surface. From Ampere’s law we have

$$\text{inside the cone: } B = 0,$$
$$\text{in the horn: } B \propto 1/r\text{, and}$$
$$\text{outside horn: } B = 0.$$

For the parallel track, the path length inside the horn (in the finite B region) is proportional to r. Thus, the total transverse momentum kick given to each particle will be

$$P_T \propto \int B \cdot dl \propto \frac{1}{r} \cdot r = \text{constant (independent of r).}$$

Thus, the horn will be focusing particles of one sign and defocusing the particles of the opposite sign, provided that they go through the horn. Trajectories inside or outside the horn will be unaffected. Focusing will be perfect for particles of a given P_T.

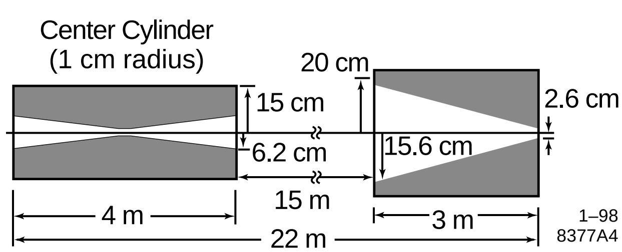

FIG. 4. Current design of the focusing horn system to be used in the NuMI beam for the COSMOS and MINOS experiments.

In practice, to focus a spectrum of particles with various values of P and P_T, more complicated systems are designed. One can vary in such a design a number of parameters, i.e.:

number of horns used,

separation between individual horns,

dimensions and shape of the horns, and

field strength (i.e., current).

A properly designed horn system can enhance neutrino flux significantly: gains of more than a factor of ten are possible. This is illustrated in Fig. 5 where we show neutrino yields for a double horn system and an unfocused system for a potential ν beam at Brookhaven National Laboratory.[21] Typical horn designs today can achieve, in the selected momentum range, neutrino collection efficiencies of the order of 50% of what one could obtain with a perfectly focused beam, i.e., one that is exactly parallel. This is illustrated in Fig. 6 where the MINOS horn design[22] is used to demonstrate this ratio as a function of momentum. The focusing efficiency as a function of neutrino energy can be changed by varying the horn parameters.

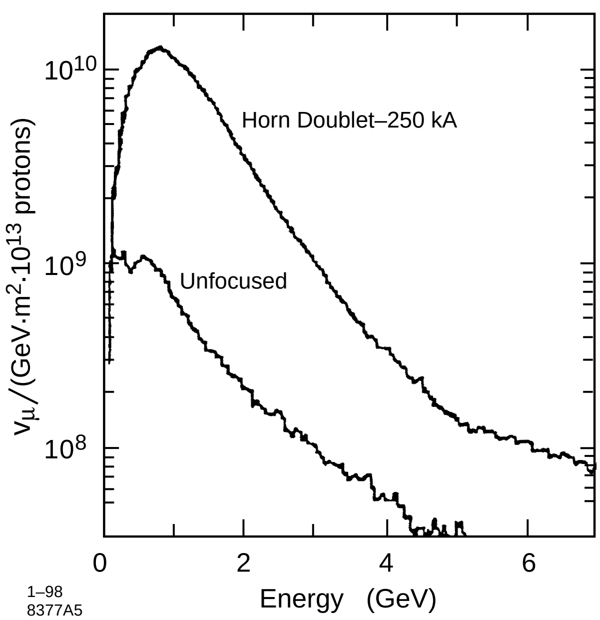

FIG. 5. Relative fluxes for an unfocused and double-horn focused beams for a BNL neutrino beam design.

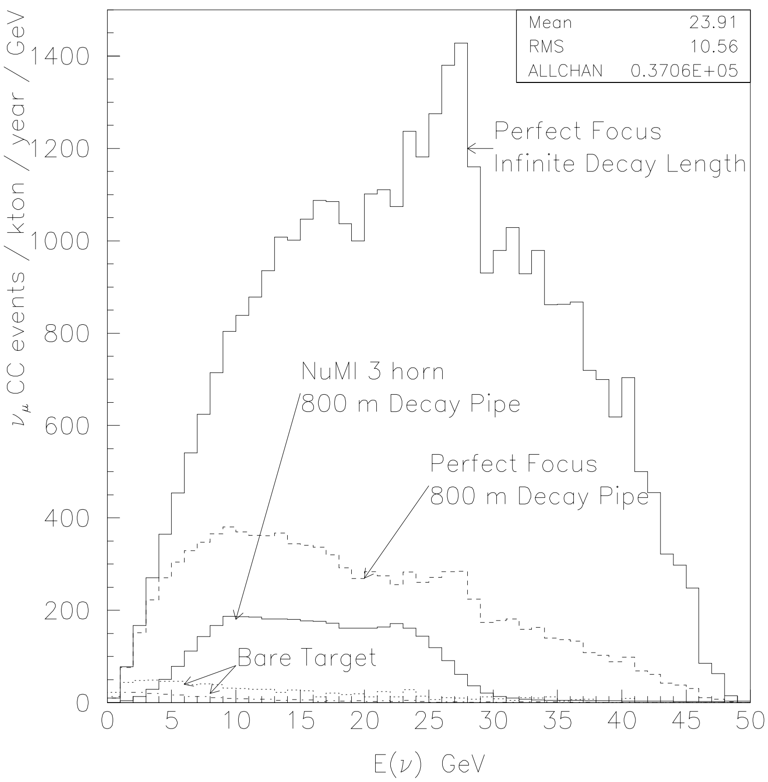

FIG. 6. Focusing efficiency as a function of neutrino energy for the NuMI horn design compared to fluxes obtained in ideal conditions and fluxes from a bare target.

Other focusing arrangements are also possible and a number of them have been used in actual experiments. The most important ones are:

(a) Quadrupole focused beam—both signs of hadrons are focused and the magnet settings are chosen to pick out a desired broad momentum range. The neutrino momentum spectrum for such a beam for the CCFR experiment at Fermilab[23] is shown in Fig. 7.

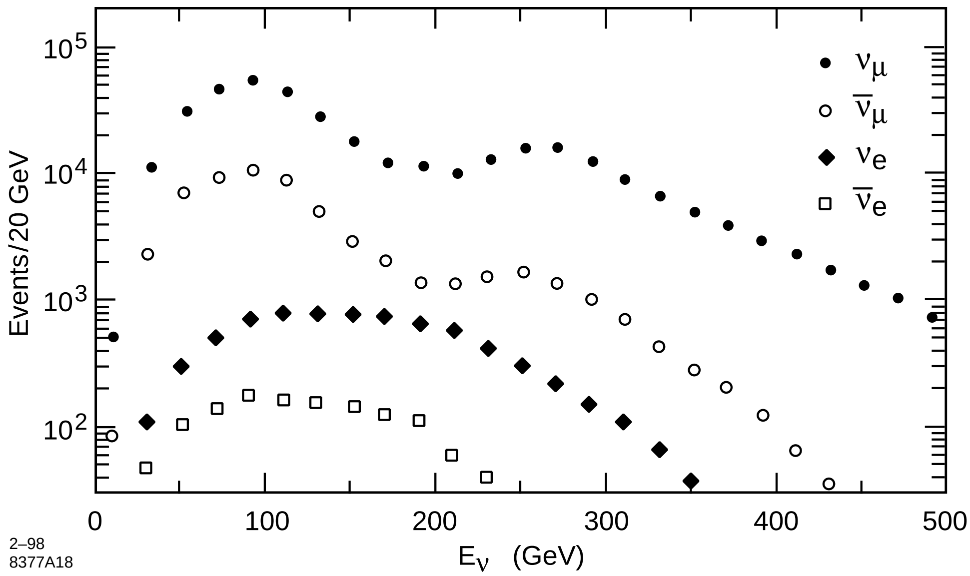

FIG. 7. Neutrino event rates from the four different neutrino flavors in the CCFR detector exposed to the Fermilab quadrupole focused beam. The ν_e (and $\bar{\nu}_e$) rates have been calculated by Monte Carlo with the normalization for the measured rates of the ν_μ and $\bar{\nu}_\mu$ flavors.

(b) Sign-selected quadrupole focused beam—this is a variant on the previous possibility with an addition of an upstream dipole magnet to select only one sign of hadrons, and hence only neutrinos or antineutrinos at the detector. The recently completed E815 experiment at Fermilab used this configuration.

(c) Dichromatic beam—such a beam uses dipoles and quadrupoles to define a relatively narrow accepted momentum band of the hadrons. The neutrino energies from π and K two-body decays are given by

$$E_\nu^\pi = \frac{m_\pi^2 - m_\mu^2}{2\,(E_\pi - P_\pi \cos\theta)}, \qquad E_\nu^K = \frac{m_K^2 - m_\mu^2}{2\,(E_K - P_K \cos\theta)} ,$$

$\cos\theta$ being the laboratory angle of the neutrino with respect to the beam axis. Because $m_K \approx 3.5\, m_\pi$, the neutrinos emitted at 0°, which come from K decays, will have a significantly higher energy than those from π decays. Furthermore, if the detector subtends an angle that is small compared to the total neutrino emission cone, the two spectra will be relatively monochromatic, hence the name dichromatic beam. This is illustrated in Fig. 8 where we show the neutrino energy spectra for the first dichromatic beam constructed at Fermilab.[24]

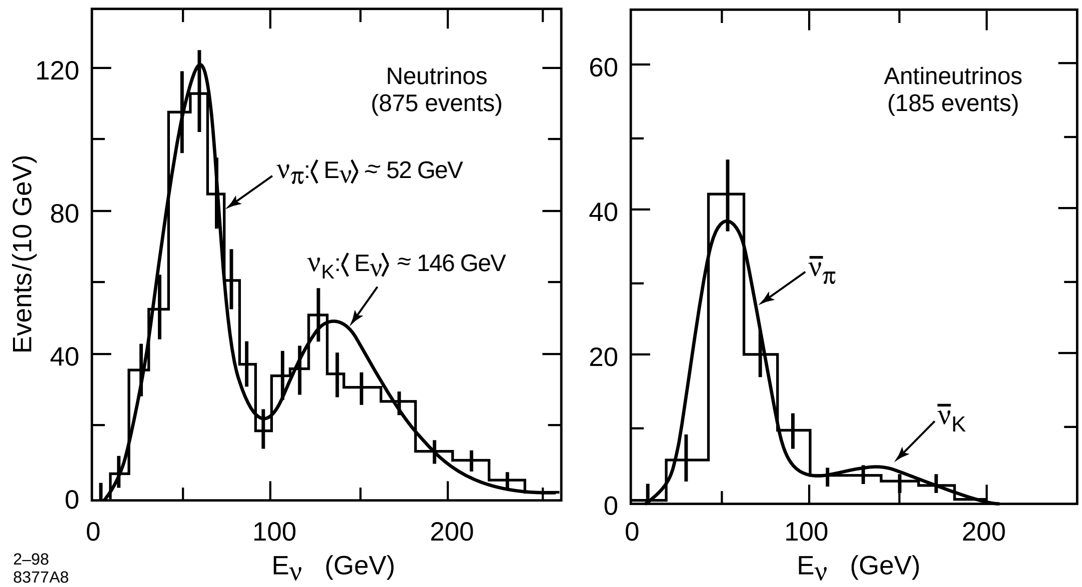

FIG. 8. ν_μ and $\bar{\nu}_\mu$ spectra (expressed in terms of observed events) for the first dichromatic beam constructed at Fermilab.

Generally, the detector subtends a significant fraction of the neutrino emission cone. In such a situation, a large part of the neutrino spectrum will be sampled, with a direct correlation between the emission angle (i.e., roughly the distance of the interaction from the beam axis in the detector) and the neutrino energy, as can be seen from the equations above. Clearly, this correlation is different for ν's with π parentage from these originating from K decays.

In principle, at least, such a correlation can be exploited to get a “good fix” on the neutrino energy. Such a situation was true in the CDHS experiment at CERN,[25] but to my knowledge this energy-angle correlation was never exploited in any physics analysis.

In addition to the focusing systems described above, other variants of neutrino beams have been proposed but never executed to my knowledge. The two important ones are:

(a) Tagged ν beams. The idea here is that by detecting the charged decay product(s) from hadron decay in coincidence with the ν event, one can obtain information about the energy and/or flavor of the neutrino causing the interaction. To date, no tagged ν beams have been implemented, even though a number of different possibilities have been discussed. The main problem in executing such a scheme is the high counting rate in the potential detector exposed to the charged decay products. Some of the possibilities that have been discussed are:

(i) Measure momentum and angle of the μ^+ in $K^+ \rightarrow \mu^+\nu$ decay. Thus, one can obtain the energy of the neutrino.

(ii) Detect μ or e in the $K_L^0 \rightarrow \pi e(\mu)\nu$. This will allow one to determine the neutrino flavor.

(iii) Detect the e^+ in $K^+ \rightarrow \pi^0 e^+ \nu$. This would allow one to veto such decays and thus obtain a purer sample of ν_μ's. The $K^+ \rightarrow \pi^0 e^+ \nu$ decay is one of the main factors limiting the sensitivity of $\nu_\mu \rightarrow \nu_e$ oscillation searches because of the ν_e contamination from this decay occurring at about a 0.5% level.[26]

(b) Off-axis beam. This idea basically allows you to obtain a relatively monochromatic low energy beam at the expense of flux.[27] The basic principle of such a beam is illustrated in Fig. 9. As can be seen, at non-zero angles, a large energy band of π's generates a rather monochromatic neutrino beam.

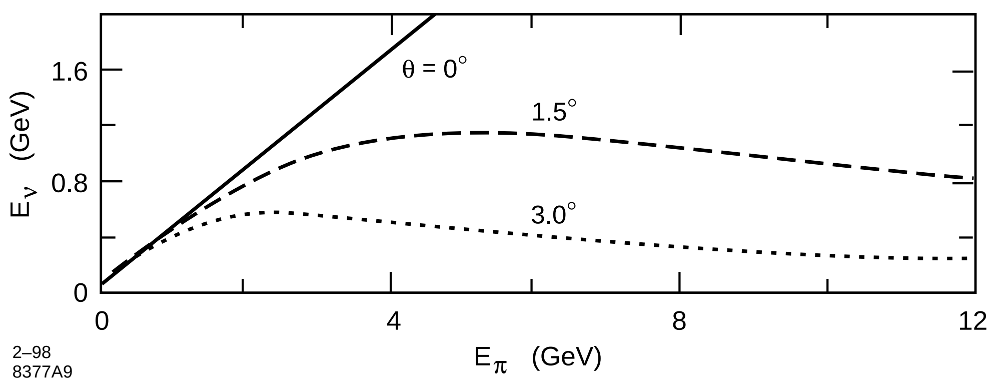

FIG. 9: Neutrino energy as a function of the parent π energy and of the laboratory decay angle.

3.2.2 Neutrinos from Beam Dumps

This method of producing neutrino "beams" differs from the one discussed above in so far that no secondary hadron beam is ever produced. We define the beam dump as a source of ν's as that experimental configuration in which the target for the primary (e.g., most likely proton) beam, in which the ν parent hadrons are produced, is at the same time also the medium for absorbing and/or stopping these hadrons. Thus, no drift space is provided for the hadrons to decay in.

The beam-dump neutrino experiments naturally divide themselves into two categories: high energy and low energy ones. We discuss each one in turn.

(a) The general motivation for high energy beam-dump experiments is to eliminate or drastically reduce the contributions of ν's from long lived and medium lived sources, described as categories 1 and 2 in Table 1. In this configuration, one could look for neutrinos from the third category of sources. i.e., decays of short lived particles, or for some new and unanticipated phenomenon.

Historically, the first beam dump experiment of this type was proposed and executed in the late '60's by Mel Schwartz and his collaborators at SLAC,[28] using the 20 GeV SLAC electron beam and optical spark chambers downstream. This was before the first observation of neutral currents and before the discovery of charm, beauty, and τ. Because of financial considerations, the design of the experiment had to be somewhat compromised and the detector moved further away from the beam dump than initially desired. The decrease in sensitivity due to this compromise contributed to a null result.

One of the first observations of charm production in hadronic interactions came from a CERN beam-dump experimental program[29] which used several detectors downstream to detect neutrinos, produced by the decays of charm particles, which in turn were produced by interactions of the primary proton beam in the dump.

The present interest in high energy beam-dump experiments is driven by the desire to observe ν_τ, a neutrino flavor known to exist from indirect evidence but never to date observed experimentally. The experiment E872 at Fermilab,[30] currently in progress, has been designed to look for ν_τ's from the production and decay of D_s mesons, the decay chain of interest being

$$D_s \rightarrow \tau + \nu_\tau \text{ and/or } \tau \rightarrow X + \nu_\tau$$

where X is some hadronic or leptonic system. The experimental challenge in the beam design is to minimize the beam-dump to detector distance and thus maximize the ν_τ event rate and at the same time keep the backgrounds in the detector from the dump down to a manageable level. The beam used for the E872 experiment is illustrated in Fig. 10. With this design, about 4% of all ν's in the detector should be ν_τ's.

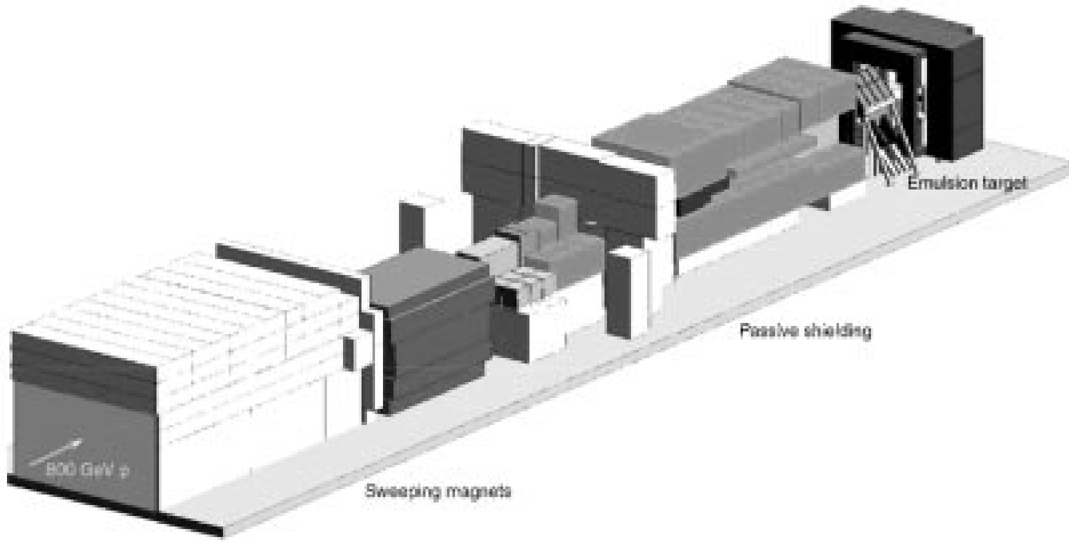

FIG. 10. E872 beam-dump beam.

(b) The low energy beam-dump experiments are designed to look at interactions of neutrinos from decays of μ^+ and π^+ stopped in the dump. This way, one can obtain a well-understood, in terms of energy and flavor, neutrino flux radiating isotropically out from a relatively small volume. If the proton beam is extracted in short bunches, one can use the time of arrival of neutrinos to determine their flavor and energy. This point is elaborated in Fig. 11. Figure 11(a) shows the neutrino energy spectra resulting from π^+ and μ^+ decay at rest. Because the lifetime of π^+ is significantly shorter than that of μ^+, the monochromatic ν_μ's from π^+ decay occur shortly after the proton beam pulse (within tens of nanoseconds); the ν_e and $\bar{\nu}_\mu$'s from μ^+ decay are spread out over a much longer period of time, i.e., of the order of microseconds due to the 2.2 μsec μ^+ lifetime. The time structure of the ν's from the ISIS spallation source at the Rutherford Appleton Laboratory[31] accelerator is illustrated in Fig. 11(b) and 11(c). In that machine, protons are extracted at a 50 Hz rate with each major pulse consisting of two short pulses about 300 nsec apart.

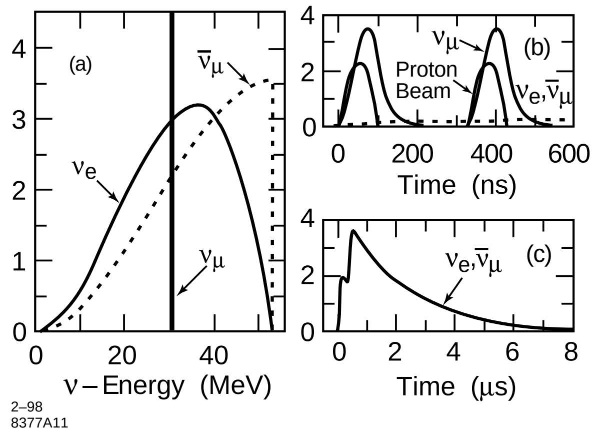

FIG. 11. The principle of a low energy beam-dump experiment. The neutrino spectra from π at rest (ν_μ) and μ at rest (ν_e and $\bar{\nu}_\mu$) are shown in (a). The time structure of the different flavor neutrinos is shown in (b) and (c) for the ISIS machine.

3.2.3 Other Accelerator-Produced Beams

There are other potential ways to use accelerators to produce neutrino fluxes for experiments. The two that have been discussed the most extensively are ν's from interaction regions and ν's from storage rings. The first method relies on the fact that high energy pp colliders, like the LHC, will produce charm and beauty particles copiously. They will generally tend to be produced in a forward direction and will decay promptly. The neutrinos from these decays will also be collimated forward reasonably well. Because π's and K's will tend to be absorbed in the calorimeters forming part of the detector, the neutrino "beam" will be dominated by products of charm decays and will have roughly equal components of ν_μ, $\bar{\nu}_\mu$, ν_e, and $\bar{\nu}_e$. In addition, one expects about 10% of the ν flux to be ν_τ's, mainly from D_s decays but with some contribution from B decays. Detailed calculations of potential ν fluxes at the LHC have been made, first by De Rújula[32] and more recently by Fernández.[33]

Another potentially interesting source of neutrinos is a storage ring for unstable particles, e.g., π's, K's or μ's. If a significant fraction of the storage ring circumference is a straight section, the decays in that section will produce a well-collimated ν beam. Interest in such a possible ν source has been recently revived[34] in connection with the studies of a possible $\mu^+\mu^-$ collider in the TeV range. The μ intensity required to obtain sufficiently high collision luminosity (typical numbers discussed are few x 10^{12} μ's/bunch at 15 Hz) is so high that the ν fluxes from such a source would be more copious than any hitherto available. Neutrino interaction rates in a typical ν detector might be of the order of few KHz.

3.3 Neutrinos from Reactors

Nuclear fission, which is the energy mechanism in a reactor, yields neutron-rich nuclear fragments as by-products. These will be unstable and decay by the fundamental process

$$n \text{ (in nucleus)} \rightarrow p\, e^- \, \bar{\nu}_e \, .$$

The ν flux is related directly to thermal power and is roughly $2 \times 10^{20} \bar{\nu}_e$/GW/sec. Clearly the neutrinos are emitted isotropically.

The ν spectra obtained from reactors are now quite well understood at the level of about 2—3%. The calculations have been verified experimentally.[35] At the low end of the spectrum there is an additional correction that needs to be made to allow for decays of the activated material in and near the core. A typical positron spectrum from reactor neutrino interactions is shown in Fig. 12. The neutrino energy is 1.804 MeV higher than the positron energy.

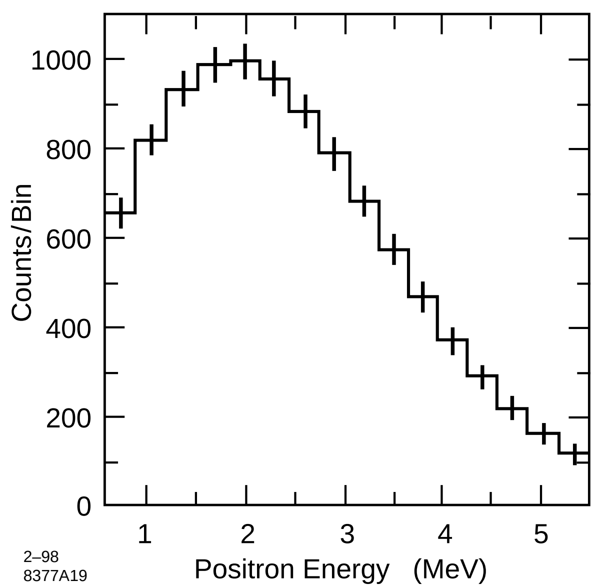

FIG. 12. Positron spectrum expected from neutrino interactions in the CHOOZ experiment (assuming no oscillations).

In addition, reactors have been used to create man-made neutrino sources by activating materials. This technique has been used to create sources whose decay neutrinos were subsequently used to calibrate solar neutrino detectors, e.g., GALLEX and SAGE.[36] In this scheme ^{50}Cr is irradiated with neutrons from a reactor to give ^{51}Cr which is unstable and gives ν's in the energy range comparable to the one characterizing the solar neutrino spectrum. Sources of 100 BCq have been obtained via this method. Figure 13 shows data from one of the GALLEX calibration runs using such a source. As required for such a calibration, neutrino flux from the source is significantly higher than the solar flux.

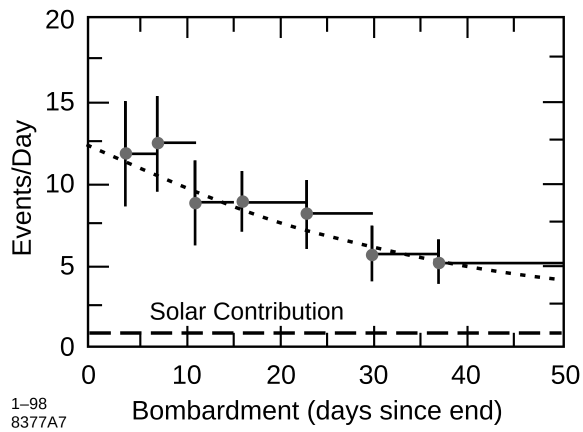

FIG. 13. The observed counting rate from the GALLEX experiment during the chromium source calibration runs. The points for each run are plotted at the beginning of each exposure; horizontal lines show duration of the exposure. The dotted line shows the predicted behavior, calculated from the directly measured source strength and the known half-life of ^{51}Cr.

3.4 Neutrinos from Natural Sources

For completeness I shall close this chapter by saying a few words about neutrinos from naturally occurring sources.

(a) Neutrinos from the sun. The sun is essentially a fusion reactor, effectively transforming four protons into a He^4 nucleus through a fusion process that reduces to

$$4p \rightarrow He^4 + 2e^+ + 2\nu_e.$$

Thus, the number of neutrinos emitted can be readily obtained from the total thermal power of the sun which is in turn directly related to the measurable quantity, i.e., the solar constant, 1.3 kW/m^2 on the surface of the earth. The spectrum of the neutrinos emitted will depend on the details of the energy producing solar cycle. Precise knowledge of this spectrum is important in the interpretation of the experimental data on solar neutrino interactions on earth. The spectrum prescribed by the current Standard Solar Model[37] is shown in Fig. 14.

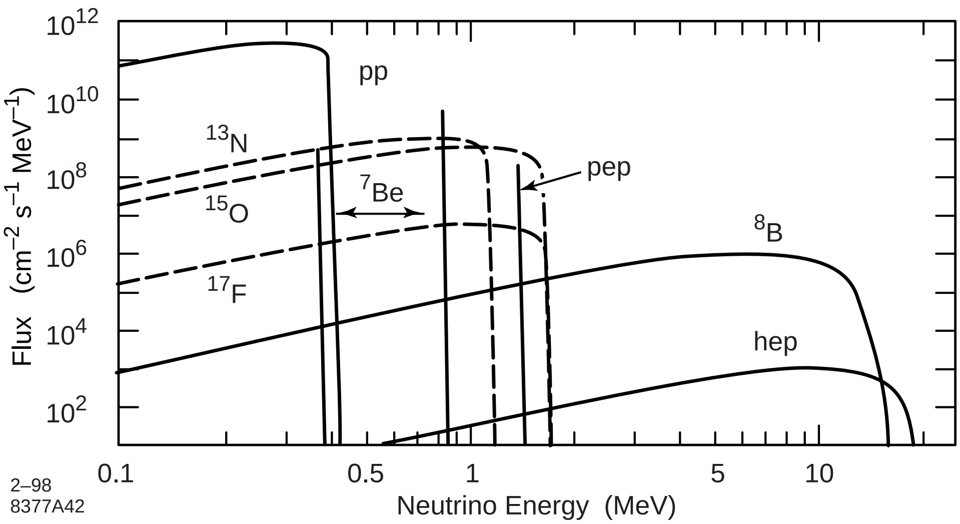

FIG. 14. Energy spectra of solar neutrinos. The pp chain is indicated by the solid curves; the less important CNO cycle by dashed curves.

It is amusing to compare the two power sources that both generate neutrinos, i.e., the sun and reactors. Such a comparison of the relevant quantities is made in Table 2.

TABLE 2.

Comparison of sun and reactor as ν sources.

Feature	Sun	Reactor
Process	Fusion	Fission
yield	1.8×10^{38} ν/sec	2×10^{20}ν/GW/sec
ν Flavor	ν_e	$\bar{\nu}_e$
Energy Spectrum	Peaks sharply below 1 MeV Extends up to 15 MeV	Few MeV
Understanding of spectrum	Some controversy	Very good
Possibility to vary L	Very little (yearly variation)	Yes
On/off capability	No	Yes

(b) Atmospheric neutrinos. The energetic hadronic particles constantly bombarding our atmosphere will generally interact in the first 10% or so of the atmosphere by weight, i.e., at about 10-20 km above the earth's surface. The density of air at that altitude is such that most of the π's and K's in the GeV range and below which are produced there will decay before interacting and most of the resulting daughter μ's will also decay. These decays (as well as the decays of subsequent generations of hadrons) are the source of the so called atmospheric neutrinos. The spectrum of these neutrinos peaks at low energies (few hundreds MeV's) and falls off as we go to the multi-GeV range. Because the relevant ν production processes are

$$\pi^+ \to \mu^+ \nu_\mu,$$
$$\mu^+ \to e^+ \nu_e \bar{\nu}_\mu,$$

the ratio of muon to electron neutrinos at low energies, where most of the μ's decay, should be about two. This ratio will increase as we go to higher energies.[38] The particles produced at different zenith angles will see different variations in atmospheric density as a function of their path. This, plus the effect of the earth's magnetic field, generates a different zenith dependence of the ν_μ and ν_e fluxes which is energy dependent.

(c) Neutrinos from supernovae. Neutrinos are generated in a supernova explosion[39]both from the inverse beta decay process, i.e.,

$$p + e^- \to n + \nu_e$$

and also through e^+e^- annihilation, i.e.,

$$e^+ + e^- \to \nu + \bar{\nu}.$$

The latter process can give neutrinos of all three flavors. Supernova neutrinos have energy in the range of MeV to tens of MeV. Their theoretically expected features have been roughly verified experimentally in the observation of ν's from the supernova SN1987A.[40]

(d) Neutrinos from extragalactic sources. Neutrinos can potentially be produced copiously in various “exotic” stellar phenomena and they might have very high energies.[41] Such possibilities imply that neutrinos might open up a new window for study of the universe since they can travel a long way and are not affected by electromagnetic fields. Observation of these neutrinos is one of the motivations for construction of large, high energy neutrino-detecting arrays like AMANDA,[42] NESTOR,[43] etc.

(e) Neutrinos from natural radioactivity. Our universe contains a number of naturally occurring neutrino emitters. Studies of such radioactive nuclei played an important role in the development of the V-A theory of weak interactions even though such neutrinos themselves have never been detected (to my knowledge). The neutrinos from the naturally occurring radioactivity in the earth's core might actually be a relevant background for some of the new ambitious reactor neutrino experiments[44] being planned currently.

In Fig. 15, we try to compile and summarize in one place in a more quantitative way the information discussed in this chapter. The figure is meant to give only a rough indication of the ν energies and fluxes from the most important sources.

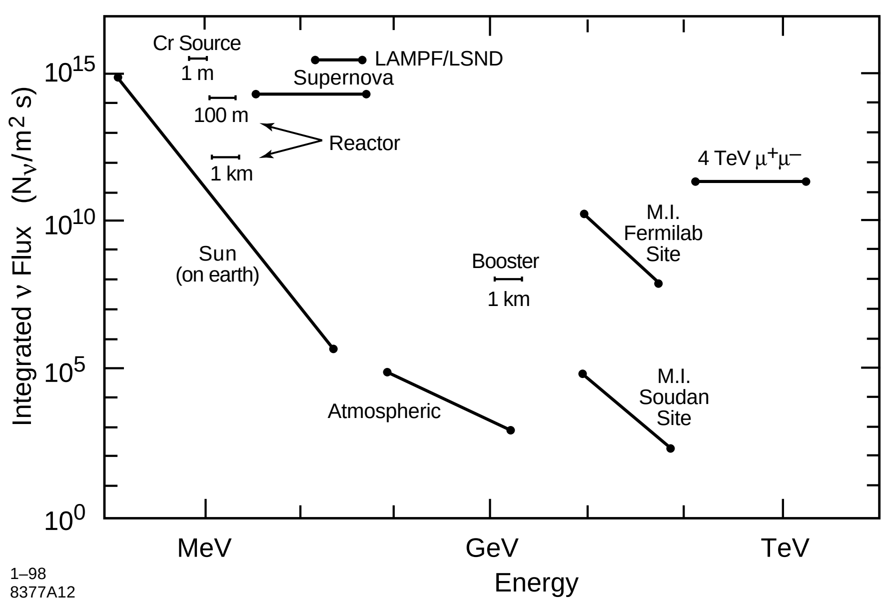

FIG. 15. A rough estimate of the neutrino fluxes from different possible sources. Booster and M.I. refer to the Booster and Main Injector rings at Fermilab; LAMPF/LSND to an accelerator/detector at Los Alamos.

4 Neutrino Detectors

Because of the low neutrino interaction probability (discussed above), neutrino detectors are seldom all-purpose detectors, like for example, an e^+e^- collider detector. Rather, depending on the physics goals of the experiment, the neutrino detector is designed to provide an optimum match to these goals.

In retrospect, looking at the past neutrino experiments, a natural classification emerges. The detectors for “standard” accelerator or reactor neutrino experiments can be divided into three general categories, depending on which specific feature they emphasize. These three categories are: calorimeters, tracking detectors, and Cherenkov detectors. This classification is somewhat arbitrary since experiments frequently use experimental apparatus that combines more than one of these features. Nevertheless, usually one specific aspect is emphasized.

In addition, there is a fourth category of neutrino detectors, quite distinct from the three groups mentioned above, i.e., radiochemical detectors, so far used only in the solar neutrino experiments. We proceed now to discuss each one of these groups in turn, describing their strong and weak points and giving some specific examples.

4.1 Calorimetric Detectors

These detectors emphasize measurement of the total energy of the final state products. They naturally divide themselves into sampling calorimeters and total absorption calorimeters. The other relevant distinction useful for sampling calorimeters is between high Z, magnetized calorimeters and (generally) low Z, nonmagnetic ones.

Total absorption calorimeters rely almost entirely on active medium as both the target for the neutrino interaction and as the detecting medium. Thus, the energy loss of final state particles can be measured without introducing uncertainties due to sampling fluctuations.

In contrast, the sampling calorimeters generally have a passive medium (iron or aluminum) interspersed with an active detector, e.g., scintillator or gas chambers. The advantage of this scheme is that a larger target mass can be obtained for the same cost with some compromise on the accuracy of the energy measurement due to potential sampling fluctuations. In general, sampling calorimeters are more appropriate for high energy experiments; total absorption calorimeters for low energy experiments, e.g.,

5 $\nu_\mu \rightarrow \nu_\tau$ Oscillation Experiments (Past and Ongoing)

The atmospheric neutrino anomaly presents a hint of possible existence of $\nu_\mu \rightarrow \nu_\tau$ oscillations with a relatively low value of Δm^2 ($\Delta m^2 << 1eV^2$). The accelerator experiments to date have not, as yet, been able to address this potentially interesting region. Rather, the focus so far has been on investigating the high Δm^2 region ($\Delta m^2 >> 1eV^2$), recently extending the reach to low values of $\sin^2 2\theta$. This chapter summarizes the current situation in this area and the prospects for the currently running experiments.

5.1 Disappearance Experiments

Three different experiments of this kind have been performed to date utilizing the CDHS, CHARM, and CCFR detectors (or their modifications). They all have very similar features, i.e.,

(a) Two detectors at different locations, the first one at 100, 100 and 400 m respectively, for the three experiments, and the second one at about 1 km away from the neutrino source.

(b) The basic measurement is a comparison of rates at the two locations.

(c) All three experiments find null results and thus can only set limits.

Because the experiments are disappearance experiments, i.e., they cannot identify the flavor of the final-state neutrino. However, because they probe the region of Δm^2-$\sin^2 2\theta$ space that has been excluded by reactor experiments (discussed below in Chapter 6) which are sensitive to the $\nu_e \rightarrow \nu_x$ oscillation mode (and hence, also the $\nu_e \rightarrow \nu_\mu$ channel) the primary interest in the results of these experiments is to see what information they can give about a possible $\nu_\mu \rightarrow \nu_\tau$ signal.

The results of these three experiments are shown in Fig. 25. The relatively small Δm^2 range investigated is a reflection of the relatively small distance between the near and far detectors. There is no sensitivity at low Δm^2 because for such values of Δm^2 the ν's did not yet have a chance to have oscillated when they arrived at the far detector. There is no sensitivity at high values of Δm^2 because for high values of that parameter the oscillations already would have occurred at the near detector. Thus, a near/far comparison would yield a null result.

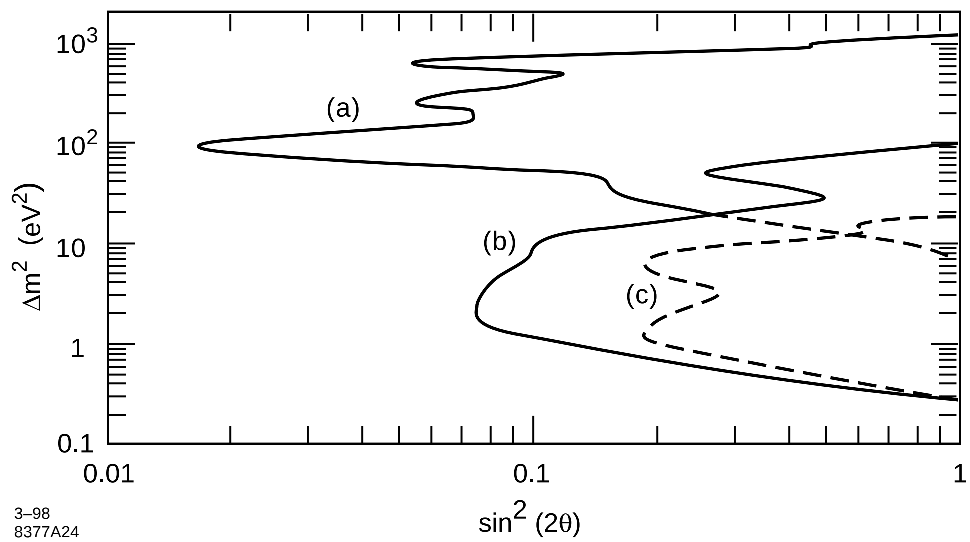

FIG. 25. Exclusion contour plots from the three early accelerator ν_μ disappearance experiments: (a) CCFR, (b) CDHS, and (c) CHARM.

The CDHS[76] and CHARM[77] experiments used the neutrino beam from the CERN PS, a beam with energy around 1 GeV. Hence, the Δm^2 region probed is lower. The CCFR[78] experiment used a much higher energy beam, from the Fermilab 400 GeV synchrotron, and thus explored a relatively higher region of Δm^2.

5.2 Completed Appearance Experiments

Up to now two $\nu_\mu \to \nu_\tau$ appearance experiments have been concluded and until very recently, they provided the best limit on possible $\sin^2 2\theta$ value for this mode of oscillations at high Δm^2.

One of these was the E531 experiment[79] at Fermilab, the first one utilizing a hybrid emulsion detector for oscillation search. It pioneered a number of general ideas subsequently used in the CHORUS experiment and which have also been proposed for the next generation of τ appearance experiments. The experiment was actually designed to study charm production by neutrinos and measure their lifetimes.[80] The $\nu_\mu \to \nu_\tau$ was a by-product, the search and potential identification of τ's being done using the same method as for the charged charm decays, i.e., looking for tracks with large kinks near the vertex. No event candidates were found.

An alternative approach was adopted by the CHARM II Collaboration[81] who searched for quasielastic τ production and subsequent decay via the exclusive mode $\tau \rightarrow \pi(K) + \nu_\tau$.

A fine-grained calorimeter was used with the plate thickness of about 1/9 of a hadronic interaction length. Thus the expected topology was a reasonably long single track, traversing many plates, followed by an interaction star. τ signatures were expected to have a large amount of energy in the star, since the pions from τ decays would be quite energetic, especially from the quasielastic ν_τ interaction.

The experiment compared the observed distributions for the required topology, both the total energy seen in the interaction and the product of that energy times the polar angle of that track (i.e., effectively the P_T of the track) with the Monte Carlo generated distributions for τ events and neutral current events as shown in Fig. 26. No τ-like excess was seen, allowing one to exclude a certain region in parameter space. The exclusion limits obtained by the E531 and CHARM II experiments are shown in Fig. 27.

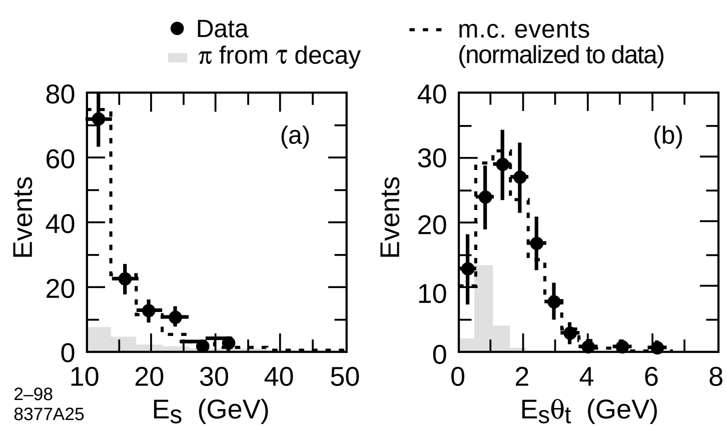

FIG. 26. CHARM II distributions of the single pion events as a function of (a) the shower energy E_s and (b) $E_s\theta_t$ for data and for Monte Carlo simulations of ν_μ N $\rightarrow \nu_\mu$ π X and ν_τ N $\rightarrow \tau$ N' with the decay $\tau \rightarrow \pi\, \nu_\tau$. Here, θ_t is the angle of the pion with respect to the direction of the incident neutrino beam.

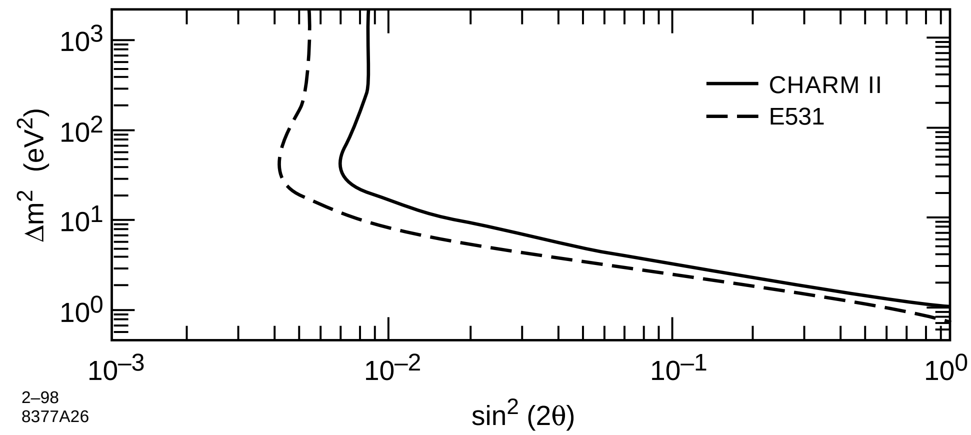

FIG. 27. Exclusion contour plots for the two $\nu_\mu \rightarrow \nu_\tau$ appearance experiments: E531 (dashed line) and CHARM II (solid line).

5.3 Statistical Analyses

Measurement of the total neutral current (NC)/charged current (CC) event ratio, as well as the differential ratio of that quantity as a function of the total hadronic energy can in principle provide us with information about the possible $\nu_\mu \rightarrow \nu_\tau$ oscillation. In practice, it is more convenient to measure the ratio of short to long events, where the division between the two is made in such a way that there is a pretty close NC/short and CC/long equivalence. If ν_μ's do oscillate into ν_τ's, then the number of ν_μ CC events, i.e., long events, will <u>decrease</u>. Furthermore, the majority of the ν_τ CC events will be short events because 83% of the τ decays do not have a muon in the final state. Thus, the number of short events will <u>increase</u> and hence the overall short/long ratio will <u>increase</u>. In addition, the behavior of that ratio as a function of hadronic energy can provide information about Δm^2 and $\sin^2 2\theta$ if a significant departure from the expected nonoscillated behavior is observed.

One should emphasize that such a determination of oscillation parameters can be made only on the <u>assumption</u> of a specific flavor oscillation made, i.e., $\nu_\mu \rightarrow \nu_\tau$ (or $\nu_\mu \rightarrow \nu_e$). The short/long ratio by itself does not allow one to determine which mode, or modes, are present and an <u>additional</u> measurement (or measurements) is necessary to make such a determination.

The CCFR Collaboration has performed such an analysis on their data[23] and found no evidence for any departure from the no-oscillation hypothesis expectations. Their data are shown in Fig. 28, and are compared with the expectation for the no-oscillation scenario and for two different oscillation scenarios. The sensitivity of this analysis is comparable to that obtained by the two appearance experiments discussed above, as is illustrated in Fig. 29.

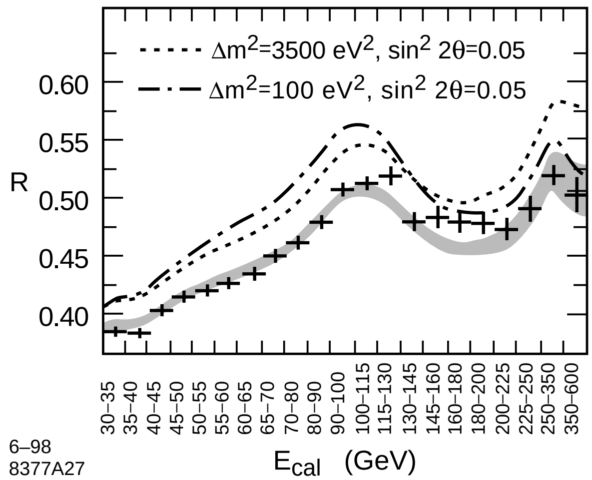

FIG. 28. Ratio of short to long events for the CCFR experiment, plotted as a function of the energy deposited in the calorimeter. The shaded band shows Monte Carlo prediction assuming no oscillations with 1 σ errors added in quadrature. The dotted and dot-dashed curves show the effect of $\nu_\mu \rightarrow \nu_\tau$ oscillations for two sets of oscillation parameters.

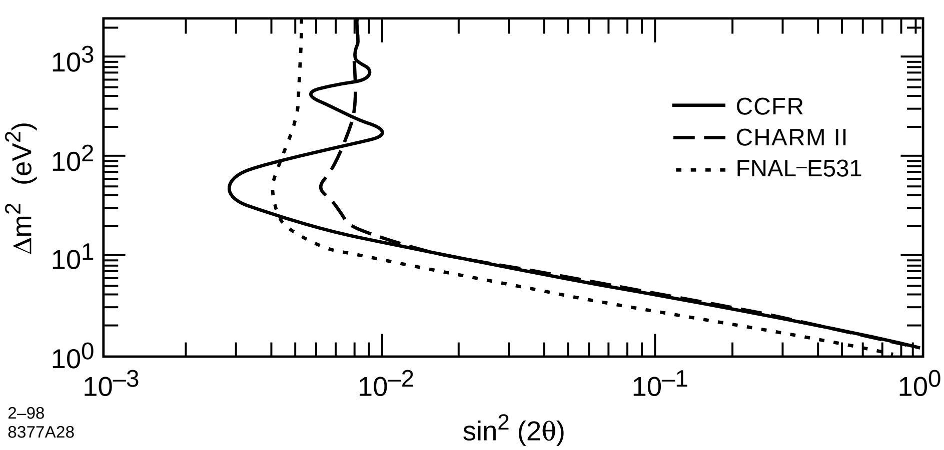

FIG. 29. Results of the CCFR experiment compared with the results from the two completed ν_τ appearance experiments.

5.4 Current Short-Baseline Program

There is currently an ongoing program to search for $\nu_\mu \to \nu_\tau$ oscillations at CERN, with two different experiments, CHORUS (CERN Hybrid Oscillation Research apparatUS) and NOMAD (Neutrino Oscillation MAgnetic Detector), attempting to push down the limits on $\sin^2 2\theta$ at high Δm^2 by another order of magnitude. This effort is motivated by a desire to explore the cosmologically interesting region in Δm^2, i.e., the region of ν masses suggested by the missing dark matter problem.[81]

Both experiments are located in the West Area of the CERN SPS,[82] in a sign-selected ν_μ beam with a mean energy of 27 GeV. The intrinsic ν_τ contamination in the beam from the D_s decay is estimated to be between 10^{-6} and 10^{-5} of the total ν flux. The ratio, averaged over the beam energy spectrum, of $\sigma_\tau^{cc} / \sigma_\mu^{cc}$ is 0.53. The length of the decay tunnel is about 300 m; the total target to detector distance is about 800 m. The experiments started in May 1994 and the expectation is that they will run through 1997, with a probable run for NOMAD also in 1998. The technique used in each experiment is quite different so we shall describe each one in turn.

The CHORUS detector, illustrated in Fig. 30, is a hybrid emulsion spectrometer, with the ν_τ interaction taking place in the emulsion target; the production of a τ is identified by a kink in the emulsion. The rest of the spectrometer is used to localize the potentially interesting events to a small region of emulsion and to measure the total hadronic energy and the direction and momentum of the muon.

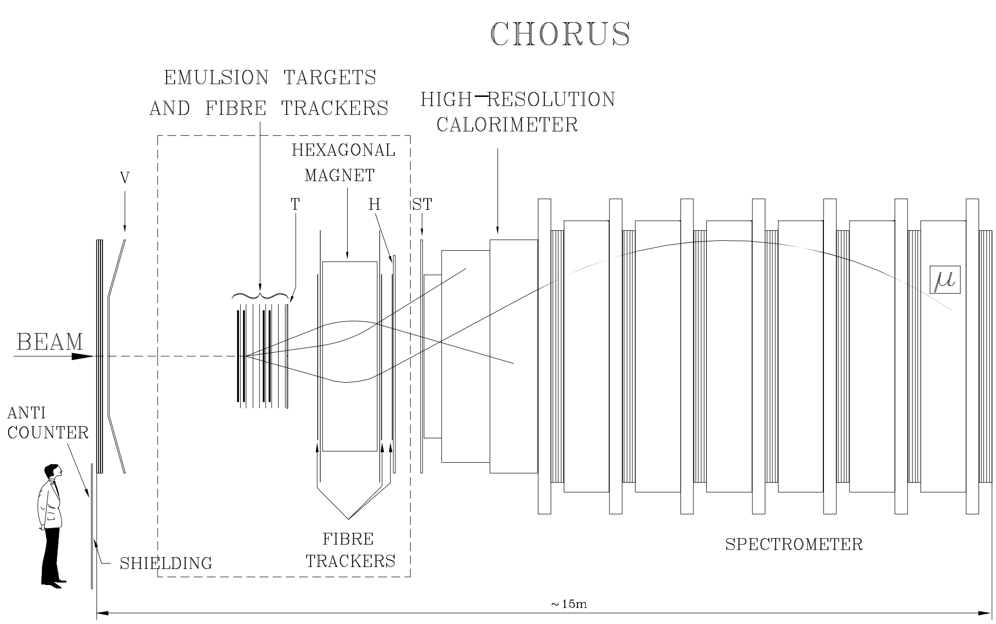

FIG. 30. The CHORUS detector.

The target region of the CHORUS detector is illustrated in Fig. 31. The downstream fiber tracking system has a spatial resolution of about 200 μm but a time resolution of 100 nsec. It is used to identify tracks that make up the neutrino interaction vertex. The changeable emulsion sheets, with spatial resolution of 1 μm, immediately upstream of the fiber tracker provide even better position and direction measurements of these tracks. They are changed every few months to aid in track finding. Finally, the bulk emulsion itself was changed twice during the run, i.e., after two years of exposure.

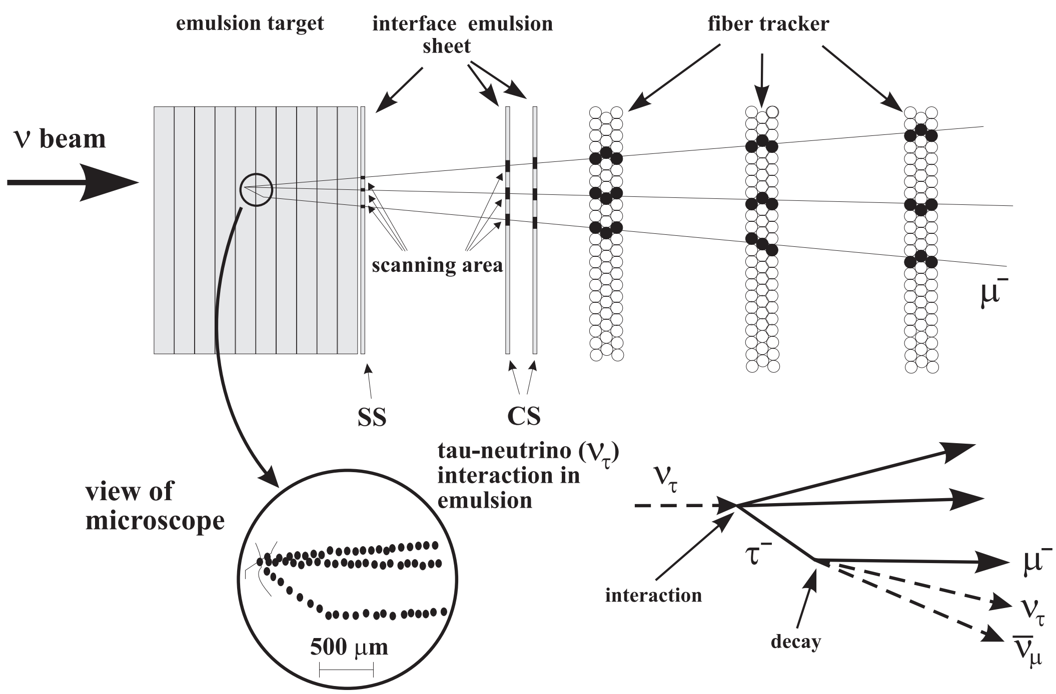

FIG. 31. The target region with an emulsion target, three interface emulsion sheets (CS and SS) and three fiber trackers is shown schematically. A ν_τ-CC interaction is shown with a “kink” structure which would be visible under the microscope is shown.

An experiment of this nature is fundamentally limited by the ability to process the data, i.e., scanning. It is important both to reduce the number of candidate events and to automate the scanning process as much as possible. The Japanese groups have made great progress in the latter area with the development of a computer-controlled automatic microscope attached to a CCD camera. Track reconstruction is done by overlapping in software the 16 frames corresponding to different z positions of the detector. The measured data are then used to obtain an impact parameter for each track reconstructed in this manner and if that value exceeds a threshold, the event is manually scanned. The distribution of the impact parameter from simulated ν_τ interactions and data is shown in Fig. 32. The manual scan checks the topology for the accepted events and rejects charm candidates, which will have an accompanying μ^- and a D^+ decay with either one positive decay daughter or with three particles. The kink is also required to have a sufficiently large P_T so as to reject the coherent scatters on a nucleus, without a visible recoil or boiloff nucleon. The observed and simulated (for ν_τ's) P_T distribution is shown in Fig. 33.

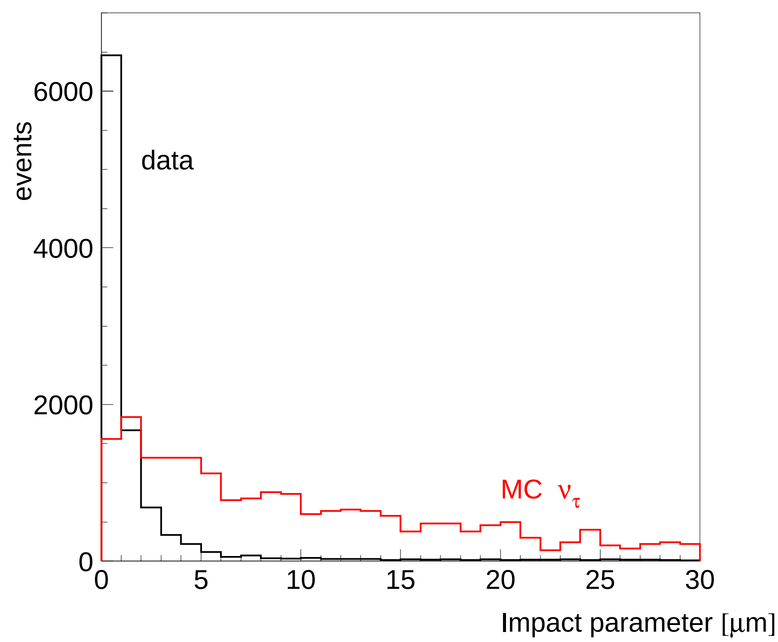

FIG. 32. Distribution of the impact parameter from simulated ν_τ interaction and data. With a cut on the impact parameter of 2--8 μm, 59% of the ν_τ interactions survive. A large fraction of data, mostly ν_μ-induced interactions, is cut.

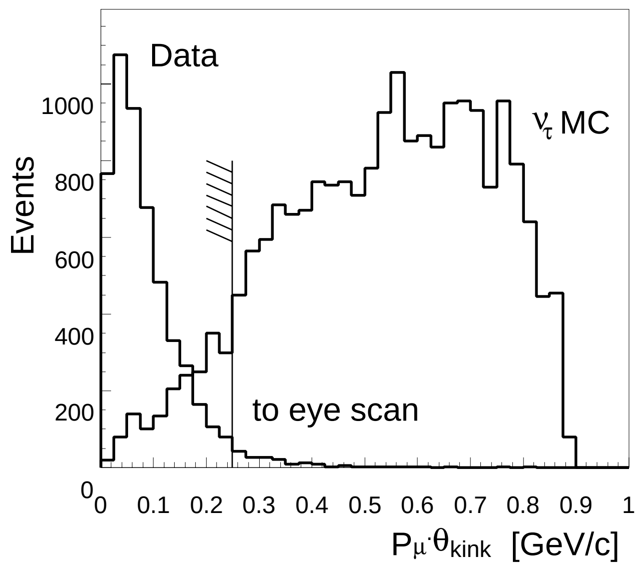

FIG. 33. Distribution of $p_\mu \cdot \theta_{kink}$ from simulated ν_τ interactions and real data. With a cut $p_\mu \cdot \theta_{kink} > 250$ MeV most of the ν_τ interactions survive.

There are expectations that all the τ decay modes will eventually be looked for, even though at this time the $\tau \rightarrow \mu$ analysis is most advanced. The efficiency for finding the $\tau \rightarrow \mu$ events is about a factor of two higher than for the other decay modes. At the time of these lectures about 10% of the potential muon decay sample was analyzed;[84] no events were found, giving a $\sin^2 2\theta$ limit of 4.5×10^{-3}. For the other decays, so far only 4% of the neutral current events have been analyzed. Three low P_T (< 250 MeV/c) kinks were found but no τ candidates. It is hoped that the full analysis of all the data can be completed by the end of 1998.

The other experiment, NOMAD, relies on a kinematical analysis to identify τ production and decay. To be able to achieve that goal, the target/detector is composed of a number of thin plane drift chambers located in a large magnetic volume, the magnet used being formerly a part of the UA1 experiment. NOMAD, like CHORUS, also hopes to have a background-free experiment. The schematic of the detector is shown in Fig. 34.

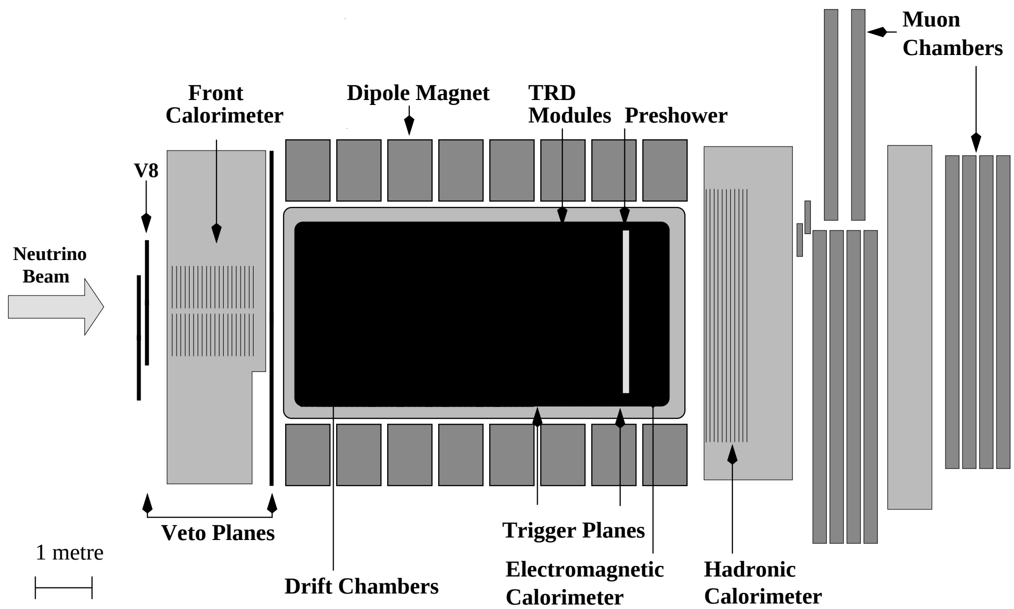

FIG. 34. Side view of the NOMAD detector.

Downstream of the 44 tracking chambers in the magnetic volume are located nine modules of transition radiation detectors (TRD's) and then an electromagnetic calorimeter, 19 radiation lengths deep, composed of lead glass Cherenkov counters. Further downstream, outside the magnet, is a hadronic calorimeter followed by muon chambers, composed of arrays of drift tubes.

The kinematical analysis used to identify the purely leptonic τ decay events relies on correlations between these vectors: P_{lepton}, P_{hadron}, and P_{miss}. For ν_μ or ν_e charged current events P_{lepton} and P_{hadron} will generally be back to back, with a relatively small P_{miss}. The last will be due to contributions from the Fermi motion in the nucleus, nuclear reabsorption and rescattering, and measurement errors (including missing particles). Thus on a two-dimensional plot, where axes are defined by the azimuthal angles between the three vectors: $\varphi_{\mu h}$ and φ_{mh}, there will be a region populated by τ events but not by μ (or e) events. This is illustrated in Fig. 35 where we show the Monte Carlo calculated scatter plots for the ν_μ events and the ν_τ CC events.

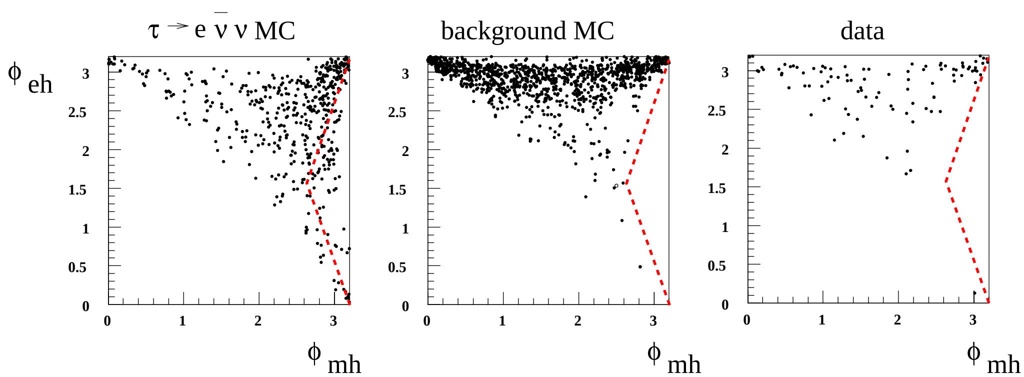

FIG. 35. Distributions of φ_{eh} vs. φ_{mh} obtained after $\tau^- \to e^- \nu_\tau \bar{\nu}_e$ selections cuts have been applied.

The initial data taken gave a measured P_T distribution for ν_μ CC events somewhat broader than what was expected from the Monte Carlo calculation: specifically one obtained $\langle P_T \rangle_{meas}$ = 770 MeV vs. $\langle P_T \rangle_{MC}$ = 610 MeV. The precise reasons for this discrepancy were not understood at the time of these lectures; they could be due to some neglected nuclear effects or easier reconstruction in Monte Carlo. Currently, the ν_μ data sample is used to calibrate and then correct for this discrepancy.

At the present time, based on 18% of the proposed statistics, no candidate events were observed (0.6 background events were expected).[85] This gives a limit: $\sin^2 2\theta < 3.4 \times 10^{-3}$ (90% C.L.) at high Δm^2.

There are expectations that the limit will be improved significantly by inclusion of more decay modes, increased statistics, and improved efficiency.

In summary, the three most sensitive experiments, E531, CHORUS, and NOMAD, have so far seen no candidate events for $\nu_\mu \to \nu_\tau$ oscillations. Thus, one can combine the whole data sample from all the experiments to obtain the current global limit on $\sin^2 2\theta$ of about 1.2×10^{-3}. The projected sensitivities of NOMAD and CHORUS as stated in the proposals are shown in Fig. 36 and compared there with the current limits from the published experiments. Finally, we might add that these experiments also set a limit on possible $\nu_e \to \nu_\tau$ oscillations which is about a factor of 50-100 worse than the $\nu_\mu \to \nu_\tau$ limit, reflecting the much smaller ν_e flux in the beam.

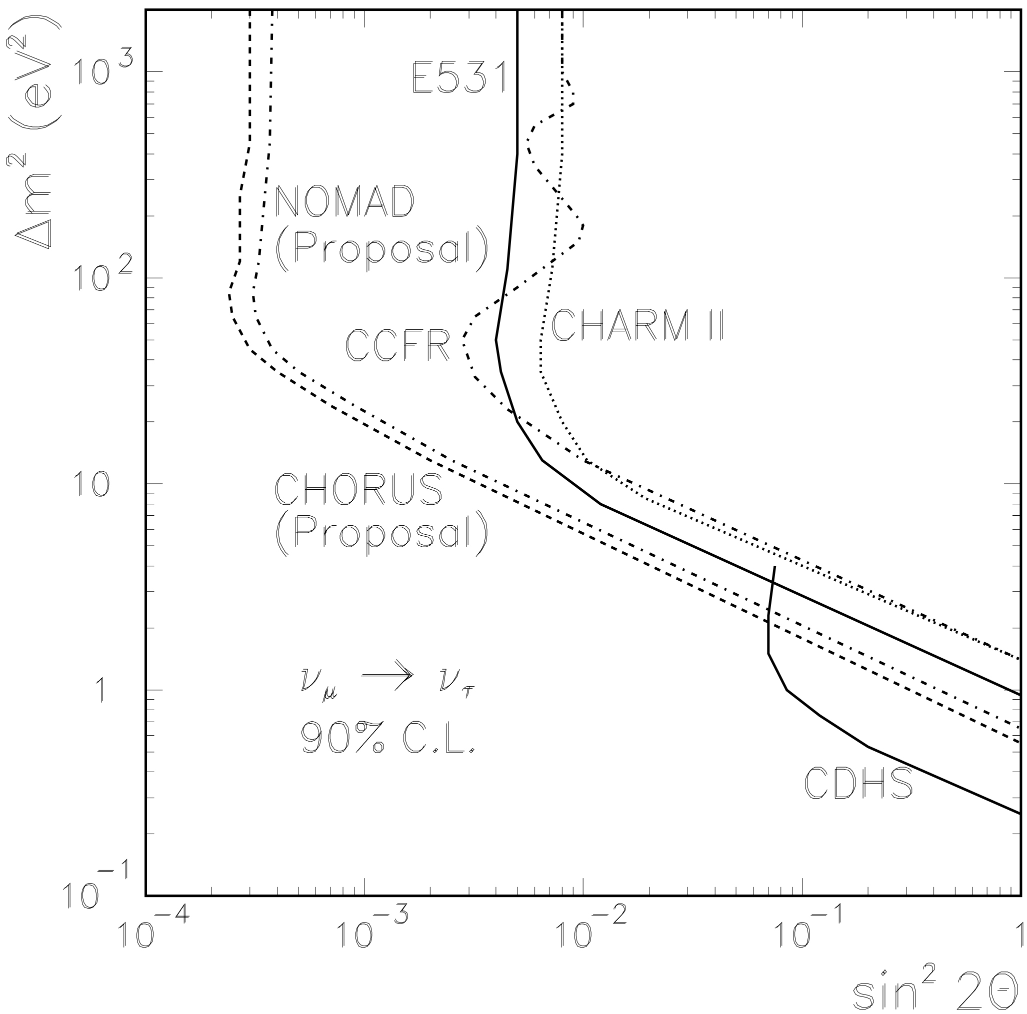

FIG. 36. Current 90% C.L. neutrino oscillation parameter limits compared to the limits achievable by the CHORUS and NOMAD experiments.

they frequently utilize neutrinos from a reactor or are used in a low energy beam-dump experiment.

The main advantage of the iron sampling calorimeters with magnetized iron is the ability to measure muon energy by curvature. Such devices (used in the CDHS and CCFR experiments) became the standard tool in the study of nucleon structure functions via neutrino deep inelastic scattering. Magnetized iron allowed one to measure the muon momentum by using tracking chambers with an accuracy ordinarily limited by Coulomb scattering. The interspersed active detectors allowed one to measure the total hadronic energy and, by measuring the energy flow, the direction of the hadronic jet.

More specialized experiments frequently required a different detector. Thus, for example, studies of ν-e scattering required a good measurement of the direction and energy of the electromagnetic shower. Low Z sampling calorimeters were generally found to be most appropriate for this purpose. Some examples of such devices are the sampling calorimeter with aluminum absorber and proportional chambers which were used at Fermilab to measure $\bar{\nu}_\mu e^-$ scattering[45] and CHARM[46] and CHARM2[47] calorimeters at CERN studying the same problem.

The total absorption calorimeters generally use liquid scintillator, either segmented or in a large tank, as the energy measuring medium. Typical recent examples would be the CHOOZ[48] or Palo Verde[49] reactor experiment detectors, or the KARMEN detector[50] looking for neutrinos from π^+ and μ^+ decays at the ISIS accelerator at RAL.

4.2 Tracking Detectors

Besides the energy measurement, another important goal of neutrino detectors is to measure tracks of individual particles. There are two general ways to attack this problem depending on the goals of the experiment. They are quite different in relative difficulty. In one approach, one tries to measure only muons (relatively easy); in another one tries to measure all individual tracks (much harder and generally requiring a significant penalty in total tonnage of the detector). In this section we shall discuss three broad categories of tracking detectors: electronic, bubble chambers, and emulsions.

(a) The first accelerator neutrino experiment[4] used what was basically a tracking detector, i.e., a massive aluminum optical spark chamber, capable of distinguishing clearly muons from electrons. Its schematic arrangement is shown in Fig. 16 and is remarkable for its simplicity.

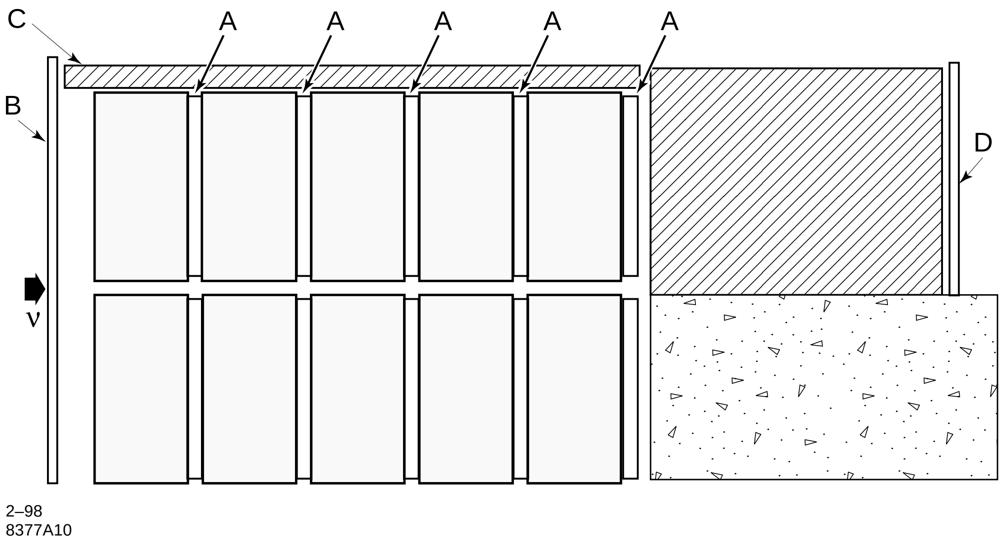

FIG. 16. Spark chamber and counter arrangement for the first neutrino accelerator experiment. A are the trigger counters. B, C, and D are the veto counters.

The subsequent evolution of neutrino detectors emphasized features typical of CCFR and CDHS detectors, i.e., a scintillator to measure hadronic components of the interaction and wire chambers to measure the muons. Thus, in some sense, these could be called hybrid detectors, combining calorimetry with tracking using two separate systems. A schematic of the CCFR detector is shown in Fig. 17.

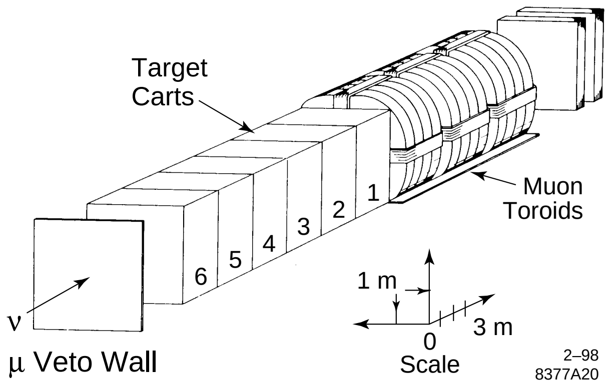

FIG. 17. The CCFR neutrino detector. Each of the six target modules contains layers of iron plates interspersed with scintillator and/or drift chamber planes. The muon spectrometer consists of three toroidal magnet units and a pair of drift chamber stations at the far downstream end.

More recently, more ambitious electronic tracking detectors have been built or are being planned. The NOMAD detector at CERN[51] uses a large number of thin low mass chambers in a magnetic field. These chambers serve both as a target and a detecting medium. Individual tracks in a hadronic shower can be seen and measured, as is shown in a “typical” NOMAD event shown in Fig. 18.

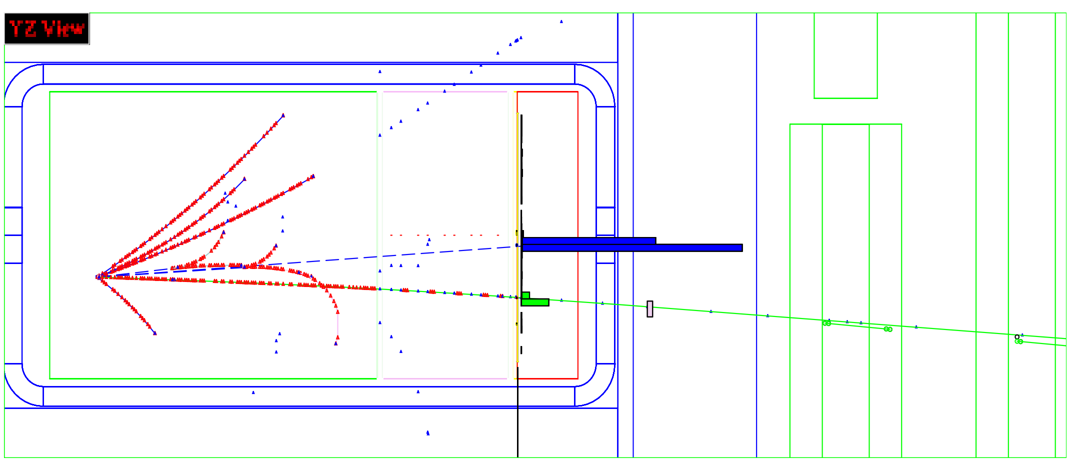

FIG. 18. A reconstructed CC candidate in the NOMAD detector. The longest track at the bottom is a muon matched to the segments in the muon chambers.

A very ambitious program centered in Italy has as its goal, construction of a massive liquid argon time-projection chamber (TPC), called ICARUS.[52] It uses the TPC principle to obtain the three coordinates and ionization associated with each space point. Prototypes up to three tons in size have been constructed and currently one full 600 ton module is being fabricated. The current plans call for several such modules to be constructed and installed in the Gran Sasso Laboratory. They could be used to search for proton decay, study solar neutrino interactions, and investigate potential long baseline oscillations if a beam from CERN to Gran Sasso is built.

(b) Bubble chambers played an important role in the development of neutrino physics. Their obvious strong point is the ability to see clearly and measure all the individual tracks. Hydrogen and deuterium exposures provided a clean simple target allowing one to study exclusive reactions as well as inclusive channels without the complexities of nuclear physics.[53] Their obvious shortcoming was the relatively low mass, difficulty of identifying muons and electrons, and very low efficiency for photon detection.

Some of the difficulties mentioned above could be alleviated by supplementing the chamber itself with high Z plates inside (to identify electrons and convert photons) and by surrounding the downstream end of the chamber with an external muon identifier (EMI).[54] A schematic of the Fermilab 15' bubble chamber with the EMI is shown in Fig. 19. Alternatively, these shortcomings could be overcome in cryogenic chambers by filling them with neon or neon-hydrogen mixture.[55] Large warm-temperature chambers filled with freon or other organic liquids were also built and played a very important role in neutrino physics.[56] The complexity of the target was compensated by higher mass, better particle identification, and high photon conversion efficiency.

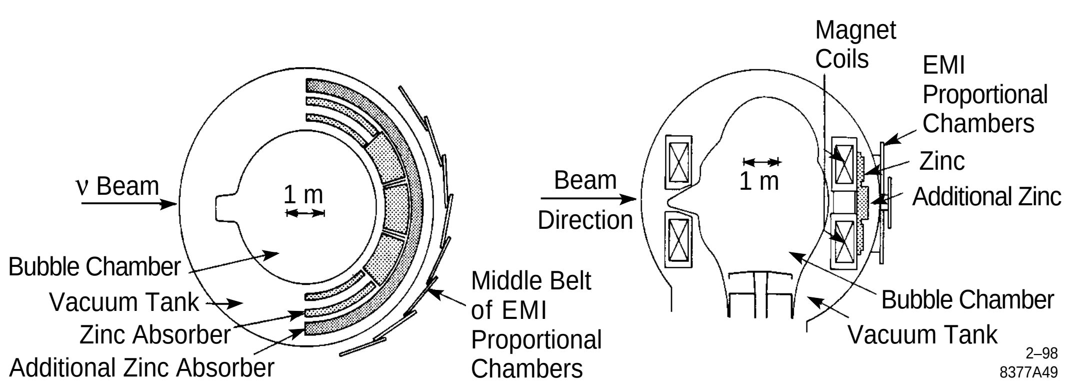

FIG. 19. Schematic of the 15' Fermilab bubble chamber with the external muon identifier.

In the waning days of the bubble chamber era there was a considerable effort made to improve the bubble chamber's spatial resolution so that one could identify charm and tau particles through their decay. Efforts of this kind led to an experiment at SLAC on charm photoproduction[57] and at Fermilab on charm production by neutrinos.[58] Even though the parallel effort, aimed at detections of ν_τ's in a beam-dump experiment,[59] never materialized, the R&D results were promising enough to lead one to believe that such a detection method of ν_τ's might be successful.

(c) In the last two decades or so we have seen a revival of the emulsion technique, again motivated by the discovery of short lived charm particles and tau leptons. This technique received a large boost by important developments in the scanning technology, which contributed to the ability to significantly increase the size of practical emulsion targets.

For τ leptons, $c\tau$ is about 89 μm. In the multi GeV energy range a typical γ will be about 5-10, resulting in the mean length of the τ track of the order of a mm or below. That number sets the scale both on the resolution and sampling frequency of the potential detection medium. So far, emulsion is the only known medium capable of such adequate resolution and thus, emulsions have been the cornerstone of detectors designed to see τ's via their decay kink.

Emulsion experiments for τ detection generally rely on electronic detectors downstream to localize the approximate volume in emulsion where the putative τ event might have occurred. This feature, combined with significant automation in the scanning technology, has resulted in a typical current processing capability of about 10^3 events/microscope/month. Further improvements are anticipated in the future.

Recently, there have also been new developments (and revival of older ideas) in how one could significantly increase the mass of the neutrino target in an emulsion-based detector, with only a very small loss in background rejection.[60] Traditionally, τ emulsion experiments used bulk emulsion so that the production and decay of the τ would occur in emulsion. Alternating thin heavy metal plates (Fe, Pb) with thin emulsion layers on a plastic sheet can increase the target mass by a factor of 100 or so for the same cost since it is the expense of emulsion that drives the total cost. The extreme form of this approach would be to look for finite impact parameter in a stack composed of a number of modules, each consisting of a metal plate followed by emulsion. Alternatively a cleaner but less efficient scheme would be to have a basic module composed of: metal plate, emulsion, air gap, emulsion. The detected τ's would ordinarily be produced in the metal plate and decay in the air gap. One emulsion on the upstream side of the air gap would measure the directions of the τ; the other one, the direction of the τ decay daughter. A significant difference between the two directions would be an indication of τ decay. Such a concept is the basis of the OPERA proposal discussed in Chapter 7.

4.3 Cherenkov Detectors

Neutrino detectors relying on detection of particles via Cherenkov light have filled an important niche in neutrino physics in recent years. In addition, they also promise to play an important role in the future. Their two most important positive characteristics are that some directional information can be obtained from the Cherenkov cone and the target/detector medium can be quite cheap e.g., water, and thus large masses are feasible. Again, in an effort to provide a systematic discussion, we choose to define four categories of Cherenkov detectors: nonfocusing, focusing, hybrid (Cherenkov/ calorimeter), and large volume detectors (no man-made containers).

(a) Nonfocusing Water Cherenkov counters have played a prominent role in recent neutrino physics, in the study of solar neutrino physics,[61] atmospheric neutrinos,[62] and detection of supernova neutrinos.[63] They were developed originally to provide a medium which would be simultaneously a detector and a source for experiments looking for proton decay.

The design that these detectors have evolved into is basically a large container (e.g., an underground cavern) filled with ultrapure water and having all of its inside surfaces covered with photomultipliers facing inwards. The latest, and most ambitious of these detectors is Super-Kamiokande:[64] a cylindrical underground cavern of 45 m height and 50 m diameter filled with H_2O (Fig. 20). The walls and top and bottom surfaces are covered with 11,200 20" photomultiplier tubes, providing a 50% coverage of the total area.

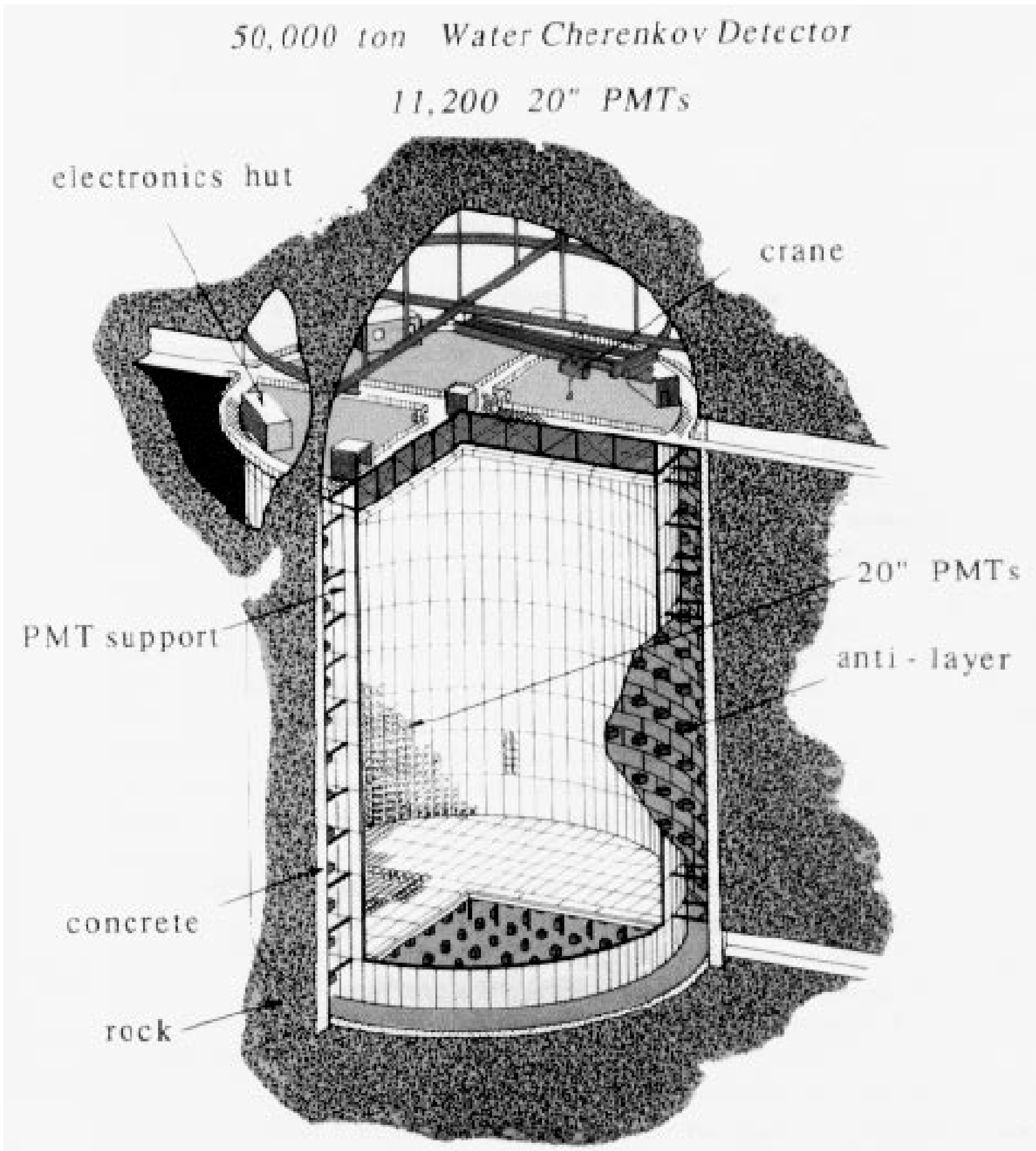

FIG. 20. Super-Kamiokande detector.

This system is nonfocusing, i.e., the Cherenkov light travels in a straight line from the point of origin to the photodetector on the wall. Because of the large detector size, the purity of the water is very important; an attenuation length of around 100 m has been achieved in the Super-Kamiokande. The purifying system must be running continuously so as to prevent growth of bio-organisms.

One can distinguish the electrons from muons by the sharpness of their Cherenkov light pattern in the photodetectors. Muons of low to medium energies will travel for a certain distance and then stop. Thus, the width of the illuminated part of the Cherenkov cone radius will be proportional to their range and its edges will be quite sharp. On the other hand, electrons will shower and thus generate a number of Cherenkov ring sources which will tend to have a variety of somewhat different directions. Thus, the resulting pattern in the photodetector will tend to be more filled in the center of the ring and more "fuzzy" on the outside. In the range of a few hundred MeV to 1 GeV separation between μ's and e's better than 100:1 is achievable as has been verified by exposing a water Cherenkov detector to muon and electron beams of well-defined energies at KEK.[65] This is illustrated in Fig. 21, which shows μ/e separation at different energies obtained by applying the Kamiokande algorithm to calculate the relative probability of an event having an electron or a muon. A typical Super-K event is shown in Fig. 22.

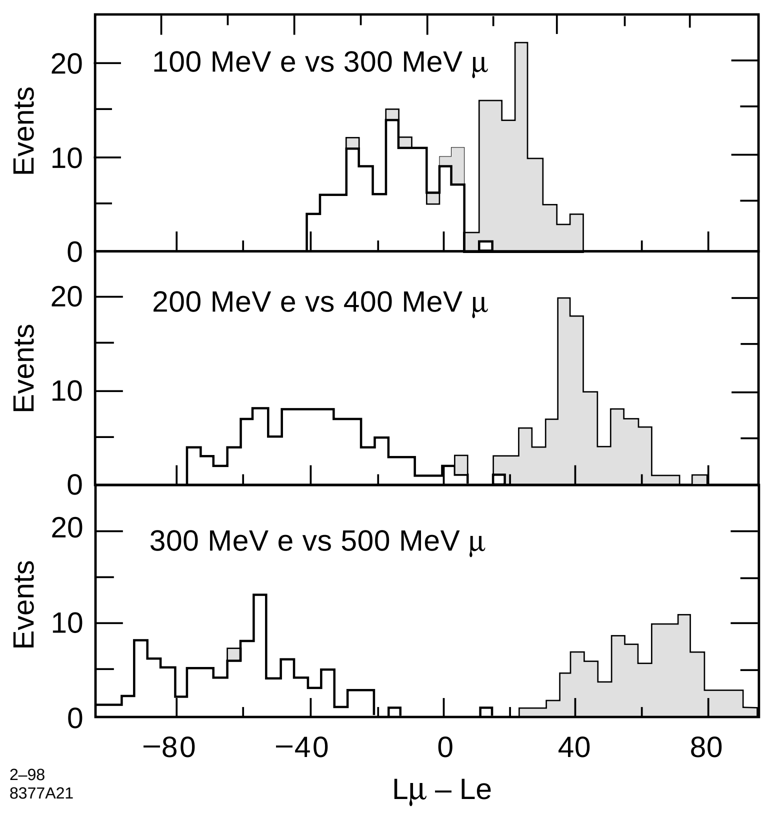

FIG. 21. The experimentally measured difference of the logs of likelihood. Shaded histogram represents muons; open histogram electrons.

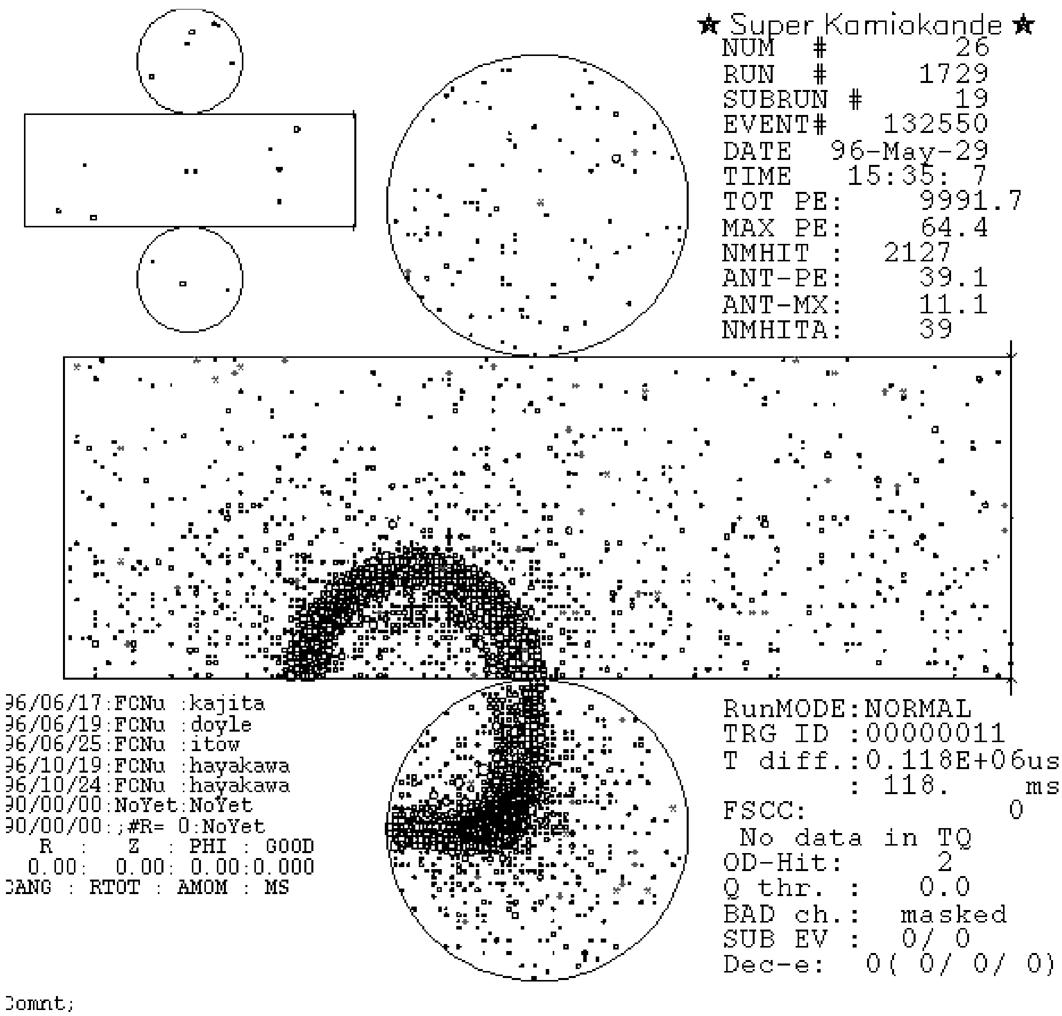

FIG. 22. Pattern of the hit photomultipliers in a typical Super-Kamiokande event.

(b) In principle, at least, the performance of a water Cherenkov detector could be enhanced by providing a focusing system, i.e., a focusing mirror which would provide sharp Cherenkov rings for a particle traveling continuously in the same direction. Such a system has never been executed before on a large scale, but is the basis of the RICH proposal for a Gran Sasso long baseline experiment utilizing a CERN neutrino beam.[66] A possible layout of such an experiment is shown in Fig. 23.

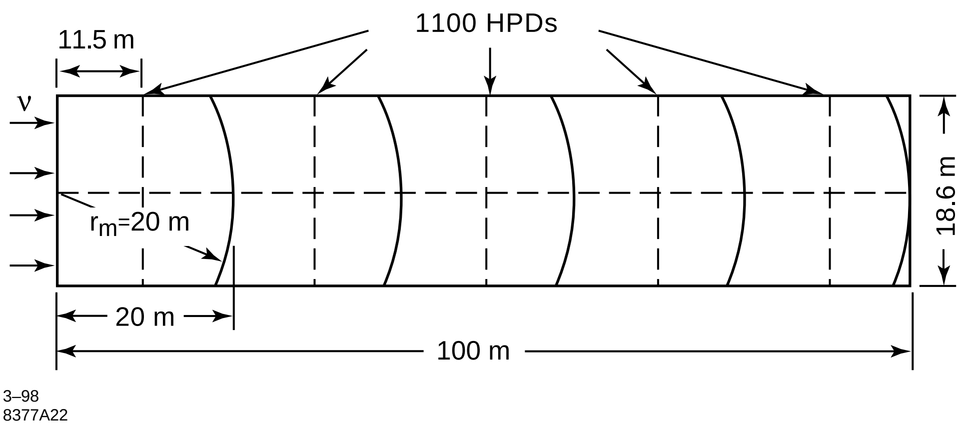

FIG. 23. Proposed layout of the 27 kt water target and radiator in the Gran Sasso tunnel. The system is composed of five equivalent sections of 20 m length, each with a reflecting mirror at the end and an array of hybrid photodetectors (HPD) 11.5 m downstream from the mirror center of curvature. 20% coverage of the area with HPD's is proposed.

(c) In certain applications, combining Cherenkov light with scintillator light might be productive. Cherenkov light is fast, and thus strongly correlated in time with the passage of a particle, and it retains the information at some level of the directionality of the particle which produced it. On the other hand, its intensity is about two orders of magnitude lower than the scintillation light from a good scintillating medium. By combining the two in a hybrid detector, the advantages of Cherenkov light could be retained and its deficiencies alleviated.

The LSND detector is a good example of such a hybrid detector.[13] The target and detector medium is mineral oil with a small amount of a scintillator additive. Thus, charged particles will give a sufficient amount of scintillator light so that their energy can be measured via calorimetry; simultaneously some time, direction, and position information is retained from the Cherenkov light.

Another kind of a proposed hybrid Cherenkov detector is the SNO neutrino detector.[67] Water (normal or heavy), is used as the medium to generate Cherenkov light from the produced positrons or electrons. But in addition, one wants to detect the neutron from the breakup of a deuteron. The SNO design aims to achieve this by providing supplementary neutron counters.

(d) Large Volume Cherenkov Counters. One can speculate how far the Cherenkov technique can be pushed. Since water (liquid or solid) is in a certain sense free, large detector arrays could be constructed in water or ice, where the main cost would be the cost of photodetectors. Such a scheme is attractive for detection of very high energy neutrinos from extragalactic sources. Because fluxes are low, large target mass is required. However, because energies to be investigated are very high, the sampling frequency, inversely proportional to the spacing between the detector elements, does not need to be very large to be able to reconstruct the muons from such high energy neutrino interactions.

The original idea for such a detector was the DUMAND underwater array in the Pacific Ocean near the Hawaiian Islands.[68] Some success in testing prototypes for this experiment has been obtained but the program has been plagued by a number of technical difficulties and a shortage of funds.

More recently, this general concept has been extended to a photomultiplier array in the ice, at the South Pole, called AMANDA.[42] The proposed AMANDA scheme is sketched in Fig. 24. The initial difficulties, associated with trapped air bubbles which caused dispersion, have been overcome by going to greater depths. The AMANDA project is proceeding and results from the deep arrays are expected to be available in the near future.

Water arrays have not been completely abandoned even though it is unlikely that DUMAND will materialize. Photomultipliers on strings have been installed and used in Lake Baikal,[69] and tower photomultiplier arrays are about to be installed in the Mediterranean off the Greek coast in the NESTOR project.[43]

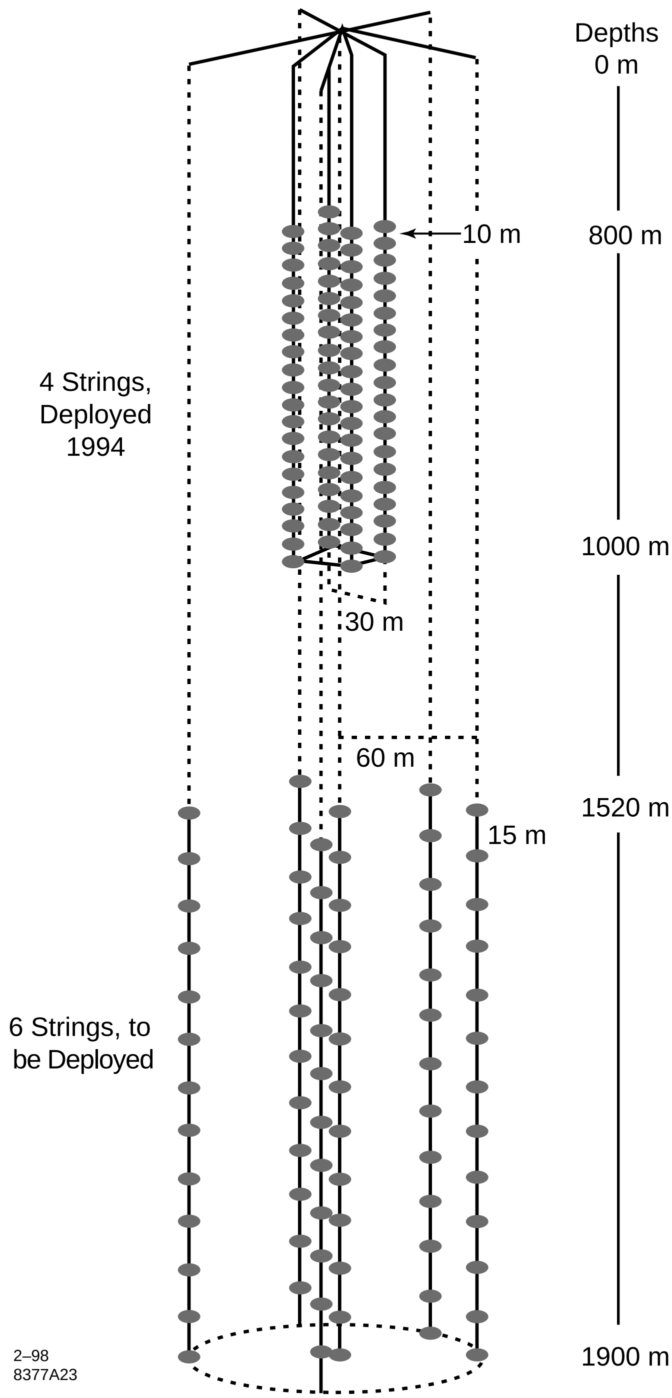

FIG. 24. Sketch of the AMANDA array located in the ice at the South Pole.

4.4 Radiochemical Detectors

These detectors incorporate the original ideas of Alvarez[70] and Pontecorvo[71] as to how one might be able to detect solar neutrinos. So far, they have been used solely for this purpose and possible applications elsewhere seem unlikely. The essence of the idea is to create (and subsequently identify) new atoms which would be produced via neutrino interactions. This is truly a heroic enterprise because typically, e.g., in the GALLEX experiment,[72] one makes 1 Ge atom per day in a tank of 30 tons of Gallium. Thus the challenge is to detect 1 atom of interest in the presence of 2.5 x 10^{29} other (uninteresting) atoms.

The neutrino channels that have been investigated so far are: in the Homestake[73] mine experiment:

$$\nu_e + {}^{37}Cl \rightarrow {}^{37}Ar + e^- ,$$

and in the GALLEX[72] and SAGE[74] experiments:

$$\nu_e + {}^{71}Ga \rightarrow {}^{71}Ge + e^- .$$

The former one has a neutrino energy threshold of 814 keV; the later of 233 keV.

The experimental technique relies on bubbling out the created atoms (in molecular or atomic gas form) by flushing the experimental tank with gas. An important feature of the technique is the fact that the produced nuclei are unstable but have relatively long (but not too long) lifetime (50.5 day half-life for ^{37}Ar, 11.4 days for ^{71}Ge). Thus after an extraction, whose frequency is determined by the lifetime of the produced unstable daughter atoms, one can count the decays of these atoms in low-background proportional counters.

Another channel that might be interesting and is actively being pursued[75] in the Homestake mine experiment is:

$$\nu_e + {}^{127}I \rightarrow {}^{127}Xe + e^- ,$$

with a threshold of 633 keV and ^{127}Xe half-life of 36 days.

6 Oscillation Experiments Involving ν_e ($\bar{\nu}_e$)

6.1 Reactor Disappearance Experiments

As discussed above in Chapter 3, reactors produce an abundant flux of $\bar{\nu}_e$'s, a flux whose energy spectrum is well understood and whose intensity is directly correlated in a known way with the power of the reactor. Because the energy of $\bar{\nu}_e$'s is relatively low, namely in the MeV range, $\bar{\nu}_\mu$'s or $\bar{\nu}_\tau$'s produced by potential oscillations will be too low in energy to interact via charged current interactions. Thus, in reactor experiments one is limited to disappearance studies, i.e., looking for a decrease in flux and/or distortion of the expected spectrum in the detector which is located some distance from the reactor.

6.1.1 Results from Completed Experiments

As of the time of these lectures (August 1997) there were several negative results from the reactor experiments, the most sensitive one coming from an experiment studying the flux from the reactors at Bugey, France.[86] The $\bar{\nu}_e$'s are detected by the sequence of reactions

$$\bar{\nu}_e + p \rightarrow e^+ + n\,,$$

$$n + {}^6\mathrm{Li} \rightarrow {}^4\mathrm{He} + {}^3\mathrm{H} + 4.8\ \mathrm{MeV}.$$

One demands a coincidence between the positron from the initial reaction and a signal from the subsequent neutron capture. The $\bar{\nu}_e$ source in the Bugey experiment is actually two reactors about 90 m apart; by utilizing detectors at two different locations, neutrino flux and spectrum can be measured for three different reactor-detector distances. The results can be compared with each other, to see if the flux intensities differ just by $1/r^2$ ratios, as expected in the absence of the oscillations, as well as with the theoretically expected spectra.

The Bugey experiment finds no evidence of oscillations. The ratios of measured and calculated (assuming no oscillation) integrated fluxes at the three distances are given in Table 3.

7 Future Experiments

As we discussed earlier, there are a number of theoretical and experimental reasons to believe that neutrinos do have mass and do oscillate. These arguments can be divided into four general categories:

(a) The need for dark matter from astronomical observations.

(b) The atmospheric neutrino anomaly.

(c) The LSND effect (discussed in Sec. 6.2).

(d) The solar neutrino deficit.

The regions in the oscillation parameter space suggested by these four general hints, and still compatible with the negative results of other experiments, are shown in Fig. 56.

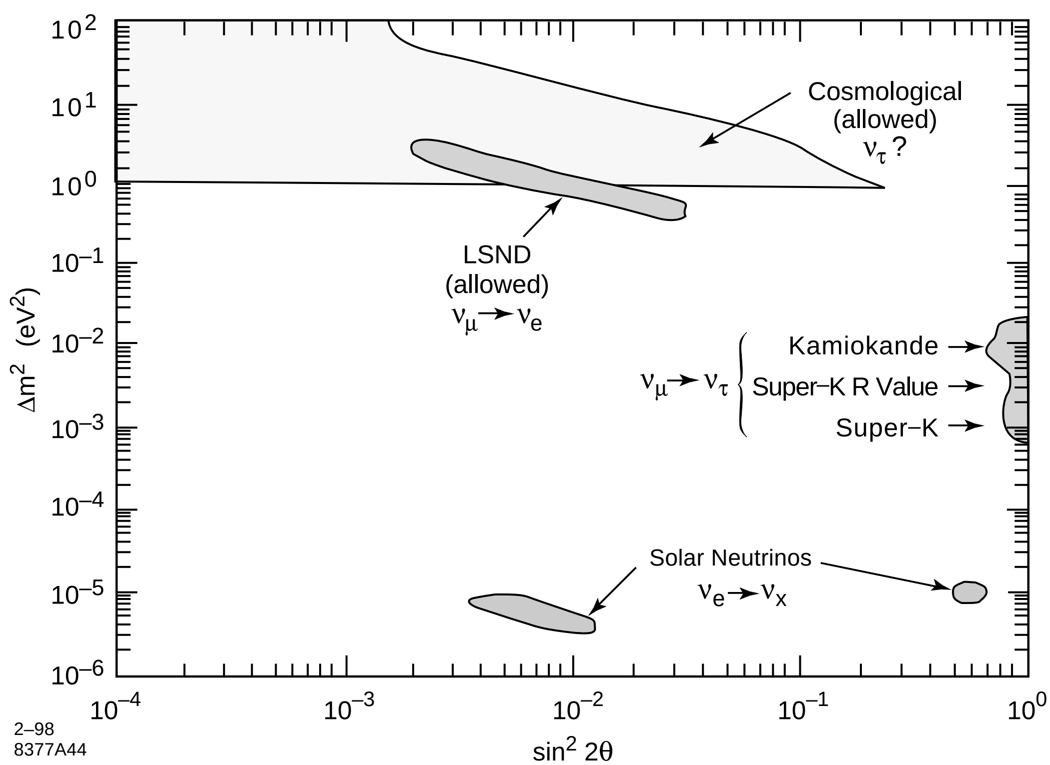

FIG. 56. Current evidence for possible neutrino oscillations. For each piece of experimental evidence (solar neutrinos, atmospheric neutrino anomaly, LSND effect) we display the suggested region in the parameter space obtained on the basis of a two-flavor fit and not excluded by other experiments. The pure vacuum oscillation possibility for solar neutrinos at low Δm^2 ($\sim 10^{-10}$ eV^2) is off the plot. The shaded region indicates roughly the neutrino mass (not Δm^2) region favored by the cosmological arguments. The higher values of $\sin^2 2\theta$ in this region are excluded by accelerator experiments.

The accelerator and reactor neutrino program planned around the world for the next decade is geared towards investigating and clarifying the above four general areas. In this final chapter, we shall briefly describe these efforts, grouped according to which of the above four issues they principally address. We first briefly outline the general thrust of activities in the accelerator and reactor neutrino area in each of the three major geographical areas of the world.

In Japan, the efforts are focussed on utilizing the Super-Kamiokande detector to search for accelerator neutrinos produced at KEK, some 230 km away, initially by the existing 12 GeV proton synchrotron, subsequently by the new 50 GeV proton accelerator of the Japanese Hadron Facility (JHF) currently in the planning stage. In addition, there are plans to convert the existing Kamiokande detector into a massive reactor neutrino detector.

In the U.S., the main thrust is centered around the NuMI project at Fermilab with both short baseline (COSMOS) and long baseline (MINOS) experiments. In addition, there is a BooNE proposal to investigate the LSND effect with the Fermilab 8 GeV Booster neutrino beam.

The situation in Western Europe is less clear. The current plan is to focus the neutrino program on a new beam pointing to the Gran Sasso Laboratory in Italy, about 730 km away. Both kinds of experiments, short baseline near the CERN site and long baseline at Gran Sasso, are being contemplated. At the present time, however, there is no definite commitment to build such a beam. There also has been some discussion about intermediate baseline experiments.

7.1 Experiments Addressing the Dark Matter Questions

7.1.1 COSMOS Experiment

The COSMOS experiment is part of the NuMI project at Fermilab, a new neutrino beam facility currently being designed together with its associated experiments. We shall first give a brief description of the NuMI beam. The source of primary protons will be the Main Injector accelerator, currently under construction at Fermilab and scheduled for completion in the middle of 1998. The energy of the extracted proton beam will be 120 GeV and it is anticipated that about 3.7 x 10^{20} protons on target will be available per year for the neutrino program. The FY98 budget includes initial funds for the engineering and design of the facility. The NuMI beam construction should start in the fall of 1998.

The neutrino beam is still in the final design stage[22] and the ideas presented here may not all be faithfully incorporated in the eventual beam. The 120 GeV proton beam will strike a segmented graphite target about 1.8 interaction lengths long. The resulting hadron beam will be transported in vacuum for about 800 m, allowing π's and K's to decay producing neutrinos along this 800 m long path. The residual hadron beam (π's, K's, and the residual primary protons) will be disposed in a dump just downstream of the decay volume.

Both wide band and narrow band beam (WBB and NBB) capabilities are being designed and it is anticipated that they can be accommodated with a rather straightforward switchover from one configuration to another. It is desired to have a beam spill approximately 1 ms in length so as to avoid pileup in the detectors on the Fermilab site where the instantaneous neutrino rates are expected to be quite high.

In the initial program, two different experiments are envisaged to coexist and take data simultaneously, COSMOS and MINOS. Pointing the neutrinos at the Soudan site for the MINOS experiment requires that the parent hadron beam be directed downward at an angle of about 52 mr. The general orientation of the beam and location of the two sites are indicated in Fig. 57.

FIG. 57. The layout of the NuMI project.

The design criteria for the beam is not only high neutrino flux, required for both COSMOS and MINOS experiments, but also a flux that is as similar as possible at the two MINOS detector locations. The two criteria are somewhat contradictory, in-so-far as a high flux requires a long decay volume. Thus, the neutrinos present an effective line source to the detectors on the Fermilab site but a point source to the far detector. This difference results in somewhat different energy spectra at the two sites. The differences at the two locations have to be well understood and a monitoring system is planned to achieve this. The current design of the WBB configuration is based on three focusing horns. The ν_e event rate is estimated to be about 0.6% of the ν_μ rate.

COSMOS (COsmologically Significant Mass Oscillation Search),[98] a short baseline component of the NuMI project, is designed to explore Δm^2 space in the cosmologically relevant domain, i.e., $1 < \Delta m^2 < 100$ eV^2. For the $\sin^2 2\theta$ parameter, 2×10^{-5} should be achievable at the upper range of Δm^2 values. It is a multinational collaboration with the participating institutions coming from Japan, United States, Europe and Israel. (Note added in proof: The proponents have recently decided not to continue with this experiment.)

The experiment is similar in its general concept to CHORUS and uses an emulsion target for production of tau leptons. The excellent resolution of emulsions, about one micron in transverse dimension, will allow one to identify tau leptons by their characteristic decay kinks. A sophisticated downstream spectrometer measures the momenta of charged tracks, converts and measures γ rays, and provides particle identification. Scintillating fiber tracker, immediately downstream of the emulsion, will allow one to trace back the trajectories of the charged particles into the emulsion region and thus provide a relatively good localization of the ν_τ interaction and τ decay. The currently envisaged apparatus is shown in Fig. 58, though the design is still undergoing evolution.[99]

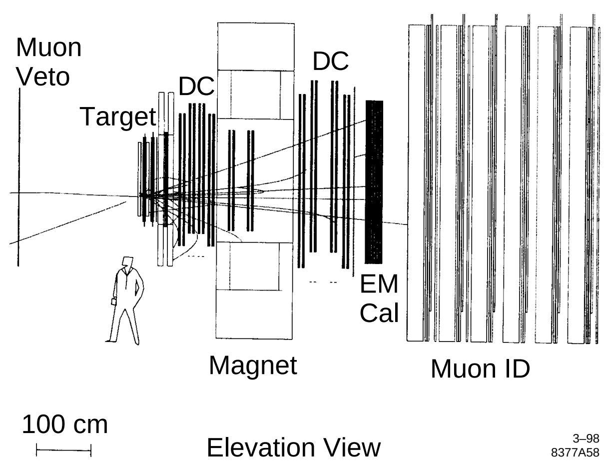

FIG. 58. Elevation view of the COSMOS hybrid emulsion spectrometer.

An important recent experimental development in this field has been the ability to do automatic scanning which significantly increases the volume of emulsion one can contemplate scanning in a finite time. The present estimated scanning capability of the collaboration is about 20,000 events/year. It is anticipated that this number will be soon raised to 100,000. A significant component of the Japanese contingent in the collaboration also participates in the DONUT (Fermilab E-872) and CHORUS at CERN experiments, where similar scanning techniques are being used and within which programs of significant development in the scanning technology have taken place.

Current estimates indicate that the experiment will be essentially background free. 1.5 background events are anticipated out of 8 x 10^6 ν_μ interactions. Because of the relatively low energy of the Main Injector, D_s production is strongly suppressed and there are no other significant sources of ν_τ production by the primary protons. Other potential sources of background like charm production, white star kinks, and decays of longer lived particles have been estimated by Monte Carlo calculations and shown to be below the one spurious event level.

Besides the presence of a kink, there are additional kinematical handles which help one to determine production and decay of a tau. Thus, for example, for the $\tau \to \pi\nu$ decay mode, in the rest frame of the τ, the pion momentum vector and missing momentum vector (due to the neutrino) have to be back to back. Similarly, the azimuthal angles of the tau and the primary hadronic jet have to be back to back. These constraints help significantly to reduce background.

The electromagnetic calorimeter is composed of about 3,500 blocks of lead glass. By detecting and measuring γ rays, other τ decay channels, like $\tau^- \to \rho^-\nu$, $\rho^- \to \pi^-\pi^o$, and $\pi^o \to 2\gamma$, can also be identified.

Figure 59 shows the expected sensitivity plot for COSMOS assuming three eight-month long runs with WBB with reasonable efficiency. The expected improvement over the current CERN experiments is about a factor of ten. There is also some sensitivity for $\nu_e \to \nu_\tau$ oscillations. It is hoped to have the experimental apparatus installed and checked out on a time scale such that the data taking can start in 2002.

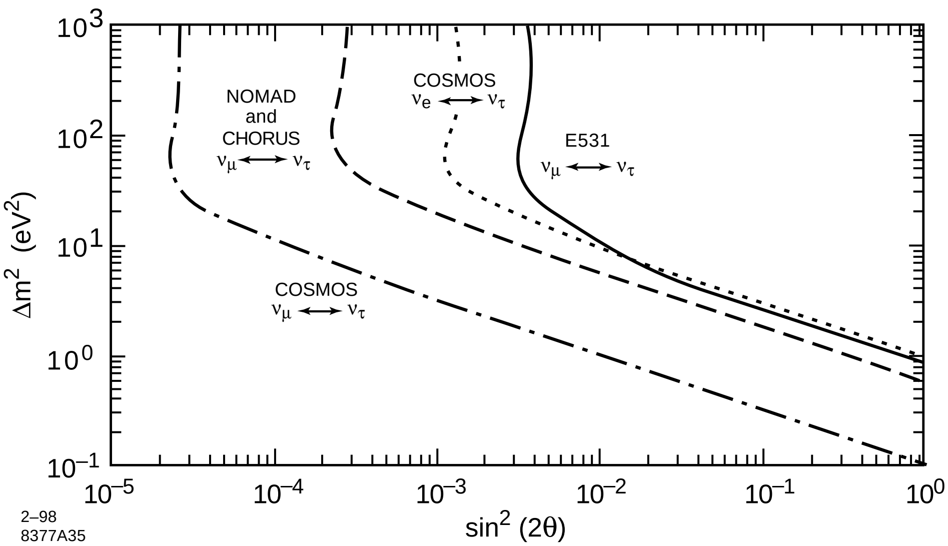

FIG. 59. The projected sensitivity for $\nu_\mu \to \nu_\tau$ and $\nu_\mu \to \nu_e$ oscillations of the COSMOS experiment and its comparison with the expected limits at the start of COSMOS run.

7.1.2 Outlook in Western Europe

About a year ago a decision was made by the CERN directorate not to continue the neutrino program in the West Area (where the current NOMAD and CHORUS experiments are situated). Instead, any new neutrino program would be based on a new neutrino beam, produced by protons from the SPS extracted in the same place where the transfer line to LHC would originate.[100] The hadron beam would be about 1000 m long and would point downward at about 5.8% so as to aim at the Gran Sasso Laboratory. A detector hall for a potential short baseline experiment could be constructed a few hundred meters downstream of the secondary hadron beam dump and would be at a depth of about 135 m. At the present time, it is not clear whether funds for such a beam line will be available. The decision is expected sometime within a year or so.

In parallel, there has been an extensive effort to design an experiment which could significantly extend the expected reach of the current CERN short baseline experiments. These efforts have resulted in a TOSCA proposal,[101] whose schematic layout is indicated in Fig. 60. The apparatus is composed of six relatively self-contained target modules located in the UA1 magnet, currently used by the NOMAD experiment. There is sufficient tracking capability within each module, as can be seen in Fig. 61, to measure directions and momenta of all tracks. Emulsions in each module are still used as the neutrino target but the modularization allows one to increase total emulsion mass without degrading track measuring capability. The calculated reach in $\sin^2 2\theta$ is 1.5×10^{-5} at large Δm^2, i.e., somewhat better than COSMOS, and $\Delta m^2 = 0.1$ eV^2 for $\sin^2 2\theta = 1$.

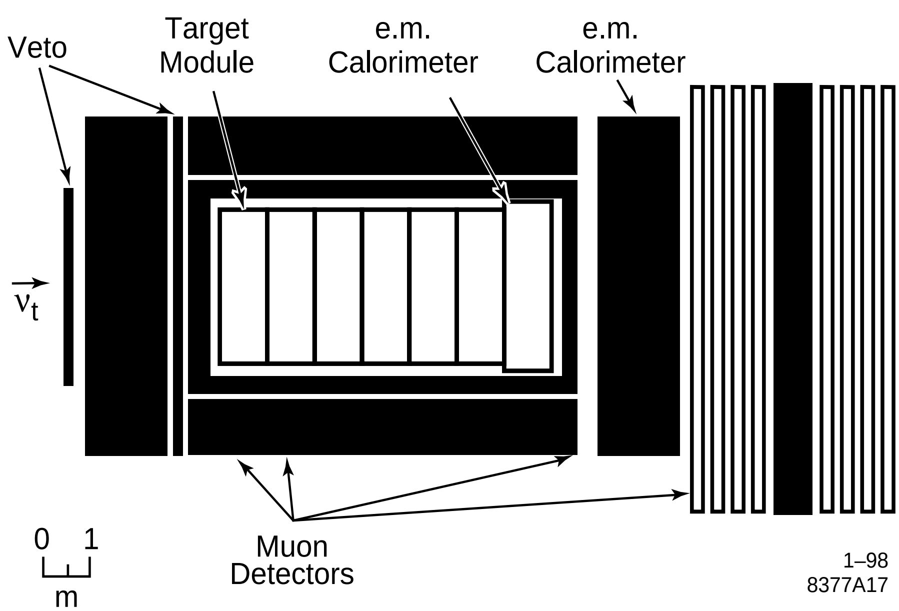

FIG. 60. Schematic layout of the proposed TOSCA experiment at CERN.

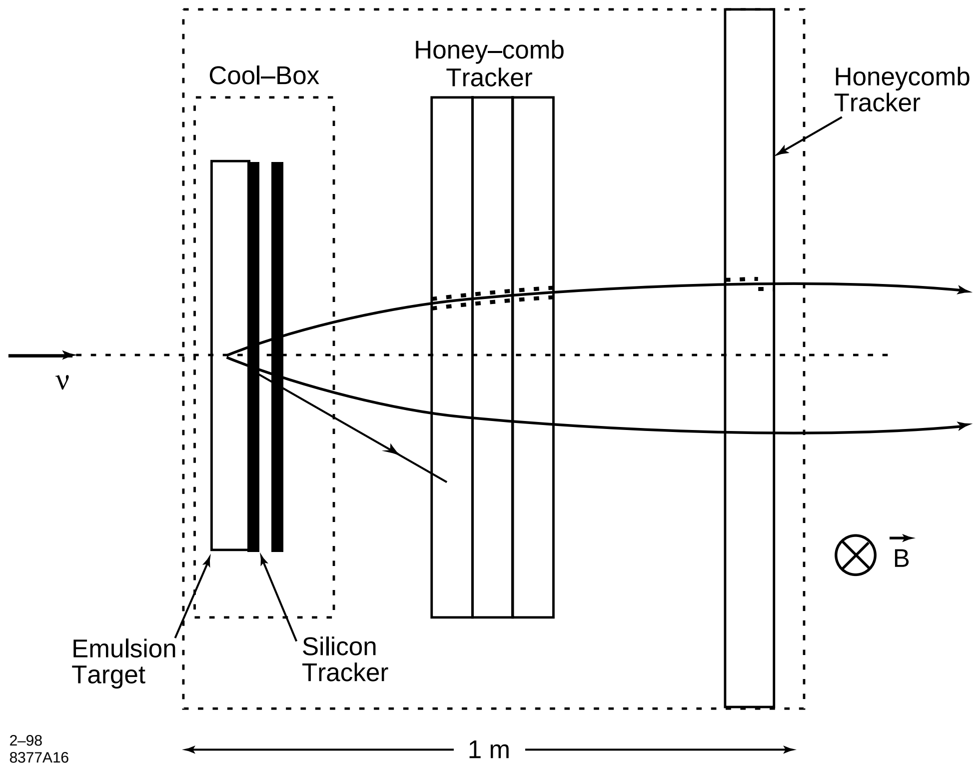

FIG. 61. Proposed design of each of the six tracking modules in the TOSCA experiment.

7.2 Experiments Addressing the Atmospheric Neutrino Anomaly

7.2.1 K2K Experiment

The first confrontation of the atmospheric neutrino anomaly with accelerator neutrinos should be within the framework of the K2K experiment in Japan, based on a neutrino beam from the 12 GeV proton synchrotron at KEK to the Super- Kamiokande detector, 250 km away.[102] The neutrino beam is currently under construction and data taking is scheduled to start early in 1999. The neutrino beam will be a relatively pure ν_μ beam with a 0.7% ν_e component with an average neutrino energy of 1.4 GeV. The expected spectrum at the Super-K site is shown in Fig. 62.

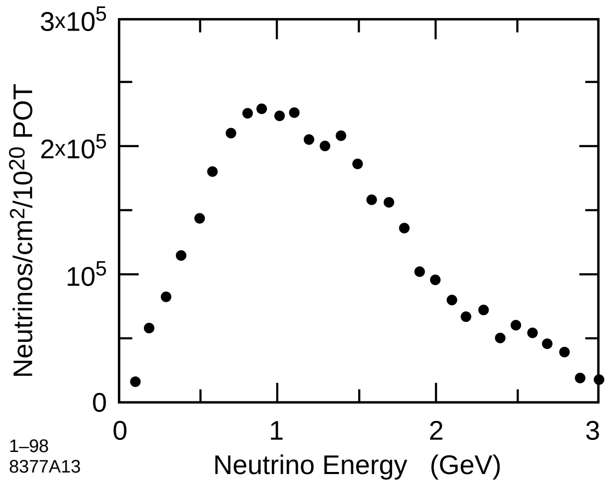

FIG. 62. Calculated neutrino spectrum at the Super-Kamiokande detector from the KEK 12 GeV proton accelerator.

Because the neutrino energy spectrum is below τ threshold, the K2K experiment can investigate only ν_μ disappearance and ν_e appearance. The beam uses a double magnetic horn system and the decay volume is 200 m long. Besides Super-K, there will be two additional detectors, both located on the KEK site: a 1 kt water Cherenkov detector for near/far comparison and a fine-grained detector whose goal is to measure precisely the neutrino flux. It consists of a main target part, composed of scintillator fiber planes interleaved with water "slabs" and followed by a downstream muon detector.

The aim of the experiment is to accumulate 10^{20} protons on target (p.o.t.), with the current synchrotron intensity of 3×10^{12} protons per pulse (ppp) and a 2 sec repetition rate; this will require two to three years of dedicated neutrino running. 10^{20} p.o.t. should give about 400 CC neutrino interactions in the 22 kt fiducial volume of Super-K if no oscillations are present. For oscillation parameters of $\Delta m^2 = 0.01$ eV^2 and $\sin^2 2\theta = 1.0$ only 148 CC ν_μ events would be observed. About 77 ν_e CC events should be observed for these parameters if the oscillation mode is $\nu_\mu \to \nu_e$.

The expected sensitivities for both $\nu_\mu \to \nu_x$ (disappearance) and $\nu_\mu \to \nu_e$ oscillations are shown in Fig. 63. As can be seen, most of the accessible $\nu_\mu \to \nu_e$ region is already excluded by the recent CHOOZ result.[89]

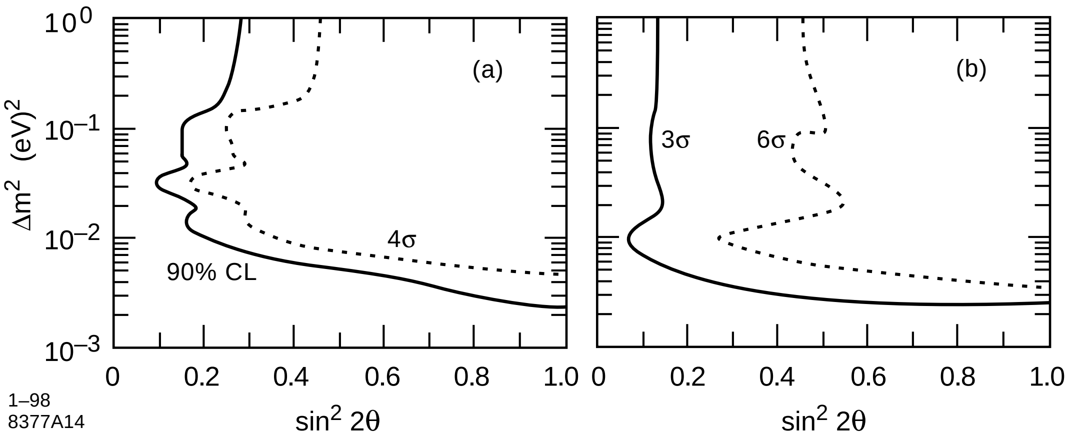

FIG. 63. The expected sensitivity for the K2K experiment for (a) $\nu_\mu \to \nu_x$ disappearance measurement and for (b) $\nu_\mu \to \nu_e$ oscillation..

7.2.2 JHF Program

A more ambitious, but also longer range, Japanese accelerator neutrino program is based on the proposed 50 GeV proton synchrotron within the framework of the Japanese Hadron Facility (JHF).[103] This accelerator is designed to deliver 2 x 10^{14} ppp with a repetition rate of 0.3 Hz. The hope is to have the project approved early in 1998 so that physics experiments could start in 2004.

The neutrino physics program at JHF would use the beam and the detectors from the K2K experiment. Thus, relatively little new construction will be necessary. The neutrino beam would have a significant fraction of neutrinos with energy above τ threshold, i.e., about 3.5 GeV. Studies have begun to see how τ production could be detected in Super-K.

A channel which looks promising is the quasi-elastic τ production followed by $\tau \to \mu\nu\bar{\nu}$ decay in a narrow band beam. The decay muon and the recoil proton can be identified relatively cleanly by the water Cherenkov technique and the subsequent kinematical analysis can reject most of the ν_μ CC background. These studies indicate that 15-20 τ events can be identified with no background for 10^{21} protons on target, if $\Delta m^2 = 0.025$ eV^2 and $\sin^2 2\theta = 1.0$. A 90% C.L. contour for the τ appearance for 10^{21} p.o.t. is shown in Fig. 64.

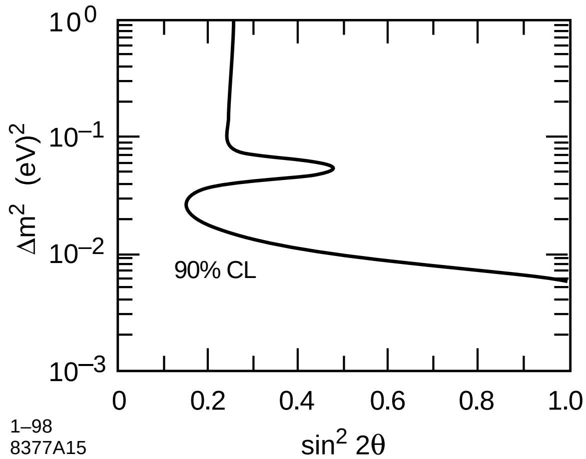

FIG. 64. A 90% C.L. contour on ν_τ appearance in the K2K experiment using the new JHF synchrotron and Super-Kamiokande as the detector.

7.2.3 MINOS Experiment

MINOS (Main Injector Neutrino Oscillation Search)[104] is a long baseline neutrino oscillation experiment designed to explore a large area in the oscillation parameter space, both for the $\nu_\mu \rightarrow \nu_e$ and the $\nu_\mu \rightarrow \nu_\tau$ oscillations. More specifically, for ν_τ oscillation levels close to 0.01 for $\sin^2 2\theta$ should be attainable, and for ν_e close to 2×10^{-3}, and sensitivity should extend to $\Delta m^2 = 0.001$ eV^2 for large mixing angles. In addition, if oscillations are observed, the experiment will be capable of identifying the specific oscillation mode; the oscillation parameters should be measurable with good precision, especially if Δm^2 and $\sin^2 2\theta$ are relatively large. For the region of parameter space suggested by the Kamiokande experiment, the experiment will be able to identify several exclusive τ decay modes on a statistical basis.

The basic experimental method relies on comparing the rates and characteristics of neutrino interactions in two detectors at two widely separated locations, under experimental conditions that are as identical as feasible. Thus the differences in the beam characteristics at the two locations have to be minimized. Furthermore, the two detectors will be made as identical as possible in the important characteristics. Several different experimental measurements will be made to provide redundancy and a check of possible systematics. Among the most important of these measurements are comparison of rates, comparison of the neutral current/charged current ratio and comparison of the total energy spectra of charged current events and of neutral current events.

The far detector will be located in the Soudan mine in Minnesota, approximately 800 m below the ground level. In the past, the Soudan mine was an important high grade iron mine but the mining now has been discontinued. Currently, the Soudan site is maintained as a state historical park, which results in a high level of safety and availability of certain infrastructure necessary for the running of the experiment. At the present time there is located in the mine an operating fine-grained detector Soudan 2, approximately 1 kt in mass.[105] It was originally designed to search for proton decay and is currently used for that investigation as well as for the study of atmospheric neutrinos. This detector will also be used as part of the MINOS experiment but its small mass would not allow achievement of the sensitivity desired by MINOS. Accordingly, it is planned to construct a new, larger detector to be located in another neighboring cavern to be excavated during the period 1998-2000. It would be of comparable size (about 80 x 14 x 14 m) as the existing cavern but would point towards Fermilab. The proposed layout of the whole Soudan MINOS experimental area is shown in Fig. 65.

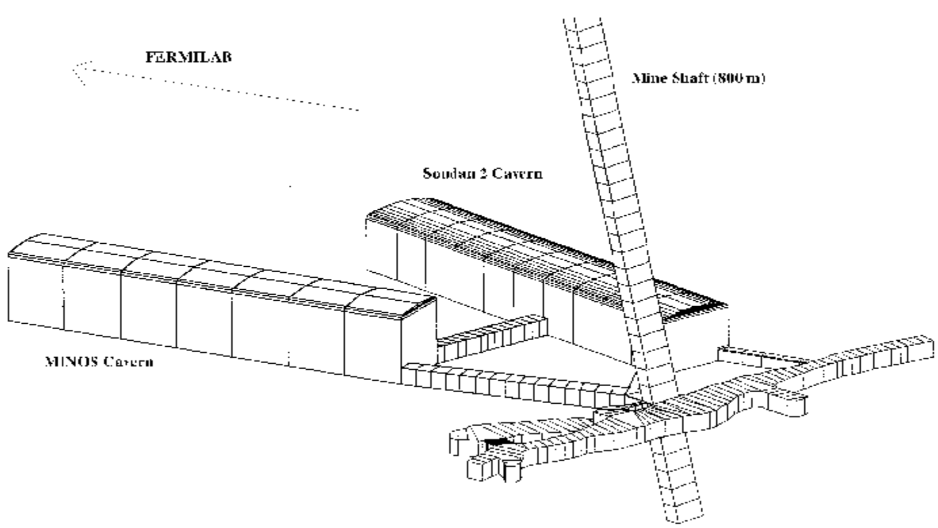

FIG. 65. The layout of the proposed Soudan MINOS experimental area together with the existing cavern housing the Soudan 2 detector.

The new MINOS far detector will be based on magnetized iron octagons, 8 m in diameter, 2.5 cm thick, with a toroidal field, and a total mass of about 8 kt.[106] The average B field will be about 1.5 T. A schematic of this detector is shown in Fig. 66. Active detector elements consisting of planes of solid scintillator strips, with wavelength shifting fiber imbedded in each strip for the readout, will be placed between the steel plates. The dimensions of the scintillator strips would be up to 8 m in length, 4 cm in transverse dimension, and 1 cm thick. A schematic of the proposed scintillator module, showing the routing of the optical signals from the scintillator to photomultiplier is illustrated in Fig. 67.

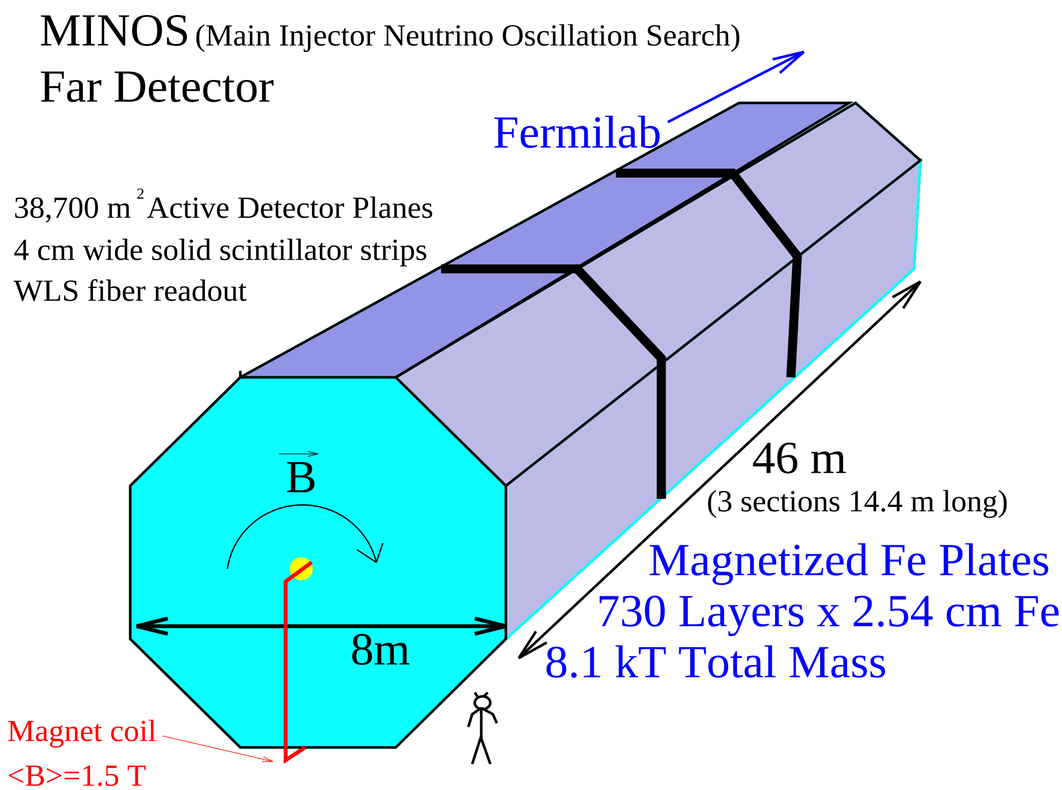

FIG. 66. Schematic drawing of the proposed MINOS detector.

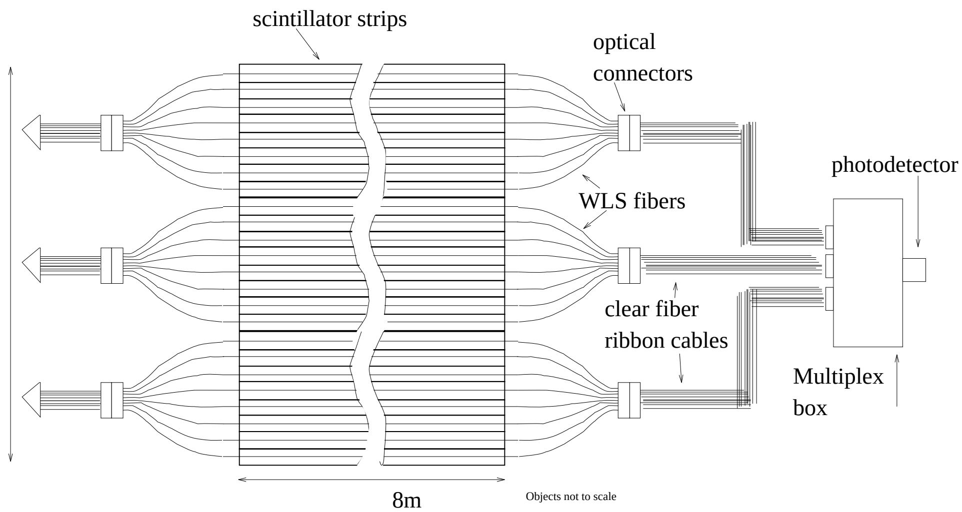

FIG. 67. Sketch of a proposed scintillator module for the MINOS detector. The system is left-right symmetric; the routing on the left side was omitted in the sketch for simplicity.

The near detector, on Fermilab site, will be as identical as possible to the far detector, except for the size. The location of the near detector will be about 500 m downstream of the end of the decay volume. The location is a compromise between the cost, which increases as one moves further downstream, and the desire to be as far downstream as possible so as to minimize the spectrum differences in the neutrino flux. It is planned to use only the central part of the near detector for comparison with the far detector for different physics measurements because the energy spectrum of the ν flux in that region is most similar to the spectrum at the far detector.

As mentioned earlier, the Soudan 2 detector will be operational during MINOS data taking and should provide complementary information. Its relatively low mass, and hence poorer statistics, will be compensated somewhat by its much finer granularity. That detector should be ready to take data immediately when the first ν flux will become available. In addition, the MINOS Collaboration is investigating the possibility of having an emulsion-based detector, capable of detecting τ's on an individual basis, upstream of the main detector.

The 90% C.L. limits that can be set on both $\nu_\mu \to \nu_e$ and $\nu_\mu \to \nu_\tau$ oscillations are illustrated in Fig. 68, assuming a two year long exposure of a 8 kt detector in the neutrino wide band beam discussed above in section 7.1.1. The several curves displayed in Fig. 68 correspond to different experimental measurements. The most sensitive test for ν_τ oscillations is the NC/CC ratio (curve A). Even though it is not as powerful statistically as the total rate measurement, it is relatively immune to differences in the ν energy spectra at the two locations and to the total relative normalization of the fluxes. The relative rate measurements of the ν_μ CC process (curve B) at the two detectors are the most powerful statistically; however, it is not clear at this time whether the systematic error on these measurements can be brought down below 2%.

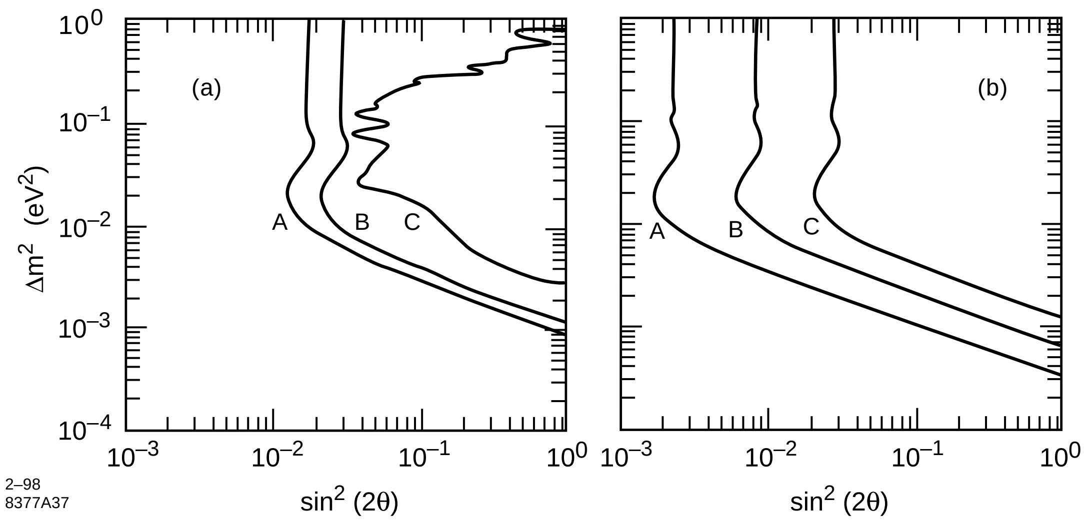

FIG. 68. Projected MINOS sensitivity to $\nu_\mu - \nu_\tau$ (a) and $\nu_\mu \rightarrow \nu_e$ (b) oscillations. Different curves correspond to different independent measurements.

Study of the CC total energy spectra (curve C) can provide an oscillation-mode-independent determination of the oscillation parameters. Good total energy resolution helps to extend the reach here, especially for large values of Δm^2. Optimization of this measurement was one argument for preferring scintillator over gas detectors. For low values of Δm^2 (around $10^{-3} eV^2$) variation in the relative energy scale could be an important source of systematic error and a limitation on this technique.

It is hoped that the construction of the far detector can start sometime in 1999. If these optimistic projections pan out, the experiment could commence taking data sometime in the year 2002 with the Soudan 2 detector and 1/3 of the MINOS far detector. The complete 8 kt detector could be finished about two years later. At the present time the MINOS collaboration consists of almost 200 individuals, representing 23 institutions from four countries: China, Great Britain, Russia, and the United States.

7.2.4 Possibilities in Western Europe

As mentioned above, the long baseline neutrino program in Western Europe, if it materializes, will be based on a new beam and detectors in the Gran Sasso Laboratory. There has been a significant amount of effort to date in the European community to design detectors optimized for study of potential neutrino oscillations with oscillation parameters suggested by the Kamiokande and Super-K atmospheric neutrino results. We shall describe these efforts below, albeit very briefly, since the situation is still quite fluid.

(a) ICARUS. The first 600 ton module of this detector is being built and is scheduled for installation in Gran Sasso in 1999. ICARUS is a large liquid argon chamber relying on the TPC principle to collect space points.[107] Its advantages are continuous sensitivity, capability of self-triggering, ability to provide three-dimensional images of ionizing tracks, and dE/dx measurements permitting some particle identification. Independent of the long baseline developments, ICARUS will be a powerful tool for studies of solar neutrinos, for proton decay search and for detection of future supernova neutrinos.

The ICARUS development program has now been in existence for over a decade. A 40 l prototype has been located now in the CERN neutrino beam for some time and a larger, three-ton prototype has been in operation at CERN since May 1991 and has provided a great deal of information about operational issues.[52]

The eventual plans call for construction of at least two additional ICARUS modules, giving a total detector mass of close to 1.8 kt. A schematic of the 600 ton module is shown in Fig. 69.

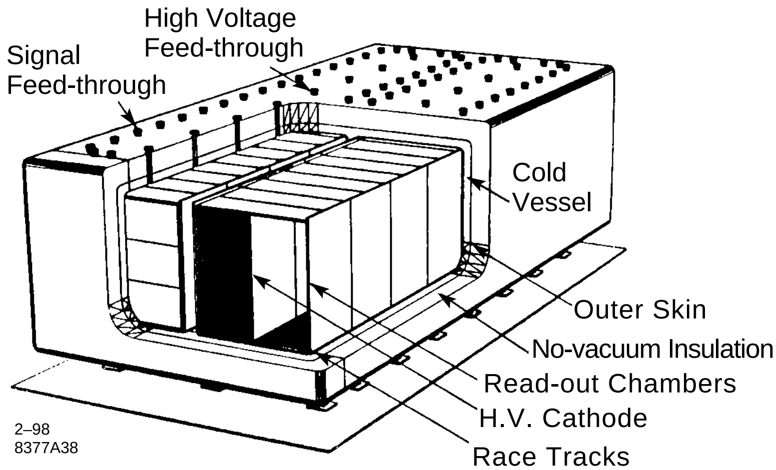

FIG. 69. Schematic drawing of the 600 ton ICARUS detector currently under construction.

(b) Neutrino Oscillation Experiment (NOE) is a more conventional detector consisting of non-magnetic target modules followed by a muon spectrometer downstream.[108] The target modules are composed of 13 cm x 13 cm x 8 m long submodules, made of scintillating fibers imbedded in taconite iron ore. They are viewed at each end by a 1.5” photomultiplier tube. The total mass of the proposed NOE detector is about 6 kt. The cross section of the target module is shown in Fig. 70.

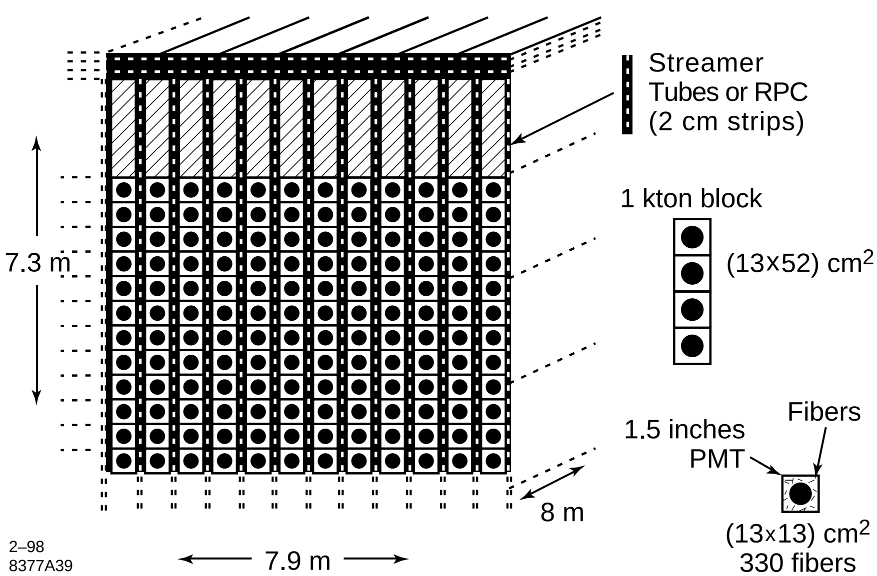

FIG. 70. Cross section of the proposed NOE detector. The detector would consist of four 8 m long target modules (illustrated above) followed by a muon spectrometer.

(c) RICH detector is a 27 kt water Cherenkov detector with focusing.[66] It is proposed as five equivalent sections, each one 20 m long and 18.6 m in diameter with a focusing mirror of 20 m curvature at the end. The focused light is detected by a planar array of hybrid photo detectors (HPD) located 11.5 m downstream of the mirror center of curvature. 20% coverage of the area with HPD's is proposed. A drawing of the proposed detector was shown earlier in Fig. 23.

(d) OPERA. This detector would be based on emulsions.[109] A module would consist of a τ detection region, composed of two emulsion sheets with a very low density material in between. Each emulsion sheet would have 50 μm layers on both sides of a 100 μm plastic sheet. Thus, two high quality track segments could be measured on each side of the low density material, allowing detection of the τ decay kink in the low density volume. The principle of this OPERA concept is illustrated in Fig. 71.

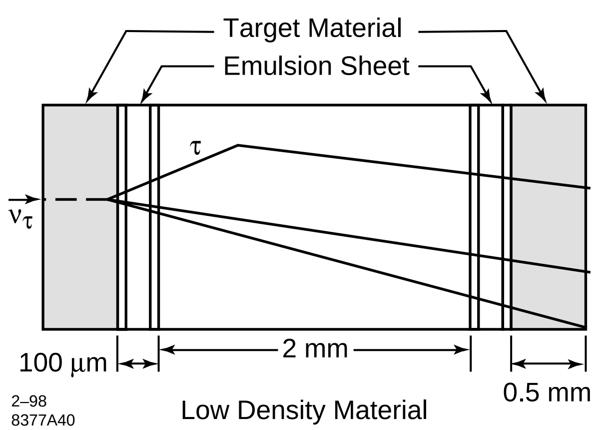

FIG. 71. Illustration of the OPERA concept for detection of tau's in a neutrino beam.

All of these detector schemes claim a comparable (within a factor of two) sensitivity to potential neutrino oscillations: about 2×10^{-3} eV^2 in Δm^2 reach and 2×10^{-2} in $\sin^2 2\theta$ reach in one to two years running.

7.3 LSND Effect

We have already discussed, in a previous chapter, the ongoing KARMEN experiment which should soon be able to confront directly the LSND oscillation result. In this section we shall focus on other efforts around the world, which, starting from scratch, aim to verify and study the LSND anomaly.

7.3.1 BooNE Proposal at Fermilab

This effort aims to study the LSND effect at neutrino energies a factor of ten higher than available at Los Alamos.[110] The proposal is to use the 8 GeV proton beam from the Fermilab booster to generate a relatively pure ν_μ beam in the energy range of 0.5 - 1.5 GeV. The relatively low K/π production ratio at these energies means that the ν_e contamination in the neutrino beam will be quite low.

The main thrust of this proposed experiment would be to look for the appearance of the ν_e signal. The proposed detector is quite similar to the LSND detector. Its proposed location is about 1 km downstream of the end of the decay pipe. The total proposed mass for the detector is 600 tons (400 tons fiducial volume); there is an inner (detector) tank volume, surrounded by an external veto shield. The inner volume is filled with mineral oil, with a possible low concentration of scintillator fluors. The outer volume would be filled with conventional, mineral oil based liquid scintillator. The plan is to use 1200 phototubes, which would provide a 10% coverage of the total detector inner area.

The particle identification would be done by combining all the available information. Thus, most of the ν_μ CC events could be identified by the presence of a muon in the outer (veto) detector region. The ratio of late and early hits (i.e., scintillation and Cherenkov light) would allow one to separate electrons from heavier particles. Finally, the opening angle between the two γ's from π^o decay would allow one some discrimination between e's and π^o's.

The proponents claim to be able to reach sensitivity of 6 x 10^{-4} for the $\nu_\mu \to \nu_e$ oscillations at high Δm^2. In the most interesting LSND-suggested region ($\Delta m^2 \sim 1$ eV^2) they claim to have sensitivity roughly a factor of five better then LSND.

7.3.2 Possibilities at CERN

A couple of years ago there was a significant interest in Europe to explore the possibility of using the West Area neutrino beam together with a detector in the Jura mountains to study possible neutrino oscillations in the intermediate L/E range (L/E of the order of unity).[111] Because of the mountainous topography in the region, several adequate locations appeared available. There were discussions about both ICARUS and OPERA detectors being located there. The recent decision by CERN to shift their neutrino effort away from the West Area puts an end (at least temporarily) to these possibilities.

There is some discussion currently about using the old neutrino beam from the CERN PS for an oscillation experiment probing this LSND-motivated region. Whether such an experiment has a chance of coming to fruition is unclear at the present time.[60]

7.4 Solar Neutrino Anomaly — KamLand

The solar neutrino anomaly, if interpreted as due to neutrino oscillations, is quite difficult to test in terrestial accelerator or reactor experiments because of the very large required value of L/E, (about 10^5) due to small Δm^2. The limitations due to the size of the earth (diameter of about 12,000 km) dictate that such an experiment would have to use neutrinos in the MeV range, i.e., reactor neutrinos. Because of the large L/E and small size of the neutrino cross section in the few MeV range, the detector would have to be quite large. Thus, the issue of backgrounds can potentially be very significant.

There is an ambitious Japanese effort, named KamLand, which may develop into a U.S.-Japan Collaboration, to overcome all of these difficulties with a large, 1 kton liquid scintillator detector, to be installed in the underground cavity where the Kamiokande detector was located.[111] A schematic cross section of such a detector is shown in Fig. 72. This detector would look for interactions of $\bar{\nu}_e$'s produced at several Japanese reactors around the site, typically some 150-250 km away. Since Japanese reactors undergo periodic maintenance, in the fall and spring of each year, there would be a periodic modulation of the $\bar{\nu}_e$ interaction rate from the reactors which would allow one to measure the backgrounds.

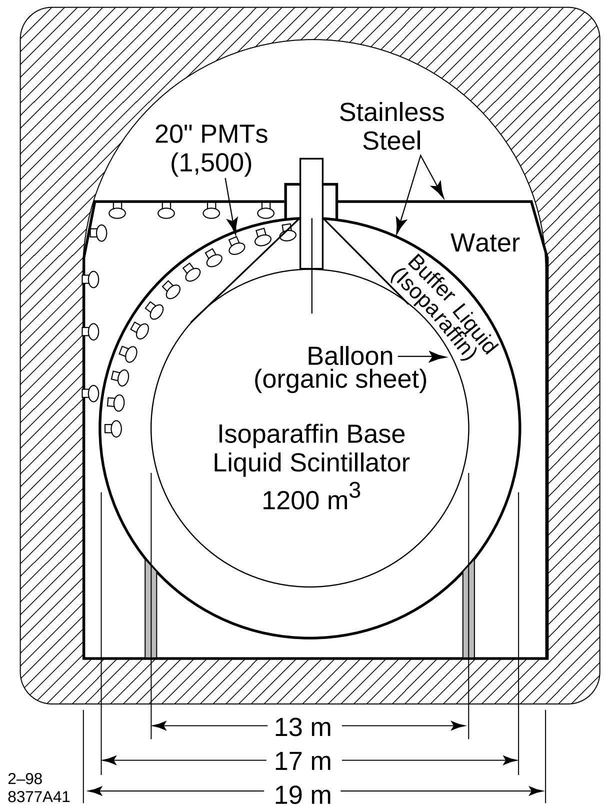

FIG. 72. Schematic drawing of the cross section of the KamLand detector.

The estimated reactor-associated neutrino signal in KamLand would be about 2 events/day, assuming no oscillations. The expected sensitivity for three years of running is $\Delta m^2 > 7 \times 10^{-6}\ eV^2$ for large $\sin^2 2\theta$ and $\sin^2 2\theta > 0.2$ for large Δm^2. According to stated plans, the data taking could begin in 2001.

TABLE 3.

Ratios of measured and calculated (no oscillations) integrated yields.

Position	Ratio
15 m	0.996 ± 0.004 (stat) ± 0.05 (syst)
40 m	0.994 ± 0.010 (stat) ± 0.05 (syst)
95 m	0.915 ± 0.132 (stat) ± 0.05 (syst)

The same ratio, plotted as a function of the positron energy, is shown for these three distances in Fig. 37. The $\bar{\nu}_e$ energy is, to a high precision, given by

$$E_{\bar{\nu}} = E_{e^+} + 1.8 \ \ \mathrm{MeV}\,.$$

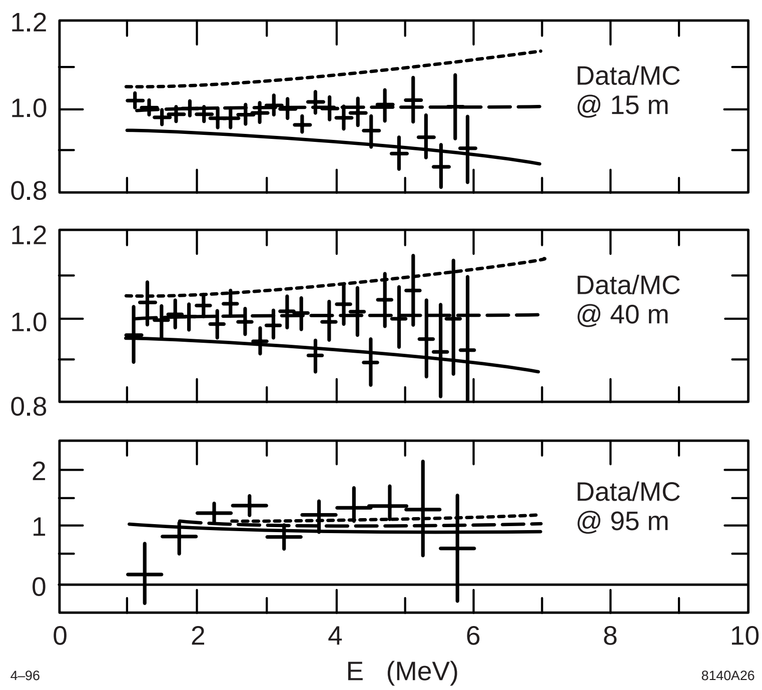

FIG. 37. The ratio of the observed and predicted positron spectra (assuming no oscillations) from the Bugey reactor experiment at detector distances of 15 m, 40 m, and 95 m. The indicated band corresponds to the estimated systematic error.

The limits imposed by the Bugey experiment, together with the limits from two other reactor experiments, at Krasnoyarsk[87] and Gösgen,[88] are shown in Fig. 38. Also shown is the region suggested by the Kamiokande results if they are interpreted under the hypothesis of $\nu_\mu \rightarrow \nu_e$ and $\nu_e \rightarrow \nu_\mu$ oscillations. As can be seen, most of the Kamiokande suggested region, except for the lowest Δm^2, is excluded by the reactor data.

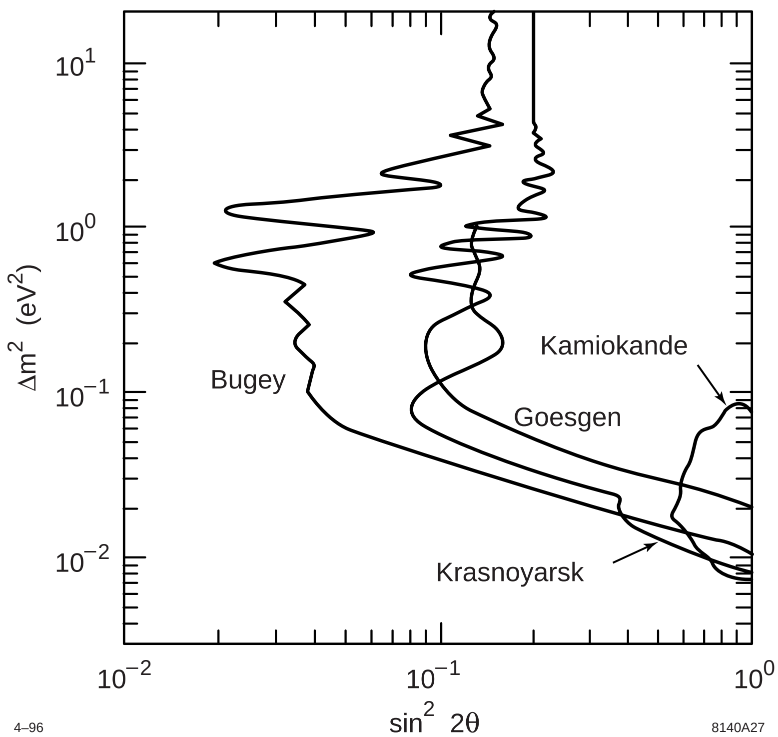

FIG. 38. The 90% C.L. exclusion contour from the Bugey experiment. Also shown are the previous limits from the Gösgen and Krasnoyarsk experiments, and the favored region from the Kamiokande experiment calculated on the basis of $\nu_\mu \rightarrow \nu_e$ oscillation hypothesis.

6.1.2 Experiments in Progress: CHOOZ and Palo Verde

The desire to explore fully the Kamiokande region by extending the sensitivity to smaller values of Δm^2 motivated initiation of two experiments with much longer baselines, about 1 km. One of these was with the $\bar{\nu}_e$ flux from the reactor near the village of Chooz in France;[48] the other at Palo Verde in Arizona, USA.[49] The detection methodology is quite similar in both cases; its main difference from the method employed at Bugey lies in the fact that one uses gadolinium (dissolved in liquid scintillator), rather than lithium to capture the neutrons. Neutron capture on gadolinium is accompanied by the release of 8 MeV of γ ray energy. The similarities and differences between the CHOOZ and Palo Verde experiments are shown in Table 4.

TABLE 4.

Comparison of CHOOZ and Palo Verde Experiments		
Experimental Characteristics	CHOOZ	Palo Verde
Reactor Power (Thermal)	8.4 GW	10.9 GW
No. Reactor Units	2	3
Reactor-Detector Distance	1000/1100 m	850/740/850 m
Detector	Homogeneous	Segmented
Detector Mass	5 Tons	12 Tons
Event Rate (no osc.)	25/Day	51/Day
Efficiency of Detection	80%	26%
Overburden	300 mwe	46 mwe
Calculated Background Rate	1-3/Day	34/Day
Start of Data Taking	March 1997	Spring 1998

As can be seen from the Table the main advantages of the CHOOZ experiment are the earlier start-up and a much lower background rate due to better shielding of the detector. The latter is due to the fact that the CHOOZ detector is located in a tunnel under a mountain; the Palo Verde detector is in a cavern, specially excavated for this experiment. At the time of these lectures no physics results were available from either experiment; since that time, however, CHOOZ has obtained significant negative results.[89] We discuss them next.

The CHOOZ experiment recently reported results based on data taken during the period from March to October, 1997, when the two reactor units ran at power levels varying from zero to full power. Thus, both the background level and the full power neutrino rate could be measured and compared with the predictions. The neutrino events were identified by having appropriate neutron capture energy (about 8 MeV), not too long a delay between the positron and neutron signals (2-100 msec) and spatial cuts on the positron and neutron locations (n--e^+ distance < 100 cm, and distance from the vessel wall > 30 cm). The relevant experimental distributions are shown in Fig. 39. The resulting neutrino counting rate as a function of the reactor power is shown in Fig. 40. The measured background rate (both from extrapolation to zero reactor power and from reactor-off measurement) is consistent with the estimated rate of 1.03 ± 0.21/day. The ratio of measured to expected neutrino signal is

$$R_{meas/exp} = 0.98 \pm 0.04 \text{ (stat)} \pm 0.04 \text{ (syst)}$$

indicating no evidence for neutrino oscillation.

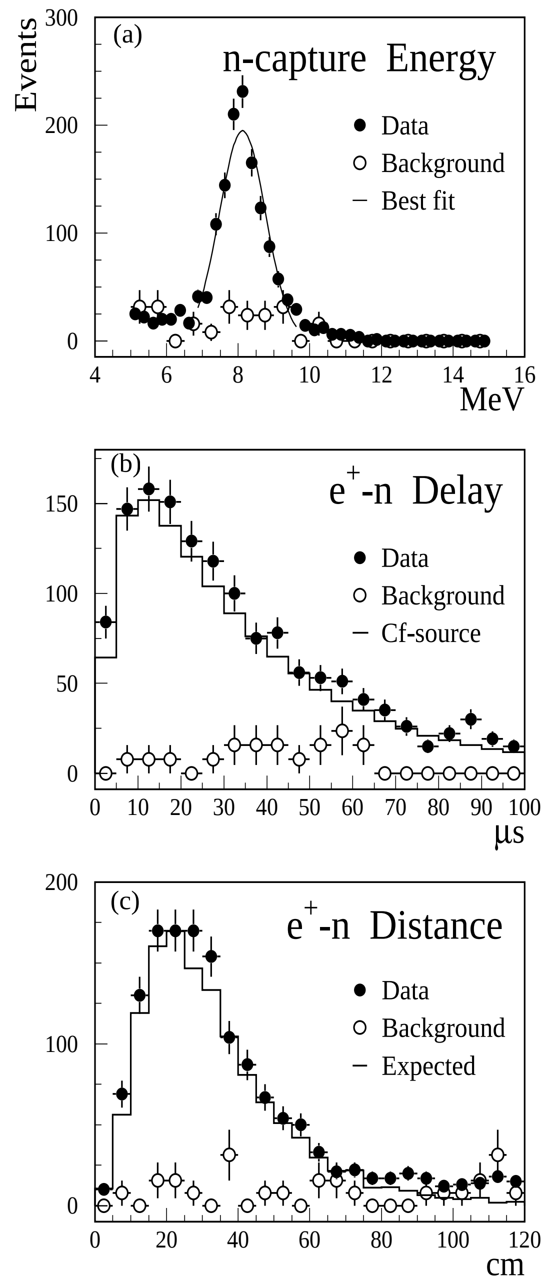

FIG. 39. Distribution of: (a) energy released by *n*-capture on Gd, (b) *n*-capture delay, (c) positron-neutron distance, measured and MC expected; the reactor-off background distribution is also shown. The histograms in (b) and (c) are normalized to the background-subtracted experimental data.

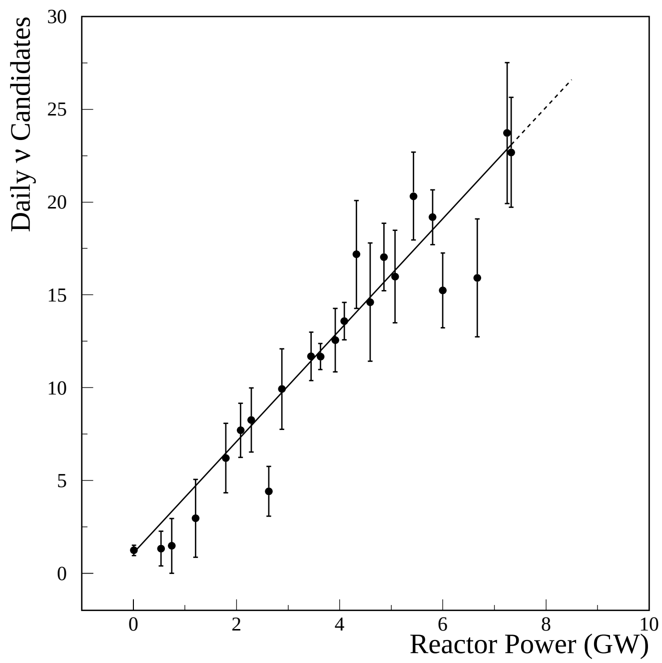

FIG. 40. Number of $\bar{\nu}_e$ -candidates per day, as a function of the reactor power.

In addition, one can compare the measured and the expected positron energy spectra. This comparison is shown in Fig. 41 and confirms the conclusion of no oscillations. The resulting 90% C.L. exclusion plot, together with the results of other relevant experiments is shown in Fig. 42. In summary, no evidence for disappearance $\bar{\nu}_e \rightarrow \bar{\nu}_x$ is seen for the parameter region corresponding to $\Delta m^2 > 0.9 \times 10^{-3}$ eV^2 for maximum mixing and $\sin^2 2\theta > 0.18$ for large Δm^2.

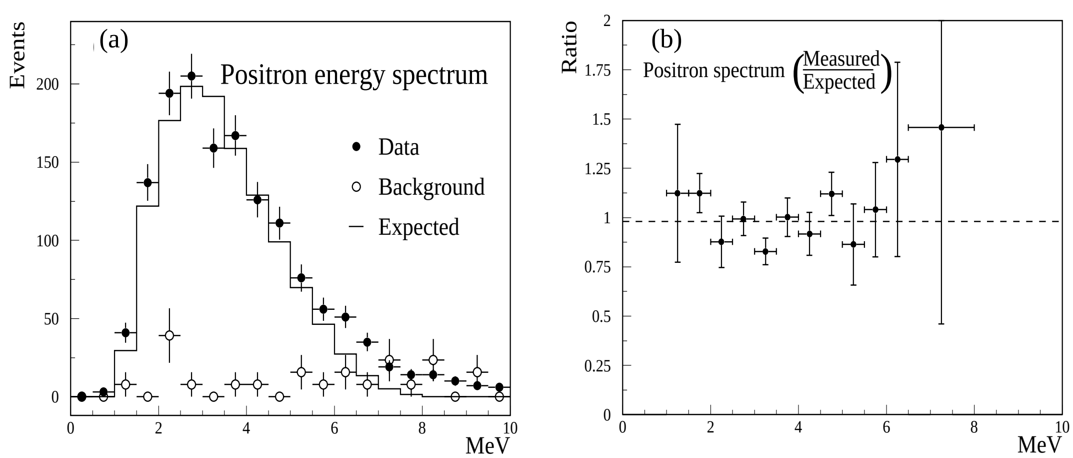

FIG. 41. (a) Positron energy spectrum and corresponding reactor-off background for the same live-time; the neutrino-signal expected positron spectrum is also shown. (b) Ratio of the measured (background subtracted) to the expected positron spectrum.

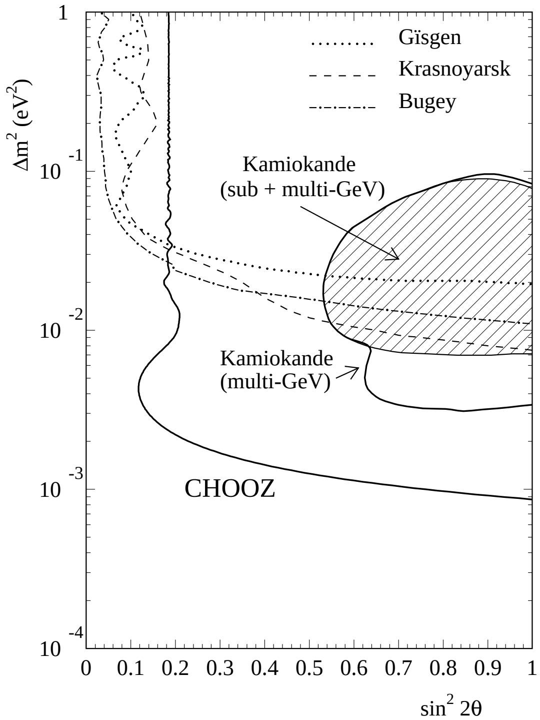

FIG. 42. The 90% exclusion contour from the CHOOZ experiment, together with the previous experimental limits and the favored region from the Kamiokande experiment calculated on the basis of $\nu_\mu \rightarrow \nu_e$ oscillation hypothesis. Note that a linear scale is used for the $\sin^2 2\theta$ axis.

The Palo Verde experiment should begin to start data taking early in 1998. As discussed above, its main challenge will be to overcome the much higher cosmic ray associated background rates due to its relatively shallow depth. The main estimated background source are the chance coincidences of neutrons produced around the detector by cosmic ray muon interactions. To reduce background as much as possible, the detector has been segmented into many individual modules, so as to get cleaner identification of the neutrino events. This segmentation allows one to require a four-fold coincidence for the signal: positron, the two annihilation γ rays, and neutron capture γ rays. The first three signals are prompt; the neutron capture signal is delayed. The detection principle is illustrated in Fig. 43. The expected sensitivity of this experiment is comparable to that of CHOOZ.

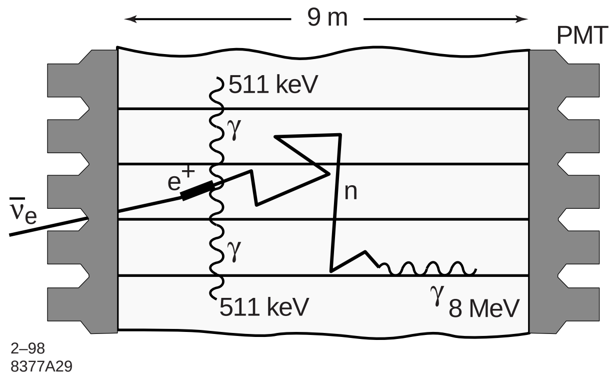

FIG. 43. The detection principle of the Palo Verde experiment.

6.2 $\bar{\nu}_\mu \to \bar{\nu}_e$ at Low Energies

At the present time the only positive indication of neutrino oscillations from accelerator or reactor experiments comes from an experiment at LAMPF looking for oscillations of $\bar{\nu}_\mu$ from μ^+ decays at rest and from ν_μ from π^+ decays at relatively low energies. These results are controversial because they still wait to be confirmed by an independent experiment. In this section we discuss the current situation in this area.

6.2.1 LSND Experiment

The initial LSND (Liquid Scintillator Neutrino Detector) experiment searched for $\bar{\nu}_\mu \to \bar{\nu}_e$ oscillations using $\bar{\nu}_\mu$ from μ^+ decays at rest.[90] A low energy beam of π^+, produced by protons in a water target, was allowed to stop in a copper dump downstream; π^+ would decay into μ^+ which subsequently would decay into e^+, $\bar{\nu}_\mu$, and ν_e. The overall layout of the experiment is shown in Fig. 44. The detector is a cylindrical tank filled with 167 tons of liquid scintillator viewed by 1280 8" photomultipliers placed on the inside walls of the tank. The fluor concentration is rather low so that Cherenkov and scintillator signals are comparable. To achieve good sensitivity one needs to suppress $\bar{\nu}_e$ from other sources, the most obvious one being the $\pi^- \to \mu^- \to e^- \nu_\mu \bar{\nu}_e$ decay chain. This is accomplished by suppressing the unwanted $\bar{\nu}_e$ in the following ways:

(a) Having the proton beam interact on a water target enhances π^+ production over π^- by roughly a factor of eight.

(b) π^- are captured when stopped. Thus the only π^- decays which can occur are those from π^- in flight, i.e., only about 5% of the total π^- flux.

(c) μ^-, when stopped in copper, undergo preferentially a nuclear capture, with only 12% of them decaying.

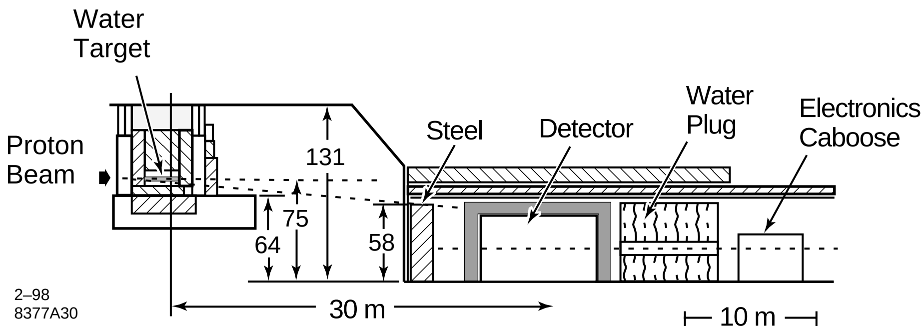

FIG. 44. Detector enclosure and target area configuration in the elevation view for the LSND experiment.

All of these factors taken together give a relative suppression of 7.8 x 10^{-4} of $\bar{\nu}_e$ from the $\pi^- \to \mu^- \to e^-$ decay chain with respect to $\bar{\nu}_\mu$ from the $\pi^+ \to \mu^+ \to e^+$ sequence.

The two other important backgrounds that need to be considered are ν_e interactions (the LSND detector does not measure sign of the electrons) and cosmic ray interactions. The first contribution is suppressed mainly by the requirement that one requires observation not only of the signal from the e^+, produced via

$$\bar{\nu}_e + p \to e^+ + n,$$

but also the signal from the subsequent neutron capture

$$n + p \to d + \gamma,$$

i.e., the 2.2 MeV γ ray. The ν_e's will not give a correlated neutron. Furthermore, the two dominant ν_e capture reactions:

$$\nu_e + {}^{12}C \to e^- + {}^{12}N$$

$$\text{and } \nu_e + {}^{12}C \to e^- + n + {}^{11}N$$

yield maximum electron energies of 36 and 20 MeV respectively. Thus, a cut on the observed electron energy can provide a significant additional suppression.

The cosmic ray background can be measured very accurately by utilizing the fact that the duty cycle of LAMPF is only 7%. Thus accumulating data during the beam-off period can give a good statistical measurement of that background.

As the above discussion should indicate, a key feature of the experiment must be its ability to identify correlated positron signals and neutron capture signatures. This is done by using an algorithm dependent on the following measurements: temporal separation of e^+ and n capture signals, spatial separation of these two signals, and number of photomultiplier hits composing the putative signal due to the γ from neutron capture. One can study these distributions for both correlated and uncorrelated signals using the cosmic ray neutron data. In the cosmic ray data the correlated signals will originate from a neutron scatter followed subsequently by neutron capture. The results of such a study are shown in Fig. 45.

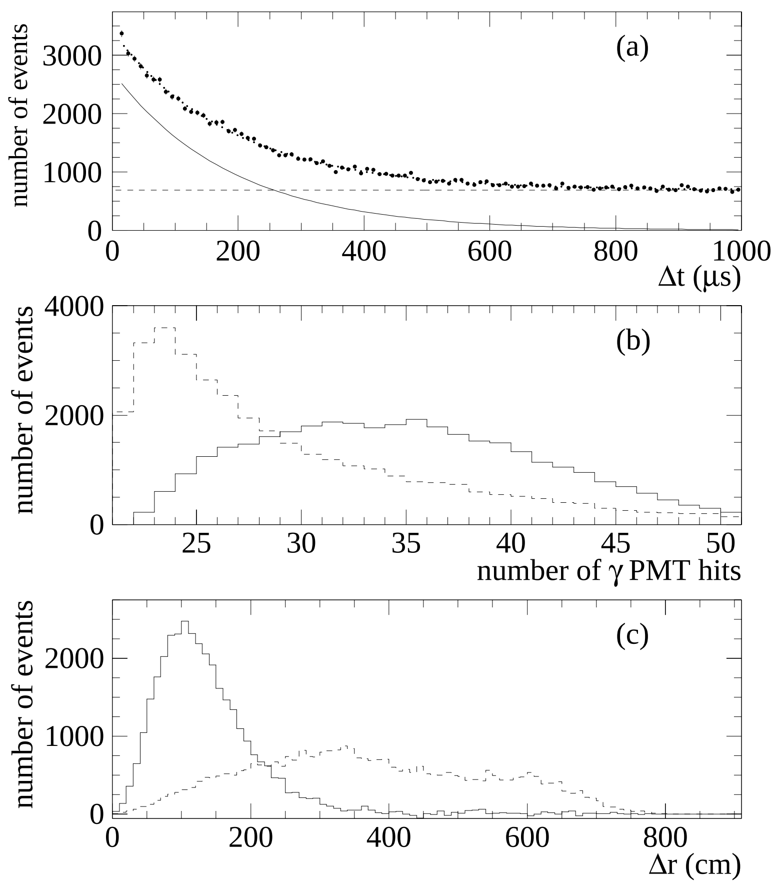

FIG. 45. Distributions obtained from cosmic-ray neutron data for γ's that are correlated (solid) or uncorrelated (dashed) with the primary event: (a) the time between the photon and the primary event;

(b) the number of photon PMT hits; (c) the distance between the photon and primary event. The raw data points are also shown in (a).

Based on the distributions discussed above, one can calculate a discriminant function R defined by:

$$R = \frac{\text{likelihood that the prompt (i.e., } e^{+}\text{) and delayed signals are correlated}}{\text{likelihood that the two signals are accidential}}$$

where the likelihood for each possibility is defined as the product of the three individual probabilities for each hypothesis, i.e.,

$$L = P(\#\text{ of hits})\ P(\Delta t)\ P(\Delta r).$$

The candidate events are subjected to a number of cuts (including $20 < E_e < 60$ MeV) and the R value is calculated for the remaining sample, both for the beam-on and beam-off conditions. The true accelerator sample can then be obtained by subtracting an appropriate fraction of the beam-off distribution. The R distribution for this sample is shown in Fig. 46, together with the best fit to the data and the expected contributions from both the correlated and uncorrelated (i.e., background) components. Clearly an excess at large R is observed if compared with the distribution due to the uncorrelated component only. This excess is interpreted as possible $\bar{\nu}_\mu \to \bar{\nu}_e$ oscillations and the sample with $R > 30$ is used for subsequent studies of this hypothesis.

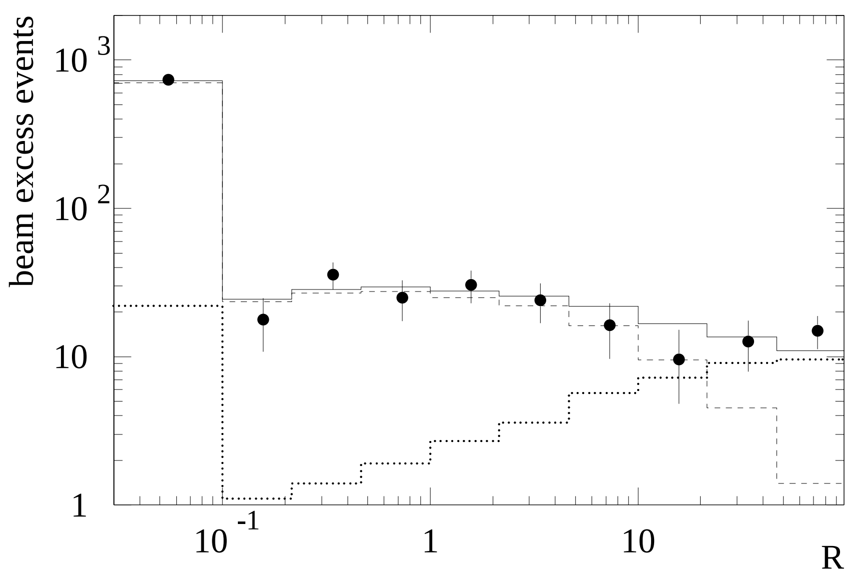

FIG. 46. The R distribution, beam-on minus beam-off excess, for events that satisfy selection criteria and that have energies in the range $20 < E_e < 60$ MeV. The solid curve is the best fit to the data, the dashed curve is the uncorrelated γ component of the fit, and the dotted curve is the correlated γ component.

The various checks performed on the data lead the authors to argue that the data are consistent with the hypothesis of $\bar{\nu}_\mu \rightarrow \bar{\nu}_e$ oscillations; after tight cuts, 22 events have been identified with the e^+ energy between 36 and 60 MeV where only 4.6 ± 0.6 background events were expected. This corresponds to an oscillation probability of $(0.31 \pm 0.21 \pm 0.05)\%$ when averaged over the experimental energy and spatial acceptance. The experiment is not able to discriminate well between different values of the two oscillation parameters, Δm^2 and $\sin^2 2\theta$. The level of its sensitivity in this area is shown in Fig. 47 where the signal events are displayed as a function of L/E_ν and compared with the expected distributions for three different oscillation hypotheses.

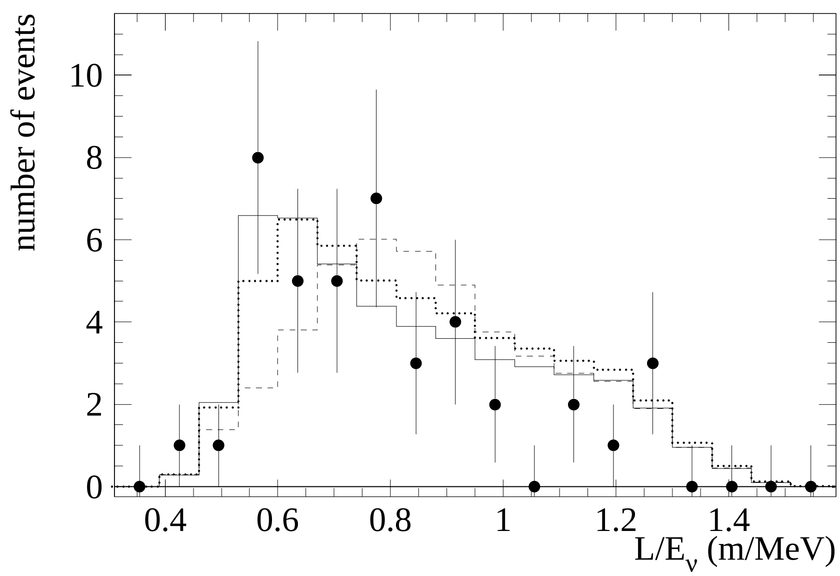

FIG. 47. Distribution of L/E_ν for the beam-on data with high R compared with the expected distributions at ($19\ \mathrm{eV}^2$, $\sin^2 2\theta = 0.006$: solid line), ($4.3\ \mathrm{eV}^2$, $\sin^2 2\theta = 0.01$: dashed line), and ($0.06\ \mathrm{eV}^2$, $\sin^2 2\theta = 1.$: dotted line).

A parallel effort has been made to investigate the behavior of ν_μ from π^+ decay in flight.[91] The systematics for this search will be quite different, but the investigation is made more difficult by the fact that there is no supplementary neutron capture signature, the searched-for reaction being

$$\nu_e + C \rightarrow e^- + N.$$

Two different analyses, labeled A and B, have been performed and they both find an excess of events above what one would expect from the known background sources. Their results are shown in Table 5.

TABLE 5.

Results from Decay-in-Flight Analyses					
Analysis	Signal Events	Backgrounds		Excess	Oscillation Probability
		Beam Unrelated	Beam Correlated		
A	23	5.3 ± 2.3	5.3 ± 2.0	12.4 ± 5.7	$(3.4 \pm 1.3) \times 10^{-3}$
B	25	8.5 ± 2.9	5.9 ± 2.5	10.1 ± 6.3	$(1.7 \pm 0.8) \times 10^{-3}$

The allowed contours in the Δm^2 - $\sin^2 2\theta$ space from the two experiments are compatible with each other. They are displayed together in Fig. 48. The data taking is continuing, with slightly altered conditions to change the systematics, and the experiment is scheduled to run for about eight months of data taking in 1998.

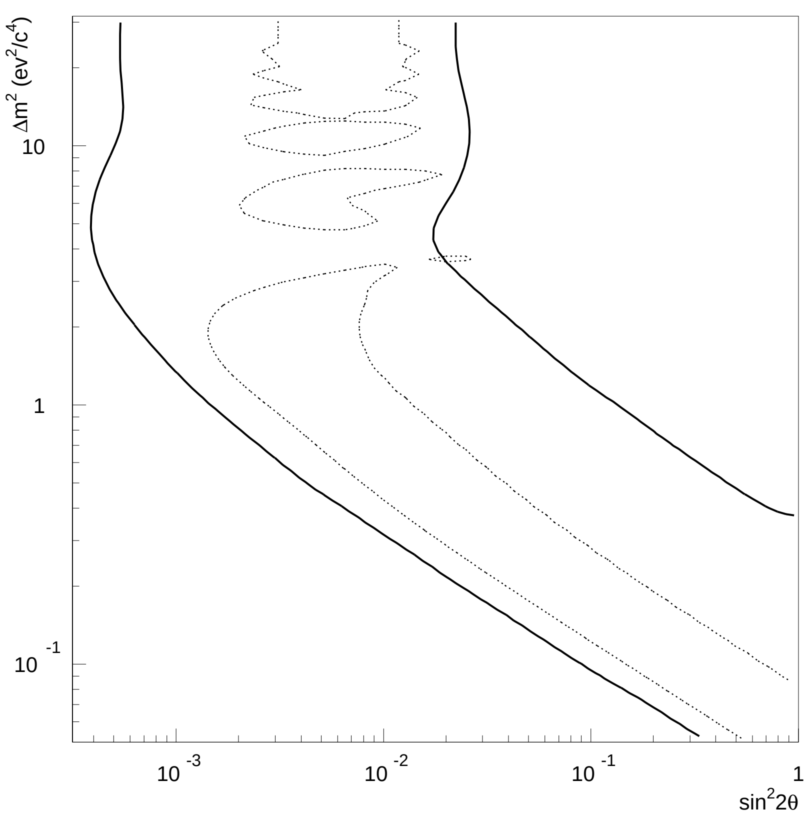

FIG. 48. The 95% confidence region for the decay-in-fight $\nu_\mu \rightarrow \nu_e$ analysis (solid) along with the favored regions for the LSND decay-at-rest measurement for $\bar{\nu}_\mu \rightarrow \bar{\nu}_e$ (dotted).

6.2.2 KARMEN Experiment

An experiment similar to LSND, named KARMEN (KArlsruhe Rutherford Medium Energy Neutrino experiment) has been performed at the ISIS spallation source at Rutherford-Appleton Laboratory in Great Britain by a British-German collaboration. The main differences between the two experiments are:

(a) The KARMEN detector is smaller, having only 58 tons of liquid scintillator.

(b) The KARMEN detector is segmented, which permits tighter spatial correlation and very good determination of L/E_ν (to a few percent).

(c) Gadolinium-loaded paper is used in KARMEN around each module to decrease the temporal and spatial separation between the e^+ and neutron capture signals.

(d) The KARMEN detector is only 17.6 m away from the neutrino source.

(e) ISIS is a pulsed machine, which decreases cosmic ray background and allows one to separate by time the neutrinos from π and μ decay.

On the whole, taking all of these differences into account, the sensitivity of KARMEN is about a factor of 2-3 worse than of LSND. They find no statistically significant signal;[92] 171 events are observed whereas the estimated background due to both cosmic ray and ν_e induced events, is 140 events. Even this small excess cannot be readily accounted for by a neutrino oscillation hypothesis. For the LSND oscillation probability, with $\Delta m^2 = 3.9$ eV^2, one would expect 77 excess events. The expected relative excess of events, for three different values of Δm^2, is shown in Fig. 49.

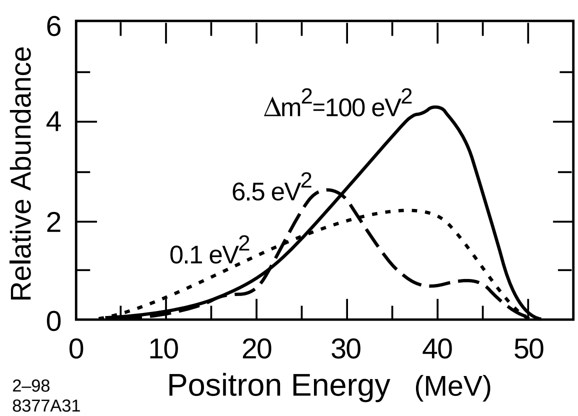

FIG. 49. The relative number of $\bar{\nu}_e$ events expected in the KARMEN experiment for three different values of Δm^2.

In addition, because of the available beam time structure and good energy resolution, KARMEN is able to make two additional measurements:

(a) Search for $\nu_\mu \to \nu_e$ via the reaction

$$\nu_e + {}^{12}C \to e^- + {}^{12}N.$$

Many examples of this process are seen, the reaction being induced by ν_e's from μ^+ decay. An oscillation signal would correspond to the process $\pi^+ \to \mu^+\nu_\mu \to \nu_e$, whose signature would be an excess of events with E_ν = 30 MeV and occurring a short time ($t \approx \tau_\pi$) after each proton pulse. No excess is seen,[93] yielding $P(\nu_\mu \to \nu_e)$ # 2.6 x 10^{-2} (90% C.L.).

(b) Search for $\nu_e \to \nu_x$ via observation of depletion of the reaction discussed above in (a). The normalization is obtained from the neutral current process

$$\nu + {}^{12}C \to \nu + {}^{12}C^*.$$

No depletion is observed,[94] giving a limit $P(\nu_e \to \nu_x)$ # 0.197 (90% C.L.).

In the data taken so far, the sensitivity of the KARMEN search for $\bar{\nu}_\mu \to \bar{\nu}_e$ process has been limited by the neutrons produced by cosmic ray μ's passing through the shielding in the vicinity of the detector. Neutron scattering can simulate the positron signature, and this signal together with the one from their subsequent capture, can give a false $\bar{\nu}_e$ signal. To reduce this background, the Collaboration has just finished installing a 300 m^2 solid scintillator shield[95] around the detector which will veto out most of this background and has been estimated to provide an additional background reduction of about a factor of 40. Preliminary results from the data taken recently with the shield appear to confirm this estimate. The current KARMEN limits for the three processes discussed above, as well as the anticipated future limit for the $\bar{\nu}_\mu \to \bar{\nu}_e$ search, are illustrated in Fig. 50.

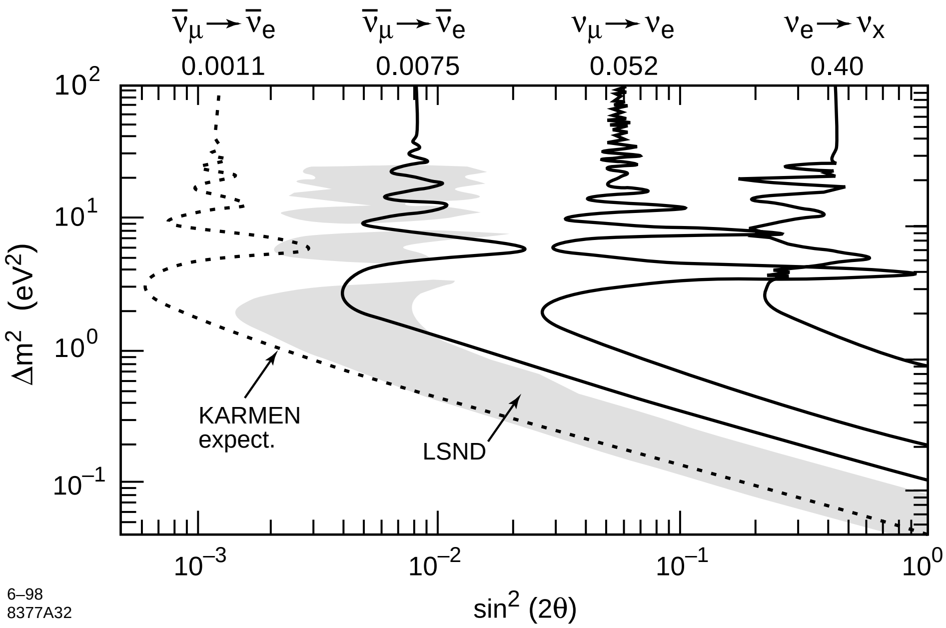

FIG. 50. The exclusion contour plots from the 3 KARMEN oscillation search measurements as well as the expected sensitivity for $\bar{\nu}_\mu \rightarrow \bar{\nu}_e$ in the new experiment. Limits for $\Delta m^2 = 100$ eV^2 and $\sin^2 2\theta = 1$ are indicated. The 90% C.L. LSND suggested contour is shown as the shaded area.

6.3 Searches for $\nu_\mu \rightarrow \nu_e$ at High Energies

There have now been reported several searches for $\nu_\mu \rightarrow \nu_e$ oscillations using accelerator beams in the energy range of 1 GeV and above. They all give negative results. In this section we first discuss these experiments and then summarize the results by showing the combined exclusion plot in the oscillation parameter space.

6.3.1 BNL E776 Experiment

This experiment, even though performed several years ago,[96] still has some of the best limits on $\nu_\mu \rightarrow \nu_e$ (and $\bar{\nu}_\mu \rightarrow \bar{\nu}_e$) oscillations in the intermediate Δm^2 range. The experiment searched for the appearance of $\nu_e(\bar{\nu}_e)$ from a wide band $\nu_\mu(\bar{\nu}_\mu)$ beam. The detector was relatively fine grained and was composed of concrete/drift tube layers followed subsequently by a muon spectrometer. It was located 1 km away from the neutrino source.

The analysis relied on an algorithm based principally on the event shape which was optimized to separate $e^{\pm}$ events from π^o showers. The data collecting was split evenly between neutrino and antineutrino beams. No statistically significant excess of ν_e or $\bar{\nu}_e$ events was observed, as can be seen from Table 6 below.

TABLE 6.

Summary of the BNL E776 Analysis		
	+ Polarity	- Polarity
ν_e/ν_μ in beam	6.8 x 10^{-3}	6.3 x 10^{-3}
No. of events	136	47
Calculated background	$131 \pm 12 \pm 20 \pm 19$	$62 \pm 8 \pm 13 \pm 9$

The three errors in the Table correspond to statistical error, statistical error on the background estimation, and systematic error. The actual data for the much more statistically significant positive polarity run (neutrino beam) are shown in Fig. 51.

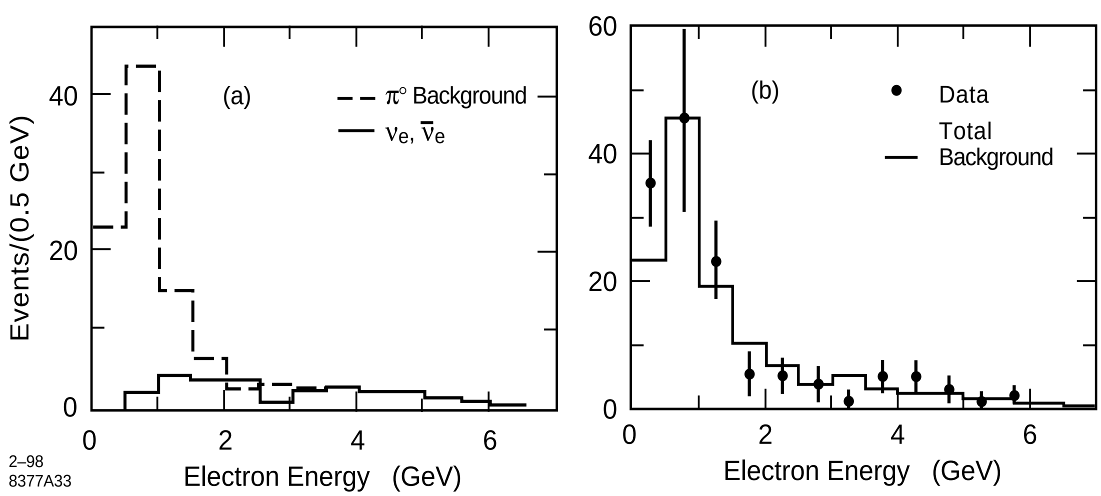

FIG. 51. The results of the BNL E776 experiment. (a) The contributions to the background from ν_μ-induced π° events (dashed line) and from beam ν_e and $\bar{\nu}_e$ (solid line). (b) The spectrum of events passing the electron cuts and the sum of the backgrounds (solid line).

6.3.2 CCFR Experiment

This experiment has been able to set limits on possible $\nu_\mu \to \nu_e$ oscillations at high Δm^2 using two different techniques. The first one of these, comparison of the measured NC/CC ratio with the prediction based on the best value of $\sin^2\theta_w$, was already discussed in Sec. 5.3 in connection with the $\nu_\mu \to \nu_\tau$ oscillation search.[23] Oscillations into ν_e would also enhance the measured NC/CC ratio, even more so than oscillations into ν_τ, because of the larger ν_e CC cross section and the fact that all ν_e CC events would be classified as NC events.

The other method relies on study of the longitudinal energy distribution of the apparent NC events[97] (i.e., "short" events). The ν_e CC events will deposit a large fraction of their energy early in the hadronic shower; the true NC events will have a much broader distribution. Quantitatively, one defines a parameter η

$$\eta = 1 - (E_1 + E_2 + E_3)/E_{vis} ,$$

where E_i is the energy deposited in the i'th scintillator plane (recall that CCFR detector is composed of 10 cm thick Fe plates each one followed by a scintillator plane) after the ν interaction. One can then calculate the expected number of events as a function of η for different values of E_{vis}, both for the ν_e CC events and for the true NC events. The latter distribution can be obtained from the ν_μ CC events by ignoring the energy deposited by the muon. The observed distributions can then be fit to a sum of the two component distributions. The actual data and these two component distributions are shown in Fig. 52 for four different neutrino energy bins: 40-50 GeV (a), 90-105 GeV (b), 150-175 GeV (c), and 250-300 GeV (d).

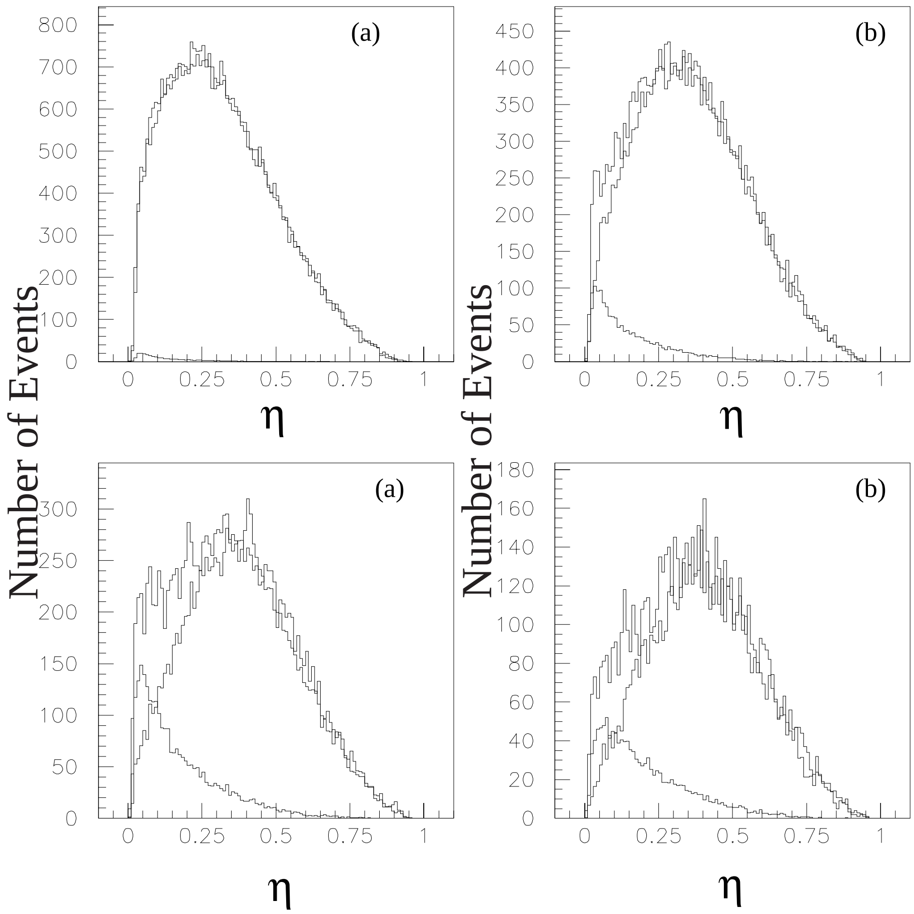

FIG. 52. Histograms of η distributions from the CCFR experiment for four different energy bands showing expected contributions from ν_e CC events (peaking near $\eta = 0$) and the NC events, and the observed experimental distributions.

Since there are some ν_e's in the beam (~2%), there should be a nonzero ν_e CC component. An oscillation signal would manifest itself as an excess of this component above and beyond what is expected from the knowledge of the beam composition. The study of the shape of the difference between these two energy spectra (the observed one and the predicted one assuming no oscillations) as a function of energy could then be used to obtain the best values of the oscillation parameters (if the difference is statistically significant) or set limits on these parameters if there are no statistically significant differences. The results of the analysis are shown in Fig. 53. No evidence for $\nu_\mu \rightarrow \nu_e$ oscillation is seen.

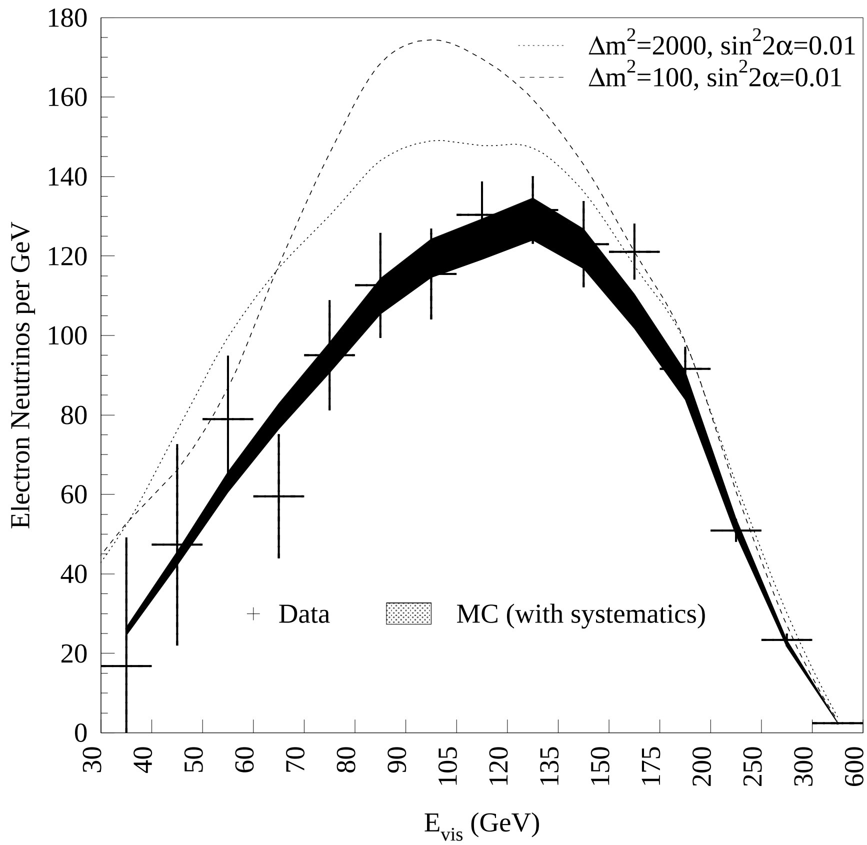

FIG. 53. Limits on oscillations from the CCFR experiment, based on the analysis of the longitudinal deposition of energy.

6.3.3 NOMAD Results on $\nu_\mu \to \nu_e$

The NOMAD detector has two characteristics that are important for possible ν_e CC event identification: good electron identification (through TRD's and electromagnetic calorimetry) and fine-grained tracking. These two characteristics allow one to identify ν_e CC interactions and also separate ν_e from $\bar{\nu}_e$ events. Thus ν_μ, $\bar{\nu}_\mu$, ν_e, and $\bar{\nu}_e$ charged current events can be separated from each other and their energy spectra measured. Furthermore, the ν_e spectrum can be uniquely predicted from the other three spectra.

The argument is basically the following. The $\nu_\mu(\bar{\nu}_\mu)$ spectra allow one to predict the primary yields of K^+ and π^+ (K^- and π^-). One can then predict the contribution of K^- flux to the $\bar{\nu}_e$ spectrum, and after its subtraction, the residual $\bar{\nu}_e$ spectrum is used to determine the flux of K_L^0's. These calculated yields of $\pi^\pm$, $K^\pm$, and K_L^0 predict uniquely the ν_e spectrum, the ν_e's originating primarily from K^+ and K_L^0 decays, with a small contribution from the decays of secondary μ^+'s. Any possibly observed excess of ν_e events would then be evidence for $\nu_\mu \rightarrow \nu_e$ oscillations. Furthermore, the energy dependence of this excess would allow one to determine the oscillation parameters. No excess is observed,[85] yielding a limit of $\sin^2 2\theta < 2 \times 10^{-3}$ at high Δm^2. The calculated contribution of each kind of parent particle to the total neutrino flux is shown in Fig. 54.

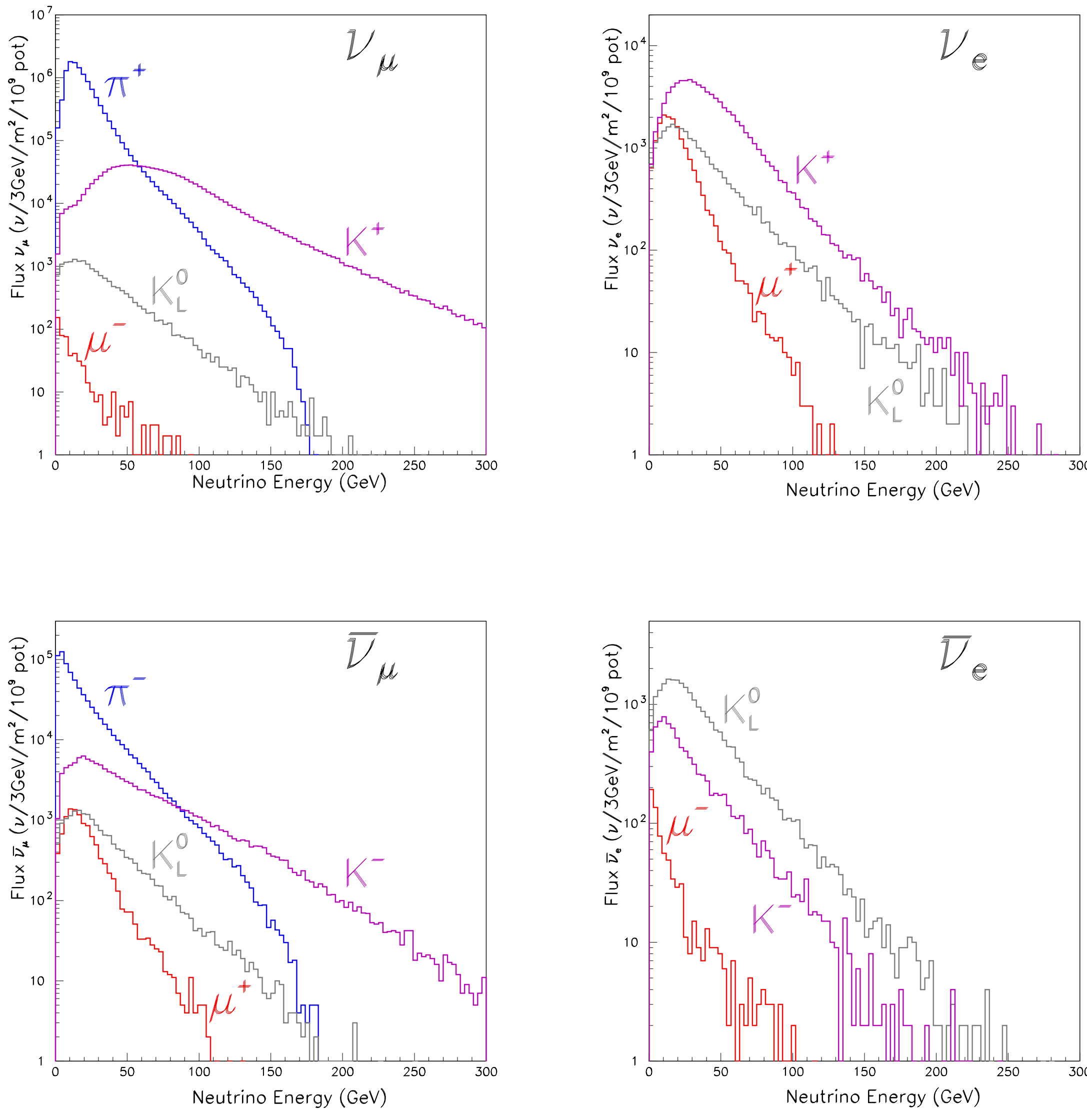

FIG. 54. Contribution of different parent particles to the different beam components in the CERN neutrino beam.

Figure 55 shows the exclusion plots in the oscillation parameter space of the four results discussed above: BNL E776, the two measurements from CCFR, and the NOMAD limits. Combining all the relevant exclusion plots, we can see that a small part of the LSND suggested region is still compatible with all of the currently existing data. The future KARMEN experiment, however, should be able to confront this region directly as has been discussed above.

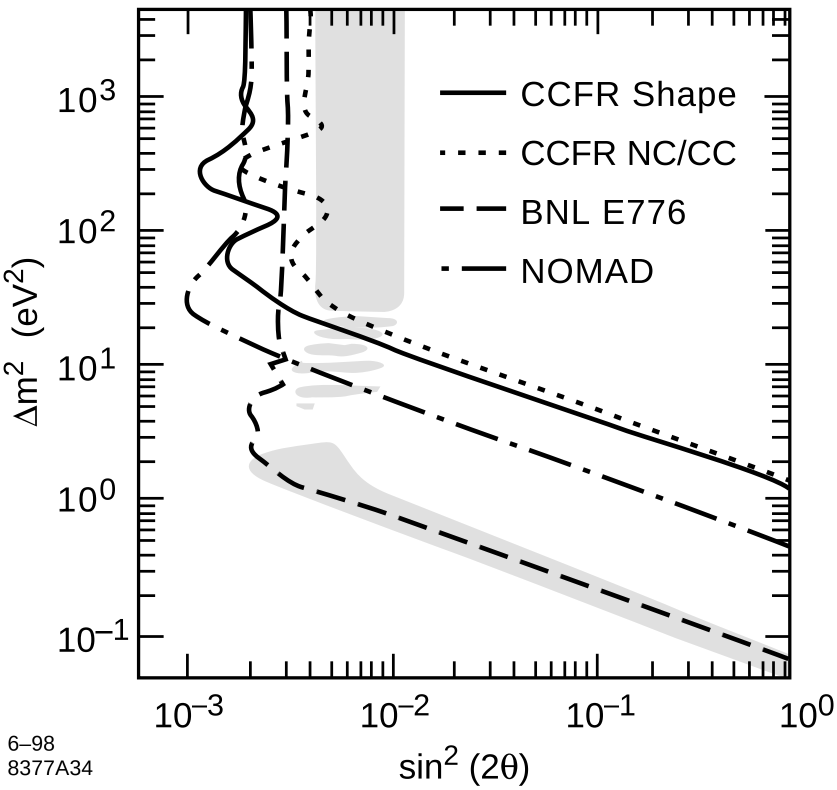

FIG. 55. 90% C.L. exclusion contours for $\nu_\mu \to \nu_e$ oscillations from the two CCFR measurements, BNL E776, and NOMAD experiments. The 90% C.L. LSND suggested region is indicated as the shaded area.

Acknowledgments

Support for this work from the U.S. National Science Foundation and the U.S. Department of Energy is gratefully acknowledged.

I would like to thank the organizers of the Summer Institute for the efficient organization and the congenial atmosphere provided. I want to thank Bob Bernstein, Bob Cousins, Byron Lundberg, Larry Wai, and Hywel White for their help in obtaining the most recent figures from their work. Finally, I owe deep gratitude to Judy Meo for the key role she played in creating this document.

References

[1] W. Pauli's bold suggestion of the existence of a new particle, the neutrino, was never published. The idea was put forth in a letter dated December 4, 1930, to the attendees of a Conference in Tubingen. It was addressed to "Dear Radioactive Ladies and Gentlemen." Pauli himself was not able to participate in the meeting because of a prior committment to attend a ball in Zurich. The letter has been reproduced in a number of places, e.g., N. Solomey, *The Elusive Neutrino* (Scientific American Library, 1997), pp. 16-17.

[2] F. Reines and C. L. Cowan., Phys. Rev. **92**, 830 (L) (1953).

[3] M. Goldhaber, L. Grodzins, and A. W. Sunyar, Phys. Rev. **109**, 1015 (L) (1958).

[4] G. Danby *et al.*, Phys. Rev. Lett. **9**, 36 (1962).

[5] Some of the key early papers are: F. J. Hasert *et al.*, Phys. Lett. B **46**, 121 (1973); F. J. Hasert *et al.*, Phys. Lett. B **46**, 138 (1973); A. Benvenuti *et al.*, Phys. Rev. Lett. **32**, 800 (1974); B. C. Barish *et al.*, Phys. Rev. Lett. **34**, 538 (1975).

[6] Some of the early papers are: B. Aubert *et al.*, Phys. Rev. Lett. **32**, 1457 (1974); B. C. Barish *et al.*, *ibid*. **34**, 538 (1975) ; D. Cline *et al.*, Phys. Rev. Lett. **37**, 252 (1976); F. A. Harris *et al.*, Phys. Rev. Lett. **39**, 437 (1977).

[7] The early work is described in: F. Reines *et al.*, Phys. Rev. Lett. **37**, 315 (1976); A. M. Cnops *et al.*, Phys. Rev. Lett. **41**, 357 (1978).

[8] R. M. Barnett *et al.* (Particle Data Group), Phys. Rev. D **54**, 1 (1996).

[9] For a comprehensive review of the subject of neutrino masses, see S. M. Bilenky and S. T. Petcov, Rev. Mod. Phys. **59**, 671 (1987).

[10] F. Zwicky, Helv. Phys. Acta **6**, 110 (1933); V. C. Rubin and W. K. Ford, Astrophys. J. **159**, 379 (1970); T. S. van Albada *et al.*, Astrophys. J. **295**, 305 (1985).

[11] The first experimental paper on the subject was by R. Davis, Jr., Phys. Rev. Lett. **12**, 303 (1964); for a recent review, see A. Y. Smirnov, in *Proceedings of the 17th International Conference on Neutrino Physics and Astrophysics* (Neutrino '96), edited by K. Enqvist, K. Huitu, and J. Maalampi (World Scientific, 1997), pp. 38-55; for a review of solar models, see J. N. Bahcall and M. H. Pinsonneault, Rev. Mod. Phys. **67**, 1 (1995); for a nonconventional point of view, arguing that the solar neutrino data are consistent with solar models if all the uncertainties are taken into account, see A. Dar and G. Shaviv, Astrophys. J. **468**, 933 (1996).

[12] The initial evidence came from K. S. Hirata *et al.*, Phys. Lett. B **280**, 146 (1992); Y. Fukuda *et al.*, Phys. Lett. B **335**, 237 (1994); R. Becker-Szendy *et al.*, Phys. Rev. D **46**, 3720 (1992); the recent data are discussed in the parallel lectures at this Institute by K. Martens.

[13] C. Athunassopoulos *et al.*, Phys. Rev. Lett. **75**, 2650 (1995); but see also J. E. Hill, Phys. Rev. Lett. **75**, 2654 (1995).

[14] K. Martens, these proceedings.

[15] The possibility of neutrino oscillations was first suggested by B. Pontecorvo, Zh. Eksp. Theor. Fiz. **33**, 549 (1957); *ibid* **34**, 247 (1958).

[16] G. S. Abrams *et al.*, Phys. Rev. Lett. **63**, 2173 (1989) for the SLC results; J. R. Carter, in *Proceedings of the Joint International Lepton-Photon Symposium and Europhysics Conference on High Energy Physics*, edited by S. Hegarty, K. Potter, and E. Quercigh (World Scientific, 1992), pp. 1-26, for a summary of LEP results from Z line shape; for a recent compendium of the latest CERN results using other methods, see S. C. C. Ting, Phys. Rep. **279**, 204 (1997).

[17] For a recent review of various possible schemes, see A. Yu. Smirnov, in *Proceedings of the 28th International Conference on High Energy Physics*,

edited by Z. Ajduk and A. K. Wroblewski (World Scientific, 1997), pp. 288-306.

[18] B. C. Barish *et al.*, Phys. Rev. Lett. **39**, 1595 (1977).

[19] K. Abe *et al.*, Phys. Rev. Lett. **58**, 636 (1987). If the neutrino has electromagnetic structure like that predicted by many extensions of the Standard Model, there will be additional contributions to the neutrino lepton scattering. See the cited paper for a comprehensive list of references discussing such possibilities.

[20] This general idea, based on a plasma lens, was first used to focus the protons from the 184" cyclotron at Berkeley. W. Panofsky and W. Baker, Rev. Sci. Instrum. **21**, 5 (1950).

[21] BNL E889 Collaboration, Long Baseline Neutrino Oscillation Experiment, April 1995, BNL No. 52459.

[22] J. Hylen *et al.*, Conceptual Design for the Technical Components of the Neutrino Beam for the Main Injector (NuMI), September 1997, Fermilab-TM-2018.

[23] K. S. McFarland *et al.*, Phys. Rev. Lett. **75**, 3993 (1995).

[24] B. C. Barish *et al.*, Phys. Rev. Lett. **32**, 1387 (1974).

[25] M. Holder *et al.*, Phys. Rev. Lett. **39**, 433 (1977).

[26] This possibility was suggested in connection with a proposal for an intermediate baseline neutrino oscillation experiment at CERN to look for $\nu_\mu \to \nu_e$ oscillations. L. Ludovici and P. Zucchelli, “An Antitagged Experiment for $\nu_\mu \to \nu_e$ Oscillation Search,” paper presented at the Fermilab Workshop on Fixed Target Physics at the Main Injector, May 1-4, 1997.

[27] This principle was to be used in the BNL long baseline neutrino experiment, Ref. 21.

[28] A. Rothenberg, ‘‘A Search for Unknown Sources of Neutrino-Like Particles,” Ph. D. thesis, Stanford University (1972).

[29] P. Alibran *et al.*, Phys. Lett. B **74**, 134 (1978); T. Hansl *et al.*, Phys. Lett. B **74**, 139 (1978); P. C. Bosetti *et al.*, Phys. Lett. B **74** , 143 (1978).

[30] Fermilab Proposal E-872, B. Lundberg, spokesperson.

[31] J. Kleinfeller *et al.*, in *Proceedings of the 17th International Conference on Neutrino Physics and Astrophysics*, edited by K. Enqvist, K. Huitu, and J. Maalampi (World Scientific, 1997), pp. 193-202.

[32] A. De Rújula, E. Fernández, and J. J. Gómez-Cárdenas, Nucl. Phys. B **405**, 80 (1993).

[33] E. Fernandez, Nucl. Phys. B (Suppl.) **31**, 326 (1993).

[34] To my knowledge, the earliest proposal to use μ storage rings as a source of copious ν_μ and ν_e fluxes was put forth by the author in 1974 in an unpublished note. For the current situation on $\mu^+\mu^-$ colliders, see: $\mu^+\mu^-$ Collider: A Feasibility Study, BNL-52503, Fermilab-Conf.-96/092, LBNL-38946.

[35] Y. Declais *et al.*, Phys. Lett. B **338**, 383 (1994).

[36] P. Anselmann *et al.*, Phys. Lett. B **342**, 440 (1995).

[37] J. N. Bahcall and M. H. Pinsonneault, Rev. Mod. Phys. **67**, 1 (1995).

[38] G. Barr, T. K. Gaisser, and T. Staner, Phys. Rev. D **39**, 3532 (1989).

[39] See, for example, A. Burrows, Astrophys. J. **334**, 891 (1988); also A. Burrows, Annu. Rev. Nucl. Part. Sci. **40**, 181 (1990).

[40] K. S. Hirata *et al.*, Phys. Rev. Lett. **58**, 1490 (1987); R. M. Bionta *et al.*, Phys. Rev. Lett. **58**, 1494 (1987); E. N. Alexeyev *et al.*, JETP Lett. **45**, 589 (1987); M. Aglietta *et al.*, Europhys. Lett. **3**, 1315 and 1321 (1987); V. L. Dadykin *et al.*, JETP Lett. **45**, 593 (1987).

[41] See, for example, F. Halzen in *Proceedings of the 1994 Snowmass Summer Study*, edited by E. W. Kolb and R. D. Peccei (World Scientific, 1995), pp. 256-266.

[42] P. O. Hulth (for the AMANDA Collaboration) in *Proceedings of the 17th International Conference on Neutrino Physics and Astrophysics*, edited by K. Enqvist, K. Huitu, and J. Maalampi (World Scientific, 1997), pp. 518-523.

[43] B. Monteleoni (for the NESTOR Collaboration), same as Ref. 41, pp. 534-538.

[44] KamLand Proposal, private communication from G. Gratta, Stanford University.

[45] R. H. Heisterberg *et al.*, Phys. Rev. Lett. **44**, 635 (1980).

[46] M. Jonker *et al.*, Nucl. Instrum. Methods A 200, 183 (1982); J. Dorenbosch *et al.*, Nucl. Instrum. Methods A **253**, 203 (1987).

[47] K. deWinter *et al.*, Nucl. Instrum. Methods A **278**, 670 (1989); D. Geiregat *et al.*, Nucl. Instrum. Methods A **325**, 92 (1993).

[48] C. Bemporad in *Proceedings of the 17th International Conference on Neutrino Physics and Astrophysics*, edited by K. Enqvist, K. Huitu, and J. Maalampi (World Scientific, 1997), pp. 242-247.

[49] G. Gratta (on behalf of the Palo Verde Collaboration), same as Ref. 47, pp. 248-255.

[50] G. Drexlin *et al.*, Nucl. Instrum. Methods A **289**, 490 (1990).

[51] P. Astier *et al.* (NOMAD Collaboration), CERN-SPSLC/91-21 (1991); J. Altegoer *et al*., Nucl. Instrum. Methods A **404**, 96 (1998).

[52] ICARUS was proposed by C. Rubbia in CERN-EP 77-8(1977); for recent developments, see A. Bonetti *et al.*, Nucl. Instrum. Methods A **332**, 395 (1993).

[53] The first hydrogen chambers used for neutrino physics were the BNL 7' chamber [see, for example, E. G. Cazzoli *et al.*, Phys. Rev. Lett. **34**, 1125 (1975)] and the Argonne 12' chamber [S. J. Barish *et al.*, Phys. Rev. D **16**, 3103 (1977)].

[54] R. J. Cence *et al.*, Lawrence Berkeley Laboratory report LBL-4816.

[55] See, for example, A. M. Cnops *et al.*, Phys. Rev. Lett. **51**, 357 (1978).

[56] The largest and most productive of heavy liquid chambers used for studies of neutrino interactions was the Gargamelle chamber at CERN; see, for example, J. Blietschau *et al.*, Phys. Lett. B **73**, 232 (1978).

[57] K. Abe *et al.*, Phys. Rev. D **30**, 1 (1984).

[58] Fermilab Proposal No. 745, Muon Neutrino, T. Kitagaki, spokesman.

[59] Fermilab Proposal No. 636, Beam Dump, T. Kitagaki and I. A. Pless, spokesmen. This experiment was approved but never took data.

[60] The key developments in the automatization of the emulsion scanning techniques have been pioneered by K. Niwa and his group at Nagoya University. For a discussion of various experimental emulsion schemes, see A. Ereditato, K. Niwa, and P. Strolin: The Emulsion Technique for Short, Medium, and Long Baseline ν_μ–ν_τ Oscillation Experiments, Report INFN/AE-97/06 and Nagoya DPNU-97-07.

[61] K. S. Hirata *et al.*, Phys. Rev. D **44**, 2241 (1991).

[62] K. S. Hirata *et al.*, Phys. Lett. B **280**, 146 (1992); R. Becker-Szendy *et al.*, Phys. Rev. D **46**, 3720 (1992).

[63] K. S. Hirata *et al.*; R. M. Bionta *et al.* (Ref. 39).

[64] Y. Itow, these proceedings; also Y. Totsuka, University of Tokyo Report No. ICCR-Report-227-90-20.

[65] Kamiokande Collaboration, presented at the 16th International Conference on Neutrino Physics and Astrophysics, Eilat, Israel, 29 May-3 June, 1994 (unpublished).

[66] T. Ypsilantis *et al.*, A Long Baseline RICH with a 27-kton Water Target and Radiator for Detection of Neutrino Oscillations, LPC-96-01, January, 1996.

[67] G. T. Ewan *et al.*, Sudbury Neutrino Observatory Proposal, Report No. SNO-87-12 (1987).

[68] See, for example B. J. Stanger, Nucl. Phys. B (proc. Suppl.) **14** A, 153 (1990).

[69] I. A. Belolaptikov *et al.*, Nucl. Phys. B **43**, 241 (1995).

[70] L. W. Alvarez, University of California Radiation Laboratory Report UCRL-328, 1949 (unpublished).

[71] B. Pontecorvo, National Research Council of Canada Report No. 205, 1946, (unpublished).

[72] P. Anselmann *et al.*, Phys. Lett. B **327**, 377 (1994).

[73] M. Aufderheide *et al.*, Phys. Rev. C **49**, 678 (1994).

[74] A.I. Abazov *et al.*, Phys. Rev. Lett. **67**, 3332 (1991).

[75] K. Lande and P. S. Wildenhain (for the Homestake Program) in *Proceedings of the 17th International Conference on Neutrino Physics and Astrophysics*, edited by K. Enqvist, K. Huitu, and J. Maalampi (World Scientific, 1997), pp. 25-37.

[76] F. Dydak *et al.*, Phys. Lett. B **134**, 281 (1984).

[77] E. Bergsma *et al.*, Phys. Lett. B **142**, 103 (1984).

[78] I. E. Stockdale *et al.*, Phys. Rev. Lett. **52**, 1384 (1984).

[79] N. Ushida *et al.*, Phys. Rev. Lett. **57**, 2897 (1986).

[80] N. Ushida *et al.*, Phys. Rev. Lett. **45**, 1049 and 1053 (1980).

[81] M. Gruwe *et al.*, Phys. Lett. B **309**, 463 (1993).

[82] H. Harari, Phys. Lett. B **216**, 413 (1989).

[83] V. Palladino, in *Proceedings of the 28th International Conference on High Energy Physics*, edited by Z. Ajduk and A. K. Wroblewski (World Scientific, 1997), pp. 1723-1726.

[84] D. Rondeshagen (for the CHORUS Collaboration), these proceedings.

[85] B. Schmidt (for the NOMAD Collaboration), these proceedings.

[86] B. Achkar *et al.*, Nucl. Phys. B **434**, 503 (1995).

[87] G. S. Vidyakin *et al.*, JETP Lett. **59**, 364 (1994).

[88] G. Zacek *et al.*, Phys. Rev. D **34**, 2621 (1986).

[89] M. Apollonio *et al.*, preprint hep-ex/9711002v1, Nov. 5, 1997 (unpublished).

[90] C. Athanassopoulos *et al.*, Phys. Rev. Lett. **77**, 3082 (1996); C. Athanassopoulos *et al.*, Phys. Rev. C **55**, 2079 (1997); see also Ref. 13.

[91] C. Athanassopoulos *et al.*, Report LA-UR-97-1998, UCRHEP-E191, submitted to Phys. Rev. C.

[92] G. Drexlin *et al.*, Nucl. Instrum. Methods A **289**, 490 (1990); see also Ref. 31.

[93] G. Drexlin, Prog. Part. Nucl. Phys. **32**, 375 (1994).

[94] K. Eitel *et al.* in *Proceedings of the XIIIth Rencontres de Blois*, June 8-12, 1996 (to be published).

[95] G. Drexlin and B. Zeitnitz, Proposal for an Upgrade of the KARMEN Veto System, internal KARMEN Report.

[96] L. Borodovsky *et al.*, Phys. Rev. Lett. **68**, 274 (1992).

[97] A. Romosan *et al.*, Phys. Rev. Lett. **78**, 2912 (1997).

[98] Fermilab Proposal no. 802, N. W. Reay, spokesman.

[99] R. A. Sidwell, in *Proceedings of the 17th International Conference on Neutrino Physics and Astrophysics*, edited by K. Enqvist, K. Huitu, and J. Maalampi (World Scientific, 1977), pp. 152-158.

[100] K. Eggert *et al.*, Nucl. Phys. B (Proc. Suppl.) **38**, 240 (1995).

[101] A. Ereditato, TOSCA—A High Sensitivity Short Baseline Experiment to Search for $\nu_\mu \to \nu_\tau$ Oscillations, paper presented at the Fermilab Workshop on Fixed-Target Physics at the Main Injector, May 1-4, 1997.

[102] Y. Suzuki (for the E362 Collaboration), in *Proceedings of the 17th International Conference on Neutrino Physics and Astrophysics*, edited by K. Enqvist, K. Huitu, and J. Maalampi (World Scientific, 1977), pp. 237-241.

[103] Proposal for Japan Hadron Facility, KEK Report 97-3, JHF-97-1, May 1997.

[104] Fermilab Proposal No. 875 (MINOS), Stanley Wojcicki, spokesman.

[105] W. W. M. Allison *et al.*, Phys. Lett. B **391**, 491 (1997).

[106] The current most up-to-date description of the experiment is in an internal MINOS note, NuMI-L-300.

[107] The ICARUS Collaboration, LNGS 94/99-II, May, 1994; see also Ref. 51.

[108] G. G. Barberino, NOE—Neutrino Oscillation Experiment, paper presented at the Fermilab Workshop on Fixed-Target Physics at the Main Injector, May 1-4, 1997.

[109] H. Shibuya *et al.* (OPERA Collaboration). The OPERA Emulsion Detector for a Long-Baseline Neutrino Oscillation Experiment, LNGS-LOI 8/97, September 1997.

[110] BooNE Collaboration, Proposal submitted to the Fermilab National Laboratory, Janet Conrad and William C. Louis III, spokespersons.

[111] ICARUS Collaboration, CERN/SPSLC/96-58/P304, December 1996.

[112] To my knowledge there is no printed proposal or a description of this effort at this time; most of my information comes from a Letter of Intent from the U.S. groups for this experiment and from private communications from G. Gratta.